Grey matter pathology in multiple sclerosis:

in vivo and post mortem

magnetic resonance imaging studies

Steven Harry Pieter van de Pavert

Thesis submitted for the degree of

Doctor of Philosophy

of the

University College London

Department of NeuroInflammmation

Queen Square Multiple Sclerosis Centre

Institute of Neurology

University College London

I, Steven van de Pavert, confirm that the work presented in this thesis is my own.

Where information has been derived from other sources, I confirm that this has been

indicated in the thesis.

Abstract

The extent and clinical relevance of grey matter (GM) pathology in multiple sclerosis (MS) is increasingly recognised. Previous work has shown that GM pathology is more closely associated with some aspects of clinical disability than white matter (WM) injury, which has been suggested to arise independently. Magnetic resonance imaging (MRI) allows the study of GM lesions, atrophy, and non-lesional injury with techniques including double inversion recovery (DIR), volumetric scans, and magnetisation transfer ratio (MTR), respectively.

This thesis includes three independent in vivo and post mortem MRI studies specifically addressing (1) the clinical impact and spatial distribution of DIR-detected GM lesions and atrophy, (2) the longitudinal development of MTR changes in thalamo-cortical systems, and (3) the histopathological substrates underlying MTR in the MS brain.

This work shows that (1) DIR-detected GM lesions are mainly found throughout the cerebellar and cerebral cortex, whereas particularly subcortical GM structures show atrophy. Both GM lesions and atrophy contribute to disability, suggesting that the substrates of disability in MS are both pathologically and spatially heterogeneous. (2) WM injury to thalamo-cortical systems is most likely to precede (both thalamic and cortical) GM damage. In addition, lower regional cortical MTR is found not to be consistently associated with lower cortical volume, suggesting that significant cortical microstructural damage can occur in the absence of atrophy. Furthermore, observed hemispheric asymmetries and WM tract inhomogeneities emphasise the need for more refined statistical models to detect disease-specific changes. (3) MTR is associated with histologically quantified myelin (and to a lesser extent neuronal content) in normal appearing grey matter and normal appearing white matter, but not in cortical lesions and chronic inactive WM lesions. Finally, the cytological make-up differs significantly between normal appearing and lesional WM and GM, and provides extra evidence for microglia-mediated mitochondria damage in normal appearing MS tissue.

Ὁ δ' ἀνεξέταστος βίος οὐ βιωτὸς

- Socrates

in Plato, Apology 38a

Acknowledgements

Over the last few years, I was continually reminded of the privilege of being able to do my PhD here at Queen Square. In every aspect of my work I was able to turn to one of my colleagues who happened to be world-leading in their respective fields, and who helped me with designing my experiments, acquiring and analysing data, and interpreting results. Without them this thesis could not have been written, and I am deeply grateful for their expertise and generous help.

I want to thank a few people in particular.

Firstly, this thesis would not have been possible without the people that donated their time, or brain tissue, and ultimately were the reason why we did these studies.

Olga Ciccarelli, I want to thank you for your endless enthusiasm and support. I enjoyed the way we worked together, and I am grateful for the trust and autonomy you gave me in our projects, while at the same time always being there when I needed help or a critical look at my work.

Claudia Gandini Wheeler-Kingshott, thank you for your help and expertise on the physics and image analysis side of these studies. While I am not a physicist by training, with your support I feel I managed to get a good handle on MRI. Thank you for making me feel part of your physics team.

Declan Chard, thank you for our weekly 'grey matter meetings' to discuss our projects and other (un)related topics. Particularly your critical look, precision, and hypothesis-driven approach have been very helpful in shaping the work in this thesis, and I am sure in many projects to come.

In no particular order I would also like to express my gratitude to the following people.

Djordje Gveric and Richard Reynolds, thank you for making available post mortem brain tissue for us to study.

Nils Muhlert, thank you for teaching me the ropes in MRI data analysis when I first arrived here.

Publications associated with this thesis

Journal articles

S.H.P. van de Pavert, N. Muhlert, V. Sethi, C.A.M. Wheeler-Kingshott, G.R. Ridgway, J.J.G. Geurts, M. Ron, T.A. Yousry, A.J. Thompson, D.H. Miller, D.T. Chard, O. Ciccarelli. *DIR-visible grey matter lesions and atrophy in multiple sclerosis: partners in crime?* J. Neurol. Neurosurg. Psychiatry 87, 461–467 (2016)

Conference abstracts

S.H.P. van de Pavert, N. Muhlert, V. Sethi, C.A.M. Wheeler Kingshott, A.J. Thompson, J.J.G. Geurts, T.A. Yousry, D.H. Miller, D.T. Chard, O. Ciccarelli. Co-localisation of grey matter volume reduction and grey matter lesions in multiple sclerosis. ECTRIMS 2012 – Lyon (Poster)

S.H.P. van de Pavert, N. Muhlert, V. Sethi, C.A.M. Wheeler Kingshott, A.J. Thompson, J.J.G. Geurts, T.A. Yousry, D.H. Miller, D.T. Chard, O. Ciccarelli. *Co-localisation and clinical impact of grey matter lesions and regional grey matter volume loss in MS.* ECTRIMS 2013 – Copenhagen (Poster)

S.H.P. van de Pavert, M. Pardini, A. Eshaghi, F. Prados, Ö. Yaldizli, V. Sethi, S. Ourselin, C.A.M. Gandini Wheeler-Kingshott, D.H. Miller, O. Ciccarelli, D.T. Chard. *Spatial and temporal characteristics of magnetisation transfer ratio changes in different corticothalamic systems in multiple sclerosis.* ECTRIMS 2016 – London (Poster)

Table of contents

List of figures

List of tables

Glossary

25TWT	25-foot timed walk test
9HPT	Nine hole peg test
BBB	Blood-brain barrier
CIS	Clinically isolated syndrome
CNS	Central nervous system
CSF	Cerebrospinal fluid
DARTEL	Diffeomorphic anatomical registration through exponentiated Lie algebra
DAWM	Diffusely abnormal white matter
DGM	Deep grey matter
DIR	Double inversion recovery
DWI	Diffusion weighted imaging
DTI	Diffusion tensor imaging
EDSS	Expanded disability status scale
fB	fraction of macromolecular protons
FA	Fractional anisotropy
FFE	Fast field echo
FLAIR	Fluid attenuated inversion recovery
FWE	Family wise error
GFAP	Glial fibrillary acidic protein
GM	Grey matter
GRE	Gradient recalled echo
ICV	Intracranial volume
LG	Lateral group
LPM	Lesion probability mapping
MBP	Myelin basic protein
MD	Mean diffusivity
MG	Medial group
MNI	Montreal neurological institute
MRI	Magnetic resonance imaging
MS	Multiple sclerosis
MSFC	Multiple sclerosis functional composite score

MTR	Magnetisation transfer ratio
NACGM	Normal appearing cortical grey matter
NADGM	Normal appearing deep grey matter
NAGM	Normal appearing grey matter
NAWM	Normal appearing white matter
OCC	Occipital cortex
PASAT	Paced auditory serial addition test
PBS	Phosphate buffered saline
PD	Proton density
PFC	Prefrontal cortex
PPMS	Primary progressive multiple sclerosis
PSIR	Phase sensitive inversion recovery
qMT	Quantitative magnetisation transfer
RD	Radial diffusivity
RF	Radio frequency
ROI	Region of interest
RRMS	Relapsing remitting multiple sclerosis
SMC	Sensorimotor cortex
SPMS	Secondary progressive multiple sclerosis
SDMT	Symbol digit modalities test
T	Tesla
TDI	Tract-density imaging
TE	Echo time
TFE	Turbo field echo
TI	Inversion time
TR	Repetition time
VBM	Voxel based morphometry
WM	White matter

Chapter 1

Multiple sclerosis pathology

In young adults, multiple sclerosis (MS) is the leading cause of non-traumatic neurological disability, globally affecting around 2.5 million people (Noseworthy et al. 2000; Preiningerova et al. 2009). MS has different clinical manifestations and is pathologically heterogeneous, complicating our understanding of the underlying pathogenic mechanisms driving the disease. The current thesis aims to provide a better understanding of the clinical impact, the spatiotemporal distribution, and underlying histopathological correlates of magnetic resonance imaging (MRI)-detected pathology in MS, specifically focussing on grey matter (GM). To outline the relevance of this work, the present chapter introduces MS and its underlying pathology.

MS can be classified in relapse onset and progressive onset. Around 80% of people with MS experience a disease course of relapses associated with accumulating neurological damage, known as relapsing remitting MS (RRMS). Relapses are associated with focal demyelinated inflammatory white matter (WM) lesions, which may occur in any part of the central nervous system (CNS) and therefore have varying clinical manifestations, including motor, cognitive, and sensory dysfunction (Compston et al. 2005). The detection of these WM lesions on MRI scans is the most common approach to diagnose and monitor progression of MS (Polman et al. 2005; Polman et al. 2011). After 10 to 15 years from disease onset the majority of people with RRMS enter a secondary progressive (SP) phase, which is characterised by a continuous decline in clinical function. A second form, primary progressive MS (PPMS), affects approximately 10 to 15% of patients and is characterised by a gradual decline in function from disease onset. Both people with relapse onset MS and PPMS reach disease milestones (e.g. requiring walking aid or being wheelchair-bound) around the same age.

In addition to WM injury, GM pathology has been found to be substantial in all MS subtypes, and in cross-sectional studies it has been shown that clinical disability is more closely associated with GM pathology than with WM lesion accrual (Fisniku et al. 2008; Roosendaal et al. 2011; Fisher et al. 2008), which has contributed to the hypothesis that the main driver of disability in MS is a pathological process occurring independently in the GM (Geurts 2008; Stys et al. 2012). For a better understanding of GM pathology, this thesis includes three independent in vivo and post mortem MRI studies specifically addressing (1) the clinical impact and spatial distribution of MRI detected GM lesions and atrophy, (2) the longitudinal development of non-lesional changes in thalamo-cortical systems, and (3) the histopathological substrates underlying MRI scans in the MS brain. The present chapter provides an overview of manifestations and underlying pathogenic mechanisms of CNS injury in MS, with a specific focus on GM damage.

1.1 White matter pathology

The traditional view of MS suggests that the disease is primarily caused by myelin-active CD4-positive T-cells infiltrating the CNS through the blood-brain barrier (BBB) and subsequently orchestrating an attack on myelin-sheaths, resulting in the characteristic inflammatory demyelinated WM lesions (McFarland & Martin 2007; Lassmann 2011). WM lesions occur throughout the entire CNS, and are predominantly found in the periventricular space and around small to medium-sized blood vessels (Fazekas et al. 1999; Filippi et al. 2012). They are sharply demarcated ranging from one millimetre to several centimetres in diameter, and can relatively easily be distinguished macroscopically. Histopathological work has shown that these lesions show severe myelin loss, axonal thinning, and axonal transection (Trapp et al. 1998), accompanied by inflammatory lymphocytes and a large presence of CD68-positive microglia/macrophages (Compston et al. 2005).

WM lesions are found in different subtypes: chronic active lesions, acute active demyelinating lesions, inactive demyelinated lesions, and remyelinated lesions. In early MS, a distinction can relatively easily be made between lesions, but in later stages of MS axonal degeneration may cause sustained diffuse inflammation (Kutzelnigg et al. 2005), making it more difficult to distinguish different confluent lesions on MRI or histopathologically. Active demyelinating lesions show ongoing inflammatory myelin sheath degradation; myelin debris can be found inside the lesions' large number of microglia/macrophage and lymphocyte infiltrates. Active demyelinating lesions can either be chronic or acute. Whereas acute lesions are characterised by a single 'wave' of demyelination, the chronic type shows continuous degradation of myelin. Inactive demyelinated lesions are the most commonly observed type in MS and do not show ongoing myelin degradation. In these lesions, inflammation and myelin debris may still be present, but the active assault on myelin sheaths has ceased. In older inactive lesions a reduced presence of inflammatory cells is seen (Esiri et al. 2006). At this stage, astrocytic glial cells form scar tissue, and the lesions are referred to as remyelinated lesions. Importantly, axonal density is severely reduced both within and outside demyelinated WM lesions (DeLuca et al. 2015; Trapp et al. 1998; Evangelou, Esiri, et al. 2000).

In addition to focal demyelinated WM lesions, diffuse non-lesional WM damage is found in MS. On conventional (proton density [PD] and T2-weighted) MRI scans, non-lesional WM may be referred to as 'normal appearing white matter' (NAWM) or 'diffusely abnormal white matter', also known as 'dirty appearing white matter' (DAWM). DAWM is defined as having ill-defined borders with hypo-intense signal on PD and T2-weighted MRI scans, and is characterised histopathologically by a reduction in myelin phospholipids and axonal loss (Moore et al. 2008). NAWM, on the other hand, shows various differences compared to WM of healthy individuals, which may be due to the

presence of pre-active lesions (De Groot et al. 2001). Histopathologically, NAWM shows increased CD68-positive microglial inflammation, BBB disruption, and oedema, suggestive of widespread inflammation (Kutzelnigg et al. 2005; Allen et al. 2001). Various pathophysiological mechanisms have been suggested to play a role in NAWM damage in addition to inflammation and axonal loss, including astrocytic activation (gliosis), reduced perfusion of the NAWM (Sowa et al. 2015), changes in vascular oxygen supply (Haider et al. 2014), cerebrospinal fluid (CSF)-mediated toxicity (Magliozzi et al. 2010), and Wallerian axonal damage from WM or GM lesions (Ciccarelli et al. 2003; Allen et al. 2001).

1.2   Grey matter pathology

Particularly in the previous decade GM damage in MS has increasingly received attention and is recognised as an important part of the disease process. As recent advances in MRI hardware, processing methods, and acquisition techniques have allowed better assessment of GM pathology in vivo, the focus of MS research has moved towards including the study of GM damage as well, and has shown that GM abnormalities develop independently (Geurts 2008) and are more closely associated with some forms of clinical dysfunction than WM damage (Fisher et al. 2008; Fisniku et al. 2008; Roosendaal et al. 2011).

GM pathology in MS has already been documented in 1887 (Charcot 1887), but has only been recognised as an important part of MS when in the 1960s a landmark histopathological study showed that significant demyelination occurs in GM as well as in WM (Brownell & Hughes 1962), hereby giving new impetus to research on GM injury in MS. This study aimed to determine the frequency and the location of lesions in 22 MS brains and found that only 74% of demyelinated lesions were located in the WM, while 26% of lesions were located in or near subcortical and cortical GM. Interestingly, there

appeared to be little relation between GM and WM pathology, indicating that different pathological processes may lead to these forms of damage.

Similar to WM injury, lesional and non-lesional GM pathology may arise in different ways, including inflammation, mitochondrial damage (Lassmann et al. 2012), iron deposition, diffuse neurodegeneration through secondary (Wallerian) degeneration from WM tract pathology (Sepulcre et al. 2009; Kolasinski et al. 2012; Bodini et al. 2016), and CSF or meninges-mediated neuronal loss (Magliozzi et al. 2010). Chapter 5 will describe the spatiotemporal relationship between non-lesional WM and GM pathology.

1.2.1 Grey matter demyelinated lesions
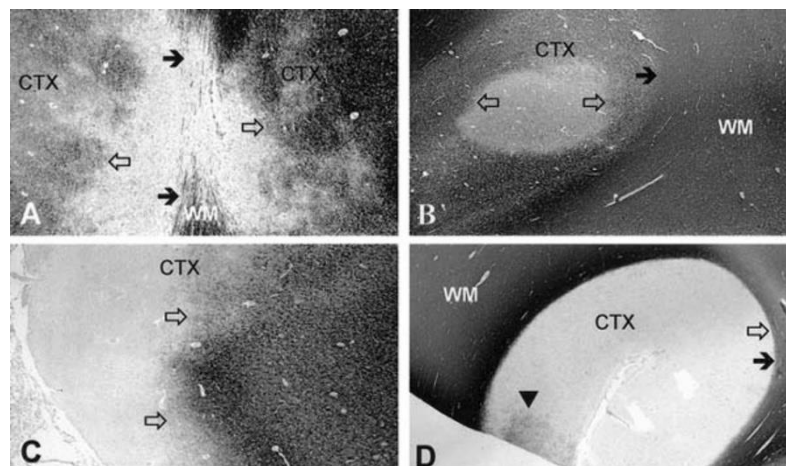
Figure 1.1. From Bø et al. 2003b. Four types of grey matter lesions on paraffin-embedded sections from MS brains immunostained with anti-myelin basic protein antibodies. Closed arrows indicate the white matter/cortical grey matter border and the open arrows indicate lesion borders. The arrowhead indicates a small area of likely remyelination. A) Type 1 lesions involve both grey and white matter. B) Intracortical type 2 lesions do not reach the pial surface or whiter matter. C) From the pial surface type 3 lesions extend inwards into the grey matter. D) Type 4 lesions comprise the entire width of the cortex, respecting the grey matter/white matter border.

After the work of Brownell and Hughes identifying GM lesions in MS (Brownell & Hughes 1962), further studies elaborated on these findings and distinguished distinct subtypes of GM lesions. Bø and colleagues investigated brains of twenty MS patients and classified four types of subpial demyelination in MS (Bø et al. 2003b), as displayed in

figure 1.1. Type 1 lesions involve both GM and WM and in this study made up 14.4% of cortical lesions. Purely intra-cortical lesions (type 2) accounted for 17% of total cortical lesions, covering just 1.2% of demyelinated cortical area. The majority (60%) of cortical lesions were classified as type 3 lesions, reaching down from the pia into the cortex without involving WM. Finally, lesions covering the entire cortical span without WM interference respecting the GM-WM boundary made up 8% of all lesions and 17% of demyelinated area and were classified as type 4 lesions.

Other immunohistochemistry work confirmed that GM damage is widespread and extensive, especially in the SP phase (Vercellino et al. 2009). Observed differences between MS subtypes in WM and GM lesion distribution are displayed in figure 1.2. This study showed that while age and disease duration are related to the extent of GM demyelination, an association between the extent of GM and WM demyelination was not found. This indicates that retrograde neuronal degeneration from WM lesions is not the only pathogenic mechanism involved in local neuronal loss in the GM, and that neuronal loss in MS can, at least partly, be attributed to damage originating within the GM (Geurts & Barkhof 2008).
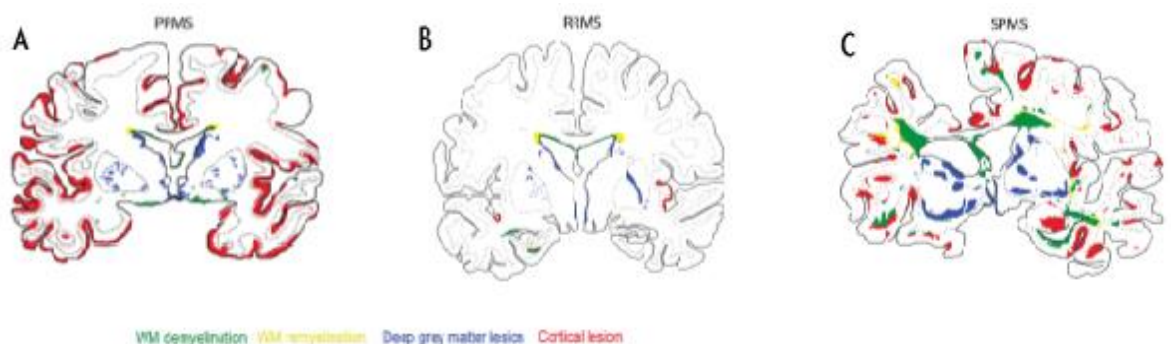
Figure 1.2. Distribution of white matter, cortical grey matter and deep grey matter lesions in different MS subtypes. The extent of white matter and grey matter pathology differs between MS subtypes, suggesting that these forms of pathology can (at least partly) occur separately. Adapted from Haider et al 2014.

WM and GM lesions both show axonal transection, reduction in synapses, as well as glial and neuronal loss. However, in contrast to WM lesions, cortical lesions are thought not to be accompanied by a similarly enhanced immune response. Immunohistochemistry studies using markers for different classes of T-cells and macrophages have shown that WM lesions have significantly increased levels of CD4-positive, CD8-positive, and CD45RO-positive T-cells as well as CD68-positive microglia/macrophages, but that intra-cortical and deep grey matter (DGM) lesions have leukocyte levels comparable to normal appearing grey matter (NAGM) in progressive MS patients and healthy controls (Bø et al. 2003a; Peterson et al. 2001; Vercellino et al. 2009; DeLuca et al. 2015). However, conversely, an immunohistochemistry study on biopsy material (Lucchinetti et al. 2011) found inflammatory cells of cortical lesions of patients with early MS, but this may be explained by a selection-bias of patients with more active disease. Furthermore, compared to the WM parts of type 1 cortical lesions, cortical parts of the same lesions showed less positivity for HLA-DR immunoreactivity and other markers of inflammation (Vercellino et al. 2009). Histopathological work has suggested that GM lesions respect anatomical GM/WM boundaries, whereas WM lesions may involve GM (Vercellino et al. 2009; Gilmore, Geurts, et al. 2009a; Bø et al. 2003b), showing that GM lesions do not to 'seep' into the WM, while WM lesions may cross the GM/WM border. However, a recent longitudinal MRI study suggests that intracortical lesions may evolve into leucocortical, involving both WM and GM (Sethi et al. 2016).

With regard to DGM structures, few post mortem studies have focused on pathology to these areas specifically. Previous work found only few thalamic lesions, while later work found evidence for thalamic lesions particularly in medial and anterior nuclei adjacent to CSF, and showed that the majority of DGM lesions are shared between WM and GM (Vercellino et al. 2009). A histopathological study assessing tissue from 75 people with MS showed that DGM lesions are found in people with early MS, and is associated with

21

infiltration of lymphocytic cells, but that this inflammation is less pronounced than in WM lesions (Haider et al. 2014). Furthermore, while the proportion of demyelinated GM tissue in the thalamus may be similar to that of the cerebral cortex (Gilmore, Donaldson, et al. 2009), the formation of demyelinated DGM lesions has been suggested to occur on a background of mild inflammation, which differs from cortical GM lesions in being associated with parenchymal and perivascular inflammatory infiltrates, compared to meningeal leukocyte infiltration (Haider et al. 2014; Kutzelnigg et al. 2007).

Combined, these studies show that GM demyelinated lesions are common in MS, are closely associated with disease severity, and may be occurring at least partly separately from WM damage. As the immune response in GM demyelinated lesions is reduced compared to inflammatory WM lesions, this suggests that different underlying pathophysiological mechanisms may lead to GM and WM lesion formation.

1.2.2   Normal appearing grey matter damage and grey matter atrophy

NAGM in people with MS differs from GM in healthy controls. In normal appearing cortical GM in MS, increased mitochondrial and neuronal loss is found, independent of the presence of cortical lesions (Dutta et al. 2006; Campbell et al. 2011). Neuronal and myelin loss ultimately manifest as atrophy, which is widespread in MS patients, particularly in subcortical GM structures, i.e. thalamus, caudate, putamen, and pallidum (Audoin et al. 2006; Sepulcre et al. 2006; Ceccarelli et al. 2008; Calabrese, Atzori, et al. 2007; Chard & Miller 2009b; Dalton et al. 2004; Henry et al. 2008).

Histopathological studies showed an overall shrinkage in cortical thickness of 10% in people with MS, specifically affecting the motor cortex, somatosensory cortex, middle frontal cortex, superior frontal gyri, and middle temporal gyri (Wegner et al. 2006; Kutzelnigg & Lassmann 2005). In normal appearing deep grey matter (NADGM) outside

demyelinated lesions neuronal loss has been found to be substantial (Vercellino et al. 2009), and has been estimated by a combined in vivo magnetic resonance spectroscopy and post mortem histology study to be reduced by around 30-35% (Cifelli et al. 2002). Several pathogenic mechanisms have been have been suggested to be involved in diffuse DGM neurodegeneration, including oxidative injury, glutamate toxicity, and anterograde or retrograde degeneration (Haider et al. 2014; Vercellino et al. 2009). The finding of mild diffuse inflammation in thalamic NADGM away from to focal demyelinating lesions may be due to the diffusion of the inflammatory autoimmune cells, or due to secondary inflammation following Wallerian degeneration causing neuroaxonal and myelin damage (Vercellino et al. 2009). Combined, these studies show that NAGM injury in MS is substantial and that this form of pathology may have a different pathogenesis from focal GM demyelination. Their relationship in vivo will be further investigated in chapter 4.

The studies described in the current chapter suggest that WM and GM pathology occur at least partly independently. Pathogenic mechanisms suggested to be involved in GM damage in MS show some similarity to those suggested for WM pathology, including inflammatory processes, Wallerian degeneration from lesions, and diffuse neurodegeneration through mitochondrial injury. The heterogeneity of pathology manifestation in MS complicates the study of the underlying pathophysiological processes, and it is therefore important to assess the spatiotemporal dynamics of these different forms of injury, to see whether they occur in the same location and how they relate to the development of other forms of injury. To this end, studies using MRI have proven invaluable due to the ability of MRI to non-invasively visualise in vivo CNS abnormalities.

Chapter 2

Magnetic resonance imaging in multiple sclerosis

Developments in MRI have greatly improved our understanding of MS. MRI has been invaluable in the diagnosis of the disease, monitoring patients' progression, and to evaluate safety and efficacy of therapeutic interventions. MRI is the most widely used tool to visualise brain pathology in clinical practice and is key in the criteria for MS diagnosis (Polman et al. 2011; Polman et al. 2005; McDonald et al. 2001). The main reason for the widespread use of MRI is that the technique is non-invasive and versatile in its ability to visualise structural, metabolic, and functional changes. This chapter will outline the basic physics on which MRI is based and how sequences allow the visualisation of different tissue characteristics. This is followed by an overview of key findings of MRI studies on MS pathology.

2.1   Magnetic resonance of hydrogen spins

MRI is based on magnetic resonance properties of hydrogen nuclei. When introduced into a static magnetic field, hydrogen nucleus spins align with and transverse around the static magnetic field in the z-direction along the scanner's bore axis. A larger share of spins will have a 'north-to-south' orientation than 'south-to-north', which is dependent on static magnetic field strength and will determine signal intensity. The speed at which these spins precess around the magnetic field is determined by the Larmor frequency:

$$\omega = -\gamma B$$

where ω is the angular frequency, γ the gyromagnetic ratio, and B the strength of the static magnetic field. Upon stimulation with a radiofrequency (RF) pulse, spins will be brought to spin in a transverse circular motion in the xy plane, perpendicular to the z direction. This is done by interacting with the spins using a pulse with the same RF as the protons.

Once the magnetisation is in the *xy* plane, the RF pulse is switched off, and the spin magnetisation acts as a vector precessing around the main magnetic field at the Larmor frequency. The cumulative current of phased spins in a volume is received by the RF coil which allows the translation of spin energies into signal intensities.

The two main metrics used in MRI are T1 and T2. Both T1 and T2 depend on the magnetic field strength through complex non-linear relationships. When the RF pulse stops, the spins return to equilibrium, which means that the magnetisation is realigned with the static magnetic field. This realignment process is referred to as T1 relaxation, and the speed at which this process occurs determines T1 signal strength. Specifically, T1 is defined as the time it takes to reach 63% of the initial magnetisation.

While T1 relaxation is the release of energy into the system, the main drivers behind T2 relaxation are local field inhomogeneities, thermal energy, and spin-spin interactions. Spins precessing in the same phase will de-phase due to these effects, reducing the cumulative current detected by the RF coil. T2 is defined as the time it takes for 63% of signal to have decayed due to de-phasing of spins. While the dephasing due to the exchange of energy between spins, i.e. due to T2 process, is not reversible, the dephasing due to local inhomogeneities can be undone by the using a 180° pulse. This is played at a certain time (1/2 × echo time [TE]) from the first excitation 90° pulse and has the effect of creating a spin-echo at time TE. TE is the echo time for the spin echo formation and can be set up by the user.

As T1 and T2 depend on the molecular environment, different tissue types are characterised by different relaxation constants, which then reflect in different intensities of the MRI signal. Fat has a shorter T1, while fluids (e.g. CSF) have a longer T1. At a static magnetic field strength of 3 Tesla (T), GM and WM have T1 times (1445ms and

791ms, respectively) that lay in between CSF (4163ms) and fat tissue measurements of T1 (Lin et al. 2001). Based on these properties T1-weighted scans allow to distinguish CSF, GM, and WM. T2-weighted scans show a high signal for CSF (1400ms), with GM and WM having a T2 of 101ms and 92ms, respectively (Lin et al. 2001).

2.2 Spatial encoding

To construct images of the MR properties of hydrogen spins, it is necessary to determine the spatial location of the spins measured by the RF coil (Duerk 1999). To this end, three gradients are used: the frequency encoding gradient, phase encoding gradient, and slice selection gradient.

Firstly, as the Larmor frequency of spins is dependent on the static magnetic field, it is possible to change the spin frequency in different locations by introducing a frequency encoding gradient (Huettel et al. 2014). This gradient changes the static magnetic field strength throughout the body, so it follows a gradient. The static magnetic field is not changed in the centre of the body where the precession of spins is determined by the static magnetic field only. Along one dimension a small magnetic force is added to the homogeneous static magnetic field, which is linearly dependent on the distance from the centre. In the opposite direction a magnetic force is introduced reducing the static magnetic force proportional to the distance from the centre.

The frequency encoding gradient hereby changes the Larmor frequency of the spins in one dimension in a gradient-like fashion. Fourier transformations of the echoes allow us to calculate the contribution of the different voxels along this encoding dimension as we intentionally change the frequency of their spins depending on their physical location. Secondly, the phase encoding gradient is used to encode a second dimension. The location of spins that precess in the same frequency can be distinguished by changing the phase in

which they spin. RF pulses are then only delivered to proton spins precessing in a specific phase, which allows for a distinction in this dimension.

The final, third, dimension is encoded by the slice encoding gradient. This gradient often encodes the z-direction and is active when the RF pulse is given. This changes the Larmor frequency of spins and ensures that the RF pulse only affects the spins of the slide within a selected frequency bandwidth. Slice thickness can be changed by changing the bandwidth or by changing the slope of the gradient.

The combination of these three gradients allows us to encode spins in three-dimensional space and the development of this technique has been awarded the 2003 Nobel Prize in medicine. In addition, several time-saving measures have been developed including multi-slice selection and turbo echo trains that significantly speed up the acquisition, but this falls outside the scope of the current chapter. Ultimately, using these techniques, allows the RF coil to receive information about hydrogen spins in different voxels, to be stored in k-space for reconstruction of the scanned object into visually interpretable images.

2.3   Sequences

Various parameters can be adjusted to obtain different types of information from the scanned tissue. The time interval between the centre of excitation and the echo formation is the TE, already mentioned above concerning the spin echo formation, and the interval between individual RF excitation pulses is the repetition time (TR). Furthermore, certain scan types make use of inversion pulses flipping the hydrogen spins by 180°. The time between the RF pulse and the 180° inversion pulse is called the inversion time (TI). An MRI sequence is a set of pulses and gradients resulting in specific MR images. The current section will describe the most commonly used MR sequences used in MS research

and will discuss how the composition, angles, and timing of these pulses and gradients determines the excitation and relaxation of spins to visualise different forms of pathology in the MS brain. The histopathological correlates of different MRI scans will be elaborated upon in chapter 6.

2.3.1 T1-weighted scans

The most widely used MRI scans are T1-weighted and T2-weighted scans and are predominantly sensitive to the T1 and T2 signals of the proton spins, respectively. As the T1 and T2 effects within voxels are estimated relative to other voxels and are not quantified mathematically, these scans are therefore referred to as T1- and T2-*weighted*. Examples of T1- and T2-weighted scans of an MS patient can be found in image 2.1. As the T1 and T2 effects are dependent on magnetic field strength, TE and TR parameters need to be optimised for tissue contrasts. T1-weighted scans have a short TR (<1000ms at 3T) and a short TE (<45ms). On T1-weighted brain scans CSF has little signal, with WM having a slightly higher intensity than GM. Tumours, haemorrhages and inflammation have low signal intensity on T1-weighted scans, while being bright on T2-weighted scans.

Three types of MS pathology are routinely visualised using T1-weighted sequences. Firstly, T1-weighted scans allow the visualisation of WM lesions as these appear hypo-intense on these images. Histopathologically these so called 'black holes' are associated with substantial irreversible myelin and axonal loss (van Walderveen et al. 1998; Bitsch et al. 2001). Secondly, gadolinium enhanced T1 scans help to distinguish active and inactive WM lesions, due to their difference in BBB permeability. The BBB breach in active lesions allows gadolinium to diffuse into the lesions, which creates a strong signal on T1-weighted MRI scans as gadolinium's strongly reduces T1 relaxation times. This gadolinium signal is not observed in inactive lesions with astrogliosis, as this scar-

formation prevents gadolinium from entering the CNS. Finally, volumetric T1-weighted scans are used to measure regional and whole brain atrophy.

Limitations of T1 scans include the following. T1-weighted MRI scans are routinely used in clinical practice, but as reviewed previously (Ge 2006), the ability of these scans to consistently detect pathology is limited due to 1) scanner hardware and particularly the field strength (Kilsdonk et al. 2016), 2) differences in concentration and dosage of gadolinium to detect active lesions (Sardanelli et al. 2003), and 3) differences in sequence set up between centres.

2.3.2   T2-weighted and proton density scans

Compared to T1-weighted scans, T2-weighted scans have longer TR (>2000ms at 3T), as well as longer TE (>45ms). On T2-weighted scans, CSF has high signal intensity, with WM having a slightly lower signal than GM. Because of the high signal intensity of fluids, T2-weighted scans are particularly good to visualise demyelination, infarction, and oedema. Proton density (PD) scans visualise the total proton pool in voxels and have long TR (>2000ms) and short TE (<45ms), resulting in high signal intensity in CSF, with WM having a lower PD than GM. PD and T2-weighted scans can be obtained simultaneously in PD/T2 scans. Similar to T1 scans, these scans are used to assess WM lesion presence in MS. Limitations to the use of T2 scans to consistently visualise MS pathology include differences between centres in terms of scanner hardware and sequence set up, as well the histopathologically observed heterogeneity of T2 detected WM pathology, highlighting the high specificity and low sensitivity of this scan type (van Waesberghe et al. 1999; Newcombe et al. 1991). Furthermore, to obtain lesion masks manual delineation of hypo intensities is required, which is a labour intensive process and is therefore nor routinely done in clinical practice. However, while manual lesion-contouring is still

considered the gold standard to obtain T2 lesions masks, this labour intensive process is being addressed by algorithms aiming to automise this step (Wang et al. 2016).

2.3.3 Fluid attenuation recovery

Fluid attenuation recovery (FLAIR) scans are a variation of T1-weighted scans and make use of the difference in TI of tissue types. After a 180° preparatory pulse, net magnetisation is inverted. Tissue types have different relaxation times for the net magnetisation to recover and signal from different tissue types therefore cross the zero longitudinal magnetisation point at different times. When the recovering magnetisation from CSF is nulled (i.e. not producing any signal), the longitudinal magnetisation from tissue is not zero. At this point a 90° RF pulse is applied that affects only magnetisation from tissue, with CSF appearing very dark (zero) on the obtained images. The time between the 180° and 90° is referred to as the TI. Annulling CSF signal creates a sharper contrast between CSF and tissue in close proximity to CSF and is therefore particularly good in detecting periventricular WM lesions, as shown in figure 2.1. The main limitation of FLAIR scans are signal inhomogeneities leading to different signal-to-noise ratios particularly in the temporal lobes and the frontal and temporal operculum. Furthermore these signal inhomogeneities are highly dependent on the field strength and receive coils used in the study (Zwanenburg et al. 2010).

2.3.4 Double inversion recovery

Double inversion recovery (DIR) scans are used to detect GM lesions. An example can be found in figure 2.1. DIR scans are similar to FLAIR scans, and make use of an additional 180° pulse to annul both CSF and WM signal, resulting in a scan in which only the GM is shown (Redpath & Smith 1994). Histopathologically, DIR scans allow prospective detection of 18% of histopathologically detected cortical lesions and retrospectively 37% of cortical lesions can be seen (Seewann et al. 2012). Despite this

relatively low detection rate, the low SNR and the presence of artefacts, DIR scans allow the visualisation of hyper-intense GM lesions that are not detectable with conventional MRI sequences and DIR scans have therefore proven valuable in the study of development of GM lesions in MS. The use of DIR in the study of GM pathology in MS will be described in section 2.4.1 and chapter 4.

DIR scans are not routinely used in clinical practice, mainly due to the previously mentioned low detection lesion-detection rate and the low signal-to-noise ratio of the scan, as well as the presence of hyper intense artefacts in the temporal poles, cinguli, and prefrontal lobes. The use of DIR is further limited due to the need for manual lesion delineation. Finally, GM lesion subtypes have different detection rates, with subpial lesions rarely being detected on DIR scans (Seewann et al. 2012).

2.3.5 Magnetisation transfer imaging

Magnetisation transfer ratio (MTR) is calculated from MT-weighted imaging. MT scans make use of cross-relaxation properties of freely moving protons and protons with restricted motion which are thought to be bound to macromolecules (Enzinger et al. 2015; Henkelman et al. 2001). The transfer of longitudinal magnetisation between these two pools of protons can be utilised by firstly acquiring signal from the freely floating proton pool (MT_{on}) and subsequently using an off-resonance excitation pulse (MT_{off}) to saturate the restricted proton pool, which do not give any signal when they exchange with the free protons; the saturated spins, originally bound to macromolecules, are not contributing to the signal and when the freely floating pool is measured again, the signal is reduced by an amount proportional to the exchanged protons. MT imaging is also influenced by the T1 relaxation time of the tissue. Areas with high macromolecule concentration have lower T1 than areas with fewer restricted protons, and a ratio (M_{on}-M_{off})/M_{on} yields the MTR. An example can be found in figure 2.1. In post mortem MS tissue, MTR has been found

to correlate with myelin and to a lesser extent with neuronal concentration (Schmierer et al. 2004; Schmierer, Tozer, et al. 2007a). The main limitations of the use of MTR is that this scan type is not standardised between centres, and secondly, that while it is hypothesised to reflect myelin (and to a lesser extent axonal) tissue content, it is unclear whether this association between myelin and MTR is the same in different tissue types. The histopathological substrates of MTR will be discussed in chapter 6.

While quantitative MT (qMT) is not used in the work presented here, this scan type offers a quantification of the MT signal. MTR makes use of a single off-resonance frequency pulse, which can be improved upon by qMT where a mathematical model of the exchange is fitted to the data to extract metrics more specific to macromolecular content. In this sequence a number of pulses at different frequencies allow a more precise quantification of the restricted proton pool and are therefore better at quantifying the macromolecule concentration (Sled & Pike 2001).

2.3.6   Diffusion weighted imaging

Diffusion weighted imaging (DWI) visualises the diffusion of protons (Enzinger et al. 2015). After a 90° pulse, a diffusion gradient is applied, which disrupts the transverse de-phasing of protons. After a subsequent 180° spin echo pulse, an opposite paired diffusion gradient is applied annulling the disruptive effect of the first diffusion gradient, allowing the protons to rephase. However, a pool of protons will have diffused along the diffusion gradient direction which will not rephrase after the application of the gradients. This change in signal, if sampled at least along six non collinear directions, together with a scan with no diffusion gradients applied, allows us to model the diffusion process in tissue with a diffusion tensor, characterised by three diffusivities (eigenvalues) along three orthogonal directions (eigenvectors). From the three eigenvalues, which are rotationally invariant, i.e. they reflect the intrinsic properties of the tissue in the voxel and do not

depend on how the subject is placed in the scanner, we can obtain various metrics about diffusivity in the tissue including mean diffusivity (MD), fractional anisotropy (FA), and radial diffusivity (RD).

MD represents the total diffusion in any direction by protons in that voxel, FA is a measure of anisotropy, i.e. the property describing that tissue restriction imposes a preferential direction for water diffusion in relation to the orthogonal directions, and RD is a metric for the amount of diffusion in the directions other than the preferential direction. Water molecules that are restricted in their movement will show lower MD. High FA values and low RD mean that molecules are free to diffuse in a particular direction, while being restricted in the orthogonal plane. These DWI metrics allow the mapping of neurons and axonal connections between areas can be visualised. In neurological diseases, including MS, a reduction in FA, or an increase in MD or RD is indicative of WM tract damage (Schmierer, Wheeler-Kingshott, et al. 2007).

The main limitations of the use of diffusion MRI are the large voxel sizes used (routinely around 2mm^3), the need for elaborate post processing steps, particularly when aiming to visualise tissue characteristics in areas where WM fibres cross, and finally the inability of diffusion MRI to readily detect GM pathology.
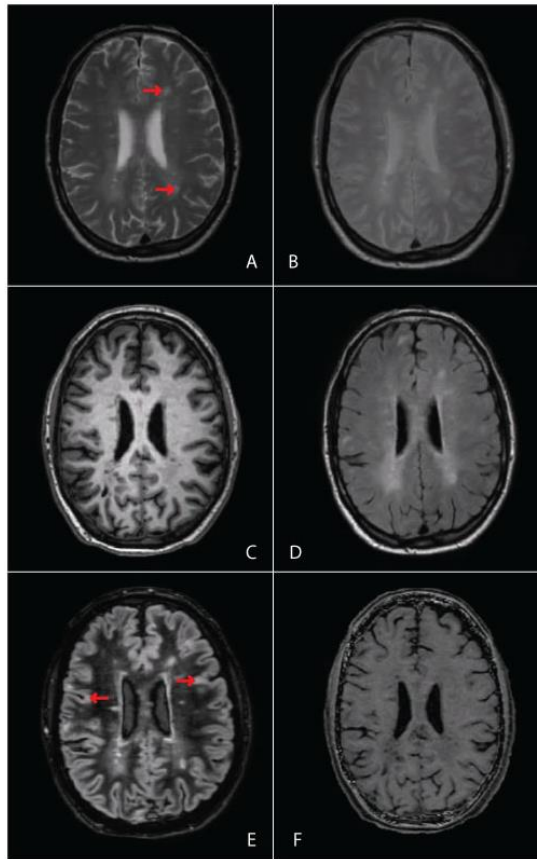
Figure 2.1. Examples of different MRI scans used to detect pathology in the MS brain. A) T2-weighted B) Proton density C) T1-weighted D) FLAIR E) DIR F) MTR. Red arrows indicate different types of pathology, visualised with different scans, i.e. white matter lesions on the T2-weighted scan (A), and cortical grey matter lesions on the DIR scan (E).

2.4   In vivo MRI studies of grey matter pathology

MRI sequences have allowed the in vivo study of macroscopic and microscopic abnormalities in the MS brain. In this section an outline is given of key findings of MRI studies of GM pathology in MS.

2.4.1   Grey matter lesions

As described in section 2.3.5, the development of the DIR MRI acquisition technique, suppressing WM and CSF signal, has allowed the study of GM lesions *in vivo* (Redpath & Smith 1994). Compared with conventional MRI acquisition techniques (e.g. T2-weighted or FLAIR scans) three-dimensional DIR scans allow detection of about five

times as many cortical lesions (Geurts, Bø, et al. 2005). However, DIR scans are not standardised between centres and are not used routinely in clinical practice as they are still suboptimal in detecting GM lesions, largely due to a relatively low signal-to-noise ratio (Hutchinson 2012; Filippi & Rocca 2012; Geurts 2012). A comparative study aiming to establish the detection rate of GM lesions on DIR scans by combining MRI with histopathology showed that only approximately 18% of all GM lesions were prospectively detected on DIR scans (Seewann et al. 2011). Even retrospectively, little more than one third of histopathologically defined lesions were observed on 3D-DIR scans. Especially type 2 and type 3 GM lesions showed poor detection rates. The poor detection rates are suggested to be caused by low contrast between surrounding GM and these lesions, lack of inflammation in these of these cortical lesions resulting in low levels of gliosis, BBB disruption, and infiltrating leukocytes.

DIR sequences, despite their low lesion detection rate, have provided insight in the distribution of GM lesions in MS, as they allow a better distinction between purely intra-cortical lesions, juxta-cortical and mixed lesions, compared to conventional MRI sequences (Hulst & Geurts 2011). These scans have allowed the study GM pathology in MS, which was previously impossible to address in vivo, and have shown that GM lesions are an important part of the MS disease process, can be found throughout the entire cerebellar and cerebral cortex, and accumulate over time (Calabrese, Battaglini, et al. 2010; Calabrese, Mattisi, et al. 2010; Calabrese et al. 2008). Cortical lesions occur early in the MS disease process (Calabrese, Battaglini, et al. 2010; Calabrese, Filippi, et al. 2009; Calabrese, Rocca, et al. 2010), and are associated with disability progression (Calabrese, Rocca, et al. 2010). Furthermore, cortical lesions are part of both PPMS and RRMS (Calabrese, Rocca, et al. 2009; Calabrese, Rocca, et al. 2010), but to a lesser extent of benign MS (Calabrese, Filippi, et al. 2009). Interestingly, people with benign MS, who remain fully functional fifteen years after disease onset, have comparable numbers of

WM lesions as people with RRMS, but do not have the same number of DIR-detected GM lesions (Calabrese, Filippi, et al. 2009), indicating that cortical pathology may be the determining factor in disability, and is further evidence for a difference in underlying mechanisms of GM and WM lesions.

2.4.2 Normal appearing grey matter pathology and grey matter atrophy

A described above, MTR allows the in vivo study of wide spread non-lesional myelin and neuro-axonal pathology in MS. GM MTR studies have shown that a reduction of MTR in NAGM is widespread and can be found in PPMS, RRMS and SPMS, and can already be seen in people presenting with clinically isolated syndrome (CIS) (Crespy et al. 2011). In the DGM of people with progressive MS, the spatial distribution of MTR reduction does not correspond to the extent of atrophy, suggesting that cortical myelin and neuro-axonal loss occurs at least partly independently from demyelination (Mallik et al. 2015). This corresponds to the finding of diffuse neuro-axonal pathology outside focal demyelinating lesions in a previous histopathological study (Vercellino et al. 2009). Ultimately, as neuro-axonal loss develops in the MS disease process, tissue volume is likely to decrease, but this appears dissociated in time.

Global and regional atrophy can be investigated using MRI analysis techniques including voxel based morphometry (VBM) and SIENA. Overall reduction of neocortical volume has been observed in PPMS (Sastre-Garriga et al. 2005), RRMS (Amato et al. 2004; Benedict et al. 2006; Calabrese, Agosta, et al. 2009), and SPMS (Benedict et al. 2006). Furthermore, it was found that people with secondary progressive MS had larger GM atrophy than people with RRMS, which was substantially larger than the detected rates of WM atrophy (Benedict et al. 2004). This further suggests that GM and WM volume loss may at least be partially independent (Calabrese, Atzori, et al. 2007).

DGM areas are particularly prone to atrophy. DGM atrophy is evident already from the first clinical event (Calabrese, Atzori, et al. 2007; Chard & Miller 2009a; Dalton et al. 2004; Henry et al. 2008) and accumulates over time (Sepulcre et al. 2006). A reduction in DGM volume is apparent in RRMS (Audoin et al. 2006), PPMS (Sepulcre et al. 2006), and SPMS (Ceccarelli et al. 2008). Because of the extent of atrophy to the thalamus, likely due to its connected nature, it has even been suggested that thalamic atrophy may serve as a "barometer" of MS pathology, and as such may be useful in neuroprotective trials (Kipp et al. 2015). Other studied anatomical areas with extensive GM demyelination are the cingulate gyrus (Vercellino et al. 2005), cerebellum (Kutzelnigg et al. 2007), and hippocampus (Geurts et al. 2007; Papadopoulos et al. 2009).

Combined, these neuroimaging studies show that GM pathology manifests as demyelinated lesions, diffuse neuro-axonal damage, and atrophy, and that GM pathology at least partly occurs independently of WM damage.

2.4.3 Clinical and cognitive decline associated with grey matter pathology

Both WM and GM pathology contribute to clinical disability in MS and are thought to complement each other in their disruption of pathways involved in cognitive and clinical function (DeLuca et al. 2015). While both WM and GM pathology are likely to be responsible for clinical disability, cross-sectional neuroimaging studies have shown that GM pathology is a better predictor of clinical and cognitive disability than WM pathology (Geurts 2008; DeLuca et al. 2015). Accumulation of DIR lesions has been shown to be associated with increased disability assessed by the expanded disability status scale (EDSS) (Calabrese, De Stefano, et al. 2007), as well as cognitive functioning assessed by the Paced Auditory Serial Addition Test (PASAT) and the Symbol-Digit Modality Test (SDMT) (Calabrese, Agosta, et al. 2009). Similarly, GM atrophy has been associated with physical and cognitive dysfunction in all MS subtypes (Amato et al. 2004; Benedict et al.

2006; Calabrese, Agosta, et al. 2009; Chard et al. 2002; Fisher et al. 2008; Fisniku et al. 2008; Roosendaal et al. 2011; Benedict et al. 2004). Both GM atrophy and GM lesions have been correlated to tests assessing disability (Chard & Miller 2009a; Rinaldi et al. 2010; Benedict et al. 2004). The spatial distribution of GM lesions and GM atrophy, as well as their individual contribution to clinical disability will be examined in chapter 4. As reviewed by DeLuca (DeLuca et al. 2015), whole brain measures including Brain Parenchymal Fraction, reflecting atrophy (Fisher et al. 2000; Kalkers et al. 2001), and studies looking at specific brain regions have shown a clear link between GM pathology and cognitive function. Smaller hippocampal volumes have been found in people with MS compared to controls, associated with reduced memory function and processing speed (Koenig et al. 2014). Similarly volumes of DGM matter structures have been found to be lower in people with MS compared to controls, and has been associated with impaired performance on tests assessing processing speed, working memory, verbal fluency, verbal and visuo-spatial learning, and executive function (Batista et al. 2012; Houtchens et al. 2007). To attempt to disentangle the contributions of WM tracts injury and cortical and thalamic GM damage in MS to impaired clinical and cognitive function, a more detailed insight into thalamic pathology and its longitudinal relationship to connected WM and cortical GM injury will be provided in chapter 5.

Chapter 3

Aims

As described in chapter 1 and 2, the importance of GM injury in MS is increasingly recognised, and MRI has proven invaluable in the study of MS pathology in vivo. A number of questions remain unanswered in our understanding of GM injury in MS. Firstly, it is unclear if the different manifestations of GM damage (i.e. focal demyelinated lesions, diffuse neuro-axonal loss, and atrophy) have a shared spatial distribution and if they contribute equally to clinical disability. Secondly, it is unclear how thalamic and cortical GM pathology is related spatiotemporally to WM tract injury. WM damage in MS is well established, and cortical and particularly thalamic GM structures are affected disproportionally and early in the disease process. However, the longitudinal relationship between these potentially separate forms of pathology manifestation has not been established. Finally, only a limited number of studies have assessed the underlying histopathological substrates of MRI-detectable abnormalities in MS. Diffuse myelin and neuronal loss are thought to be detected by MTR MRI, but it is unknown if this association between is the same in normal appearing and lesional GM and WM.

3.1 Aim and hypotheses

The current thesis aims to provide insight into the pathophysiology of CNS pathology in MS with a focus on GM. The overarching tested in the current thesis is as follows.

> There are different manifestations of GM pathology in MS, which arise (at least partly) independently from WM damage and all forms of pathology contribute to clinical disability.

This work consists of three independent studies which include in vivo, post mortem, and histological investigations, and specifically aims to answer the following questions, which are addressed in the next three results chapters.

1) Do GM lesions and GM atrophy co-localise, and what is their independent contribution to clinical disability in vivo?

2) Can thalamic and cortical GM pathology, as detected by in vivo MTR MRI, be explained by prior damage to connecting WM tracts, or vice versa?

3) What are the independent underlying histopathological substrates of MTR abnormalities of CNS pathology in MS? Are they the same in NAGM, NAWM, and lesional GM and WM?

The overarching of the current thesis is tested through specific sub hypotheses tested in chapters 4, 5, and 6, which are related to the above questions and are as follows.

1) GM lesions and GM atrophy do no co-localise to a large extent, and disruption of clinically relevant regions by either form of pathology results in clinical dysfunction.

2) WM tract degeneration precedes diffuse non-lesional neuro-axonal and/or myelin loss in the connected thalamus and cortex. Injury to any part of thalamo-cortical systems affects clinical function associated with the respective system.

3) Lesional and normal appearing GM and WM differ substantially in terms of histopathological make-up and MRI-visualised pathology.

3.2   Structure of thesis

To answer these questions, Chapter 4 investigates if GM lesions and GM atrophy co-localise and what their individual contributions are to clinical disability. I show that DIR-detected GM lesions are found throughout the entire cerebellar and cerebral cortex, while GM atrophy is mainly affecting DGM structures. Chapter 5 investigates the longitudinal relationship between pathology to thalamic nuclei, WM tract injury, and cortical pathology, to establish the spatiotemporal distribution of these forms of damage. I show that MTR abnormalities in NAWM of thalamic-tracts precede (both thalamic and cortical) GM MTR changes. Finally, chapter 6 investigates the underlying histopathology of CNS abnormalities in MS, using a combination of post mortem MRI and histology, and shows that whereas MTR is associated with myelin in NAGM and NAWM, this association appears absent in lesional tissue.

Chapter 4

Co-localisation and clinical impact of grey matter lesions and atrophy in different subtypes of multiple sclerosis

4.1 Introduction

As introduced, GM pathology has emerged as a significant and clinically relevant component of MS. This is in part due to advances in MRI technology, which allows the systematic assessment of GM pathology in MS in vivo. GM volume loss and focal GM lesions both occur, and both have been correlated with neurological and cognitive deficits (Amato et al. 2004; Calabrese, Agosta, et al. 2009; Benedict et al. 2006; Chard & Miller 2009a; Rinaldi et al. 2010; Calabrese, De Stefano, et al. 2007; Chard et al. 2002; Fisher et al. 2008; Fisniku et al. 2008; Roosendaal et al. 2011). However, a key unanswered question is whether they share a common pathogenesis, in particular whether lesions are the cause of atrophy, or represent independent processes that contribute separately to clinical outcomes.

Histopathological studies have identified extensive cortical demyelination in people with MS, and in those with progressive disease GM lesion volume may exceed that of WM (Bø et al. 2003b). However, in vivo it has proven difficult to detect GM lesions using conventional MRI techniques. Only 6.8% of GM lesions are identified on T2-weighted scans, and 11.4% on FLAIR scans (Geurts, Bø, et al. 2005). The development of DIR MRI has improved on this, prospectively detecting 17.1% to 18% of GM lesions (Geurts, Pouwels, et al. 2005; Seewann et al. 2012), and DIR studies have shown that GM lesions are spread throughout the cortex, appear early in the course of the disease, and accumulate over time (Calabrese, Battaglini, et al. 2010; Calabrese, Filippi, et al. 2009; Calabrese, Rocca, et al. 2010).

Previous in vivo work provides insight into the mechanisms of GM injury in MS. DGM and CGM atrophy is now well-recognised in MS (Audoin et al. 2006; Ceccarelli et al. 2007; Chard & Miller 2009a; Chard et al. 2002), occurs early in the disease (Labiano-Fontcuberta et al. 2016; Deppe et al. 2016), and appears to accelerate as people with MS enter a progressive phase (Fisher et al. 2008). Three studies have assessed the relation between GM atrophy and WM injury showing that while lesions in connecting WM tracts are associated with DGM atrophy (Sepulcre et al. 2009; Mühlau et al. 2013), WM lesion independent microstructural degeneration is thought to drive atrophy (Deppe et al. 2016). GM atrophy is thought to mark irreversible tissue loss, and it is likely that a combination of neuronal morphological changes and loss, and glial abnormalities contribute (Geurts & Barkhof 2008). Lesions could directly cause localised atrophy, as suggested by pathological studies showing axonal transection and loss in cortical lesions (Peterson et al. 2001). There has been little histopathological work looking for co-localisation of cortical atrophy and demyelination, but in the only study I am aware of, local cortical thickness did not correlate with demyelination (Wegner et al. 2006). However, fixation can affect cortical thickness (which was correlated with fixation time (Wegner et al. 2006)), and so it is possible that this may have obscured an association. As such, it is preferable to look for associations in unfixed tissue samples or, better still, in vivo.

The study presented in the current chapter sought to clarify the spatial overlap between GM atrophy and GM lesions, and their independent relationship with cognitive and physical disability, in a large cohort of patients with MS and in different MS subtypes. I hypothesise that GM lesions and GM atrophy do no co-localise to a large extent, and that disruption of clinically relevant regions by either form of pathology results in clinical dysfunction.

4.2 Methods

4.2.1 Participants and clinical assessment

Eighty people were recruited with clinically definite MS (Polman et al. 2011), who had not had a relapse or received corticosteroids within the preceding four weeks, were less than 65 years old and had no other neurological conditions, as well as 30 healthy volunteers with no known neurological disease. All participants gave written informed consent and this study was approved by our local institutional ethics committee. Patient recruitment, clinical assessment and obtaining of MRI data was done prior to my involvement with this project.

Clinical status was assessed using the EDSS (Kurtzke 1983) and the MS functional composite (MSFC) score which includes walking speed on the 25-foot timed walk test (25TWT), 9-hole peg test (9HPT), and the PASAT. Z-scores of these tests were calculated using published means and standard deviations (Burgess & Shallice 1997).

All subjects underwent cognitive testing to assess executive function and memory. Executive function was assessed using the Hayling Sentence completion task (Burgess & Shallice 1997) and Stroop task (Trennery 1989), from which averaged z-scores were calculated on the basis of healthy control performance, and SDMT, from which the age-adjusted z-scores were calculated based on published normative values (Smith 1982). Memory function was evaluated using a composite score of story recall (immediate and 30-minute delay) and figure recall (immediate and 30-minute delay) from the Adult Memory and Information Processing Battery (Coughlan & Hollows 1985) and word and face recognition from the Recognition Memory Test (Warrington 1984); z-scores based on the performance of the control sample were also calculated for these tests.

4.2.2　MRI protocol

Brain MRI was performed on a Phillips 3T Achieva TX system (Philips Healthcare, Best, The Netherlands) using a 32-channel receive-only coil. T1-weighted (TR=6.9ms, TE=3.1ms, TI=824.5ms, SENSE=2, voxel size=1×1×1mm), turbo FLAIR (TR=8000ms, TE=125ms, TI=2400ms, SENSE=1.3, voxel size=1×1×3mm), and DIR (TR=16000ms, TE=9.9ms, TI=2400/325ms, SENSE=4.16, voxel size=1×1×3mm) sequences were acquired.

4.2.3　Image registration and lesion mapping

All pre-processing was carried out with SPM8 (http://www.fil.ion.ucl.ac.uk/spm/). All subsequent data analysis, statistical analysis and interpretations were performed by SvdP. To limit the impact of WM lesions on tissues segmentations, T1-weighted hypo-intense lesions were filled (Chard et al. 2010) and the lesion-filled T1-weighted images were then segmented. Anatomical normalisation to MNI space was achieved via a custom diffeomorphic anatomical registration through exponentiated Lie algebra (DARTEL) template (Ashburner 2007; Ashburner & Friston 2009), generated from all subjects' (N=110) GM tissue segmentations. Compared to the use of other templates (e.g. MNI) the use of this cohort-specific template reduces the amount of deformation required to nonlinearly register individual brains to the template, which would be larger for more atrophic brains than for healthy brains, and therefore allows improved detection of disease effects. The DARTEL GM template was affine-registered to the MNI standard space, and each subject's T1-weighted image was first nonlinearly registered to the DARTEL template, and subsequently affine registered to MNI using the DARTEL to MNI transformation, moving it into MNI template space. This pipeline reduces the adverse effect of disease-associated brain atrophy on the registration accuracy to MNI space. When spatially normalising the segmented GM images to MNI space (via the DARTEL

and affine transformations), the images were modulated to preserve native tissue volumes. All registrations were reviewed to confirm their accuracy. Modulated, normalised, segmented GM images were smoothed with an 8-mm full-width at half-maximum Gaussian kernel.

GM lesions were marked on the DIR scans using JIM (version 6.0, Xinapse Systems, Northants, UK) by one rater (VS) according to consensus guidelines (Geurts et al. 2011). These lesion masks were then assessed by rater two (SvdP), and in case of a differing opinion on the lesion contouring, the lesion was discussed and a consensus was reached on all lesions between VS and SvdP. Subsequently, similarly, one in five lesion masks were analysed by DC, after which a final consensus was reached between all three raters. Total GM lesion volume was then calculated.

Each participant's DIR scan was affine registered to their T1-weighted scan, and their DIR-to-T1 affine transformation, T1-to-DARTEL deformation field and DARTEL-to-MNI affine transformation were combined and used to move the binarised GM lesion mask into MNI space. An 8mm full-width at half-maximum Gaussian Kernel was then used to smooth the normalised lesion masks.

Two people (one with SPMS, one with PPMS) were excluded from the subsequent imaging analysis due to inadequate registration.

4.2.4 Co-localisation of grey matter atrophy and lesions

VBM and GM lesion probability mapping (LPM) analyses were carried out in SPM8. Two types of analyses were carried out: voxel-wise comparisons and region of interest (ROI) analyses. For voxel-wise VBM-map comparison between groups, an alpha value of 0.05 (family wise error [FWE] corrected) was used. For voxel-wise LPM, an alpha

value of 0.001 (uncorrected) was used. This threshold was used as no lesion clustering was found at 0.05 (FWE corrected). For neither approach a prior power calculation was performed. In both VBM-map and LPM comparisons, people with MS were compared to healthy controls to assess areas significantly more affected in people with MS.

To determine co-localisation of volume loss and GM lesions, permutation tests were run using Randomise implemented in FSL (FMRIB's software library, http://www.fmrib.ox.ac.uk/fsl). For each of the MS groups the following regression model was tested per voxel:

$$\text{VBMmap} = \text{LPM} \times B1 + \text{age} \times B2 + \text{gender} \times B3 + \text{total intracranial volume} \times B4 + \text{intercept}$$

Total intracranial volume (ICV; was estimated by summing the thresholded GM, WM and cerebrospinal fluid volumes using the 'get_totals' function in SPM8).

FSL Randomise tests per voxel whether random permutations of values for each independent variable yield significant associations with the dependent variable, after which the ratio of significant associations to non-significant associations is considered for each independent variable using t-tests. As the test makes use of random permutations, the test does not make assumptions about the normality of the data. The tests were performed using an inclusive GM mask (thresholded at 0.5), with 5000 permutations and an uncorrected alpha of 0.01 with a cluster-threshold of 5, meaning that if more than 50 of 5000 permutations reject the null-hypothesis of independence, the variables were considered to be significantly correlated.

The second analysis employed an ROI approach. ROIs involved in tasks assessing clinical and cognitive functioning in MS (Audoin, Ibarrola, et al. 2005; Cardinal et al. 2008; Genova et al. 2009; Lockwood et al. 2004; Audoin, Au Duong, et al. 2005) were chosen

a priori. These regions were the bilateral cerebellum, medial temporal lobe, postcentral gyrus, precentral gyrus, insula, prefrontal cortex, and thalamus (Figure 4.1). Masks for these regions were created by using Freesurfer to automatically segment the MNI-space cohort-specific T1-weighted template (Fischl et al. 2002; Desikan et al. 2006). For each GM ROI, and in each patient, the total GM lesion volume and the GM volume were extracted from the VBM and LPM images and co-localisation between atrophy and lesion load was assessed using linear regression analyses, correcting for age, gender and ICV.
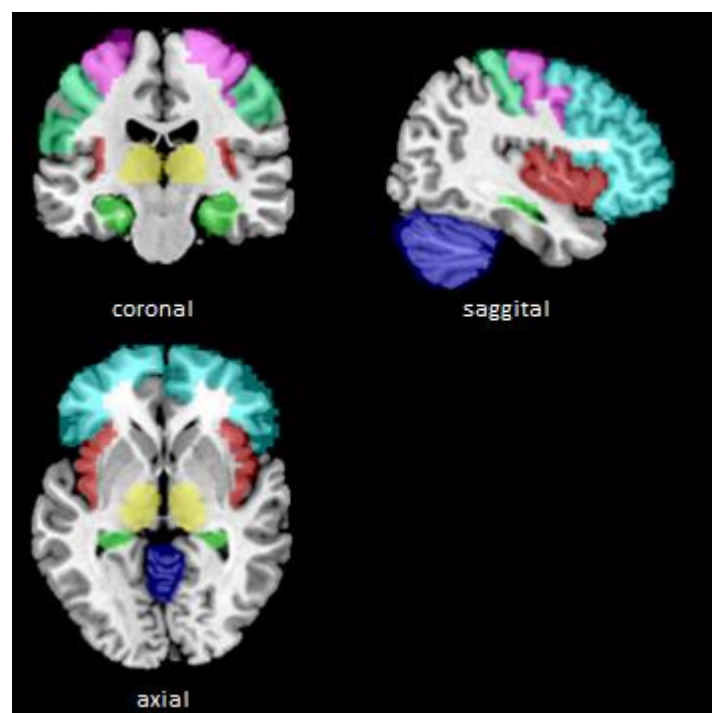
Figure 4.1. A priori defined regions of interest: Cerebellum, insula, precentral gyrus, postcentral gyrus, prefrontal cortex, medial temporal lobe, and thalamus. Regions are overlaid on the cohort-specific MNI-space template (x=37, y=-24, z=-6).

4.2.5 Associations of disability with grey matter lesion load and grey matter atrophy

To explore the associations of GM lesion load and GM atrophy with clinical measures (EDSS, PASAT, 9HPT, 25TWT, executive function, and memory function), voxel-wise and ROI analyses were carried out. The first analysis, based on a voxel-wise factorial design, was conducted in SPM8, including age, gender, and ICV and using VBM-map or LPM values. In all voxel-wise comparisons a cluster threshold of five voxels was applied.

Linear regression models using EDSS, PASAT, 9HPT, 25TWT, executive function, and memory function as the dependent variables, and GM lesion load and GM volume extracted from the ROIs were used as the independent variables. Age, gender, and ICV were also added to the model as additional covariates. SPSS (version 21.0. Armonk, NY: IBM Corp) was used to conduct this analysis. Differences between subtypes in scores, volume loss and lesion load were analysed using unpaired t-tests (for VBM-map values) or nonparametric tests (for lesion-loads since they were non-normally distributed). When both GM lesion load and GM atrophy within a given ROI were associated with clinical performance, a linear regression model including lesion load, total GM volume, age, and gender was run to determine the independent contribution of each to the outcome of interest. Shapiro-Wilk tests were used to assess normality of residuals of the linear regression analyses and unpaired t-tests.

4.3 Results

4.3.1 Demographics and clinical performance

Thirty of the MS group had relapsing RRMS, 25 had PPMS, and 25 had SPMS (Lublin & Reingold 1996). Demographics are shown in table 4.1. SPMS patients had a longer

disease duration than PPMS and RRMS patients (both p<0.001). People with MS performed worse than healthy controls in all clinical domains, and MS subtypes showed differences in cognitive performance. EDSS scores differed significantly between MS subgroups (p<0.001), with the SPMS group having a higher EDSS than PPMS group, and people with PPMS having higher EDSS scores than those with RRMS (both p<0.05). People with MS had worse executive function and memory scores than controls, with SPMS being worse than PPMS, and PPMS being worse than RRMS (p<0.05 and p<0.01, respectively).

	PPMS	RRMS	SPMS	All patients	Healthy controls	P value
Females/Males	14/11	20/10	14/11	48/32	18/12	
Age (*yr*)[a]	52.5 (9.8)	42.5 (9.6)	52.8 (7.6)	48.8 (10.2)	37.8 (11.8)	<0.001
Disease duration *(yr)*[b]	12.0 (7.4)	11.5 (10.5)	24.0 (8.2)	15.6 (10.5)	-	<0.001
Median EDSS *(range)*[c]	6.0 (0.0-6.5)	1.75 (1.0-6.5)	6.5 (4.5-8.5)	5.75 (0.0-8.5)	-	all <0.05
z PASAT	-0.70 (1.38)	-0.69 (1.32)	-0.94 (1.12)	-0.77 (1.27)	0.12 (1.05)	
z 9HPT	-1.00 (1.13)	-0.66 (0.65)	-1.16 (0.90)	-0.93 (0.92)	0.63 (0.61)	
z 25TWT	0.32 (0.97)	0.00 (1.03)	0.56 (1.01)	0.24 (1.02)	-0.44 (0.08)	
Composite z MSFC	-0.62 (0.81)	-.041 (0.76)	-0.77 (0.66)	-0.56 (0.76)	-	
Hayling	4.80 (2.02)	5.17 (2.09)	4.64 (2.43)	4.89 (2.16)	6.17 (1.76)	
Stroop	174.4 (76.7)	135.83 (36.9)	174.58 (80.9)	158.59 (66.7)	109.80 (20.0)	
z SDMT	-1.02 (1.62)	-0.52 (1.13)	-1.22 (1.21)	-0.88 (1.34)	0.53 (1.11)	
Composite z executive[d]	-1.58 (1.69)	-0.71 (1.09)	-1.51 (1.55)	-1.23 (1.48)	0.23 (0.69)	0.006
Story recall immediate	30.04 (10.96)	33.97 (11.35)	27.76 (11.44)	30.80 (11.42)	37.13 (10.35)	
Story recall delay	27.20 (12.29)	31.57 (10.93)	24.80 (12.22)	28.09 (11.97)	34.90 (10.31)	
Figure recall immediate	51.09 (15.41)	62.20 (11.14)	51.57 (16.17)	55.80 (14.86)	67.67 (11.94)	
Figure recall delay	48.73 (15.84)	60.07 (11.22)	48.67 (14.83)	53.37 (14.72)	66.30 (12.06)	
RMT Words	46.17 (3.63)	47.60 (2.43)	45.61 (3.69)	46.56 (3.31)	49.00 (1.26)	
RMT Faces	40.21 (5.27)	42.33 (4.23)	37.43 (5.53)	40.21 (5.31)	44.27 (3.20)	
Composite z memory[e]	-1.30 (1.15)	-0.55 (0.89)	-1.63 (1.27)	-1.13 (1.18)	0.00 (0.58)	both <0.05

Table 4.1. Demographics and clinical performance. Mean values are presented, unless specified otherwise. Values in parentheses are standard deviations. Clinical scores presented in bold are used in image analyses. a) RRMS patients were significantly younger than PPMS and SPMS patients (both p<0.001). b) SPMS patients had longer disease duration than RRMS and PPMS patients (both p<0.001). c) All MS subgroups differed significantly (all p<0.05) with SPMS having a higher EDSS than PPMS patients, who had a higher EDSS in turn than RRMS patients. d) Patients had poorer executive functioning than healthy controls (p<0.01). e) Memory functioning was better in controls than patients (p<0.01), and best in RRMS patients, followed by PPMS patients, who in turn performed better than the SPMS subgroup (p<0.05, and p<0.01, respectively).

4.3.2 Grey matter atrophy

All MS patients together showed significant GM atrophy predominantly in DGM structures (thalamus, pallidum, putamen and caudate), in addition to a few small regions in the frontal (0.09 cm^3), insular (0.06 cm^3), and temporal lobes (0.12 cm^3), compared to controls (Figure 3.2). Similarly, in the a priori defined ROIs (i.e. cerebellum, medial temporal lobe, postcentral gyrus, precentral gyrus, insula, prefrontal cortex and thalamus, Figure 3.1), mean GM volume was significantly smaller in patients than controls in the thalamus ($p<0.001$) and insula ($p<0.05$).

Subgroup analyses revealed that DGM volume loss was present in all MS groups compared to controls, with additional temporal lobe volume loss in the PPMS group, and volume loss of the occipital lobe, amygdala, and hippocampus in the SPMS group (table 3.2, table 3.3 and figure 3.2a). Voxel-wise comparisons between patient groups yielded no significant results, though ROI analyses revealed significant subgroup differences in insular and thalamic volumes. SPMS patients had a significantly reduced insular volume compared to both healthy controls and PPMS patients (both $p<0.01$, Bonferroni corrected for multiple comparisons). Thalamic volume was also reduced in SPMS compared to both healthy controls and PPMS patients ($p<0.001$ and $p<0.05$, respectively).

4.3.3 Grey matter lesions

In patients, 1476 lesions were found throughout the GM (neocortex: 1276, cerebellum: 154, deep GM: 46). Mean number of GM lesions was 17.0 (SD=10.2) for PP patients (neocortex: 14.5, deep GM: 0.6, cerebellum 1.92). Mean number of lesions for people with SPMS was 21.2 (SD=9.4) (neocortex: 18.3, deep GM: 0.8, cerebellum: 2.4), and 15.0 (SD=10.1) for RR patients (neocortex: 13.5, deep GM: 0.3, and cerebellum: 1.4). Mean GM lesion volume was 1.33 cm^3 (SD=1.04 cm^3) for PP patients (neocortex: 1.15, deep GM: 0.03, cerebellum 0.16 cm^3). Mean GM lesion volume was 1.39 cm^3 (0.85) for

SP patients (neocortex: 1.20, deep GM: 0.03, cerebellum 0.16 cm^3), and 0.93 cm^3 (0.82) for RR patients (neocortex: 0.84, deep GM: 0.01, cerebellum 0.08 cm^3). Fourteen GM lesions were identified in healthy controls (in four participants).

At a threshold of $p=0.001$, patients had significantly higher GM lesion probability only in the right cerebellar hemisphere when compared with healthy controls (70 voxels, $t_{max}=3.37$). No DGM structures showed a significantly increased lesion probability at this threshold or at a lower threshold ($p=0.01$, uncorrected). However, at this threshold, additional cortical areas showed increased lesion probability, notably the right pre- and postcentral gyri, bilateral supplemental motor area, and bilateral temporal lobes (data not shown). People with MS had significantly more lesions in every a priori defined ROI than healthy volunteers (all $p<0.001$).

Group wise whole brain analyses at $p<0.001$ (Table 4.2 and Figure 4.2b) revealed that PPMS patients had a significantly higher lesion probability in the left supplemental motor area (354 voxels), right medial frontal lobe (48 voxels), right postcentral (29 voxels), right supra-marginal gyrus (92 voxels), and the right cerebellum (375 voxels) than controls. The RRMS subgroup did not show any significant lesional clusters than controls. The SPMS group showed consistent clustering of lesions in the supplemental motor area (47 voxels) compared to controls. All MS groups had significantly more lesions in every ROI than healthy volunteers (all $p<0.001$), and was comparable for all ROIs between MS groups, with the exception of the cerebellum, in which those with SPMS showed more lesions than those with RRMS ($p<0.05$, Bonferroni corrected).

4.3.4   Co-localisation of grey matter atrophy and lesions

In the combined MS group, voxel-wise analyses showed a significant association between a higher probability of a voxel being lesional and smaller GM volume in regions

throughout the entire brain, particularly in the cerebellum (Table 4.2). ROI analyses found that increased GM lesion load was significantly associated with reduced GM volume within the cerebellum (B=-17.76, p<0.001) and postcentral gyrus (B=-4.77, p=0.037).

In analyses examining the co-localisation between volume loss and lesion load across MS subtypes (Tables 4.2 and 4.4, and Figure 4.2c) the PPMS group showed spatial overlap between the two pathological abnormalities throughout the cerebellar and cerebral cortex. While RRMS patients showed co-localisation of these forms of pathology mainly in the cerebellum, SPMS patients showed very little co-localisation, mainly in the post-central gyrus. The least co-localisation was found in the SPMS patients (0.01cm^3), whilst the RRMS patients (0.18cm^3) were in between the PPMS (0.30cm^3) and SPMS groups in terms of number of regions showing both forms of MR changes. None of the groups showed co-localisation in the DGM (where significant atrophy was found in the absence of GM lesions). ROI-wise regression analyses in the RR group showed a significant association between cerebellar lesion load and volume loss (B=-33.46, p<0.001).

4.3.5   Associations of grey matter atrophy and lesion load with clinical status

Voxel-wise models at p<0.05 (FWE corrected) in people with MS revealed an association between lower executive function scores and decreased left putamen volume (104 voxels), which was the only significant association of volume loss with any clinical metric. Furthermore, at p<0.001 (uncorrected), increased lesion probability in the cerebellum in particular was associated with lower performance in executive function, TWT speed, and PASAT (Appendix I, supplemental table 4.1).

In the combined MS group cerebellar volume loss and increased GM lesion volume were associated with poorer functioning in all cognitive domains tested (Appendix I, supplemental table 4.2). In addition, lesions and volume loss within the postcentral gyrus

were associated with cognitive performance and physical disability in almost all domains tested (i.e. executive function, memory function, TWT speed, PASAT, 9HPT). Overall, lower functional scores were only weakly linked to GM lesion or atrophy clusters.
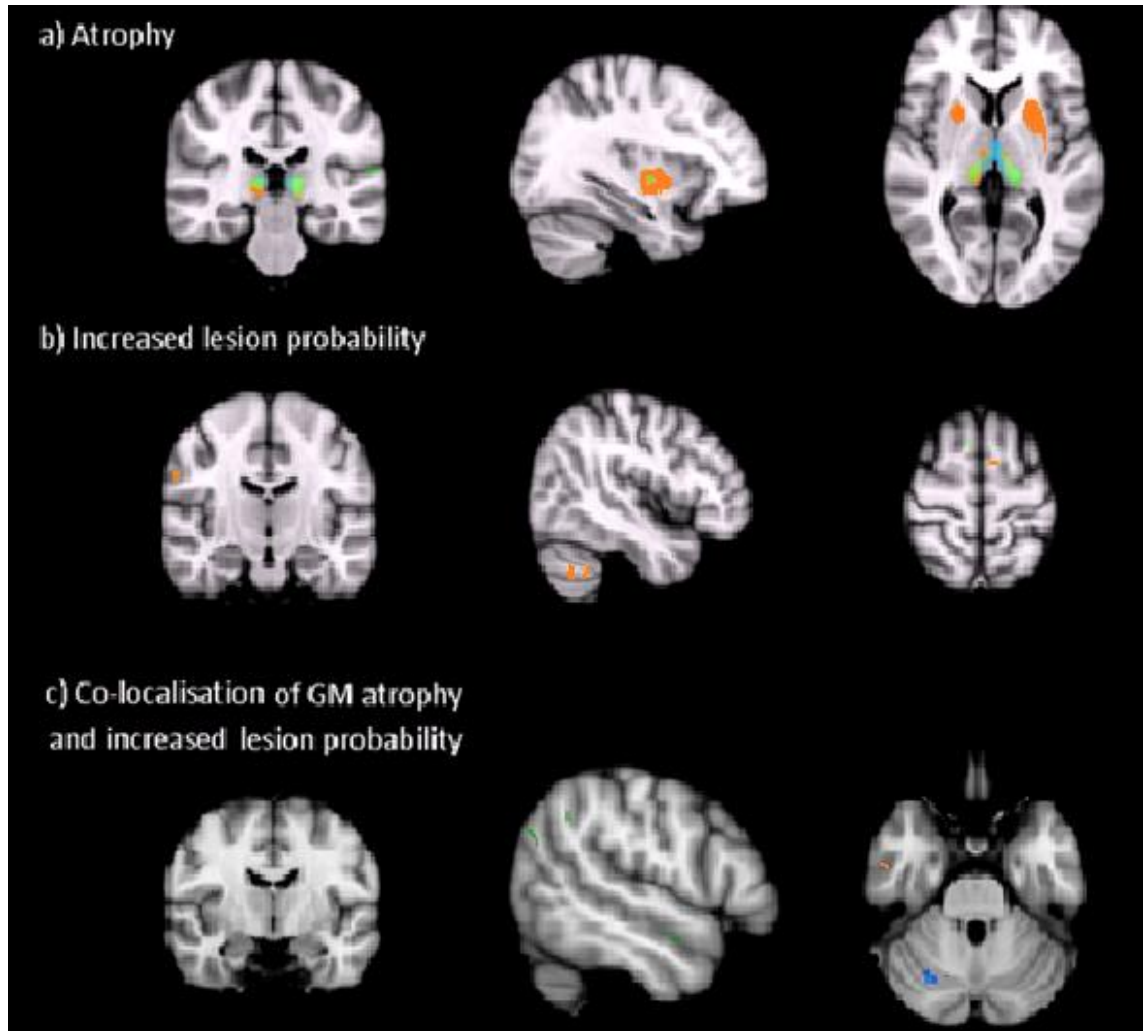
Figure 4.2. Grey matter pathology in MS subtypes. The PPMS group is presented in green, RRMS in blue, and SPMS in orange on the cohort-specific MNI-space template. A) All MS subtypes show large deep volume loss compared to controls at p=0.05 (FWE corrected). Particularly patients with relapse onset have severe deep atrophy. Coordinates of sections are x=35, y=30, z=3. B) Areas showing clusters of higher grey matter lesion probability in patients compared to controls at p=0.001, uncorrected. The RRMS group did not show clusters of increased grey matter lesion probability at this threshold, while SPMS showed increased cerebellar lesion load and PPMS had clusters of increased lesion probability throughout the cerebral, and especially the cerebellar cortex. Coordinates of sections are x=39, y=-20, z=60. C) Areas showing a significant correlation of atrophy and higher probability of a grey matter voxel being lesional (at p=0.01, uncorrected) in all patient together. Coordinates of sections are x=29, y=-66, z=-28.

	PP	RR	SP	All patients
Atrophy				
Cerebral cortical GM	0.13	0	0.14	0.35
Deep GM	0.73	3.48	10.91	15.5
Cerebellar GM	0	0	0	0
Lesion clustering				
Cerebral cortical GM	0.52	0	0.05	0.07
Deep GM	0	0	0	0
Cerebellar GM	0.38	0	0	0
Atrophy and lesion clustering				
Cerebral cortical GM	0.27	0.01	0.01	4.33
Deep GM	0	0	0	0.4
Cerebellar GM	0.03	0.17	0	3.47

Table 4.2. Total volume of voxels (in cm^3) consistently showing atrophy (at p=0.05, FWE corrected), lesion clustering (at p=0.001, uncorrected), and areas where these two forms of pathology was significantly associated (at p=0.01, uncorrected). Consistent atrophy was seen in all MS subtypes predominantly in deep grey matter structures. Lesion clustering and co-localisation of atrophy and lesions were consistently found in cerebral and cerebellar cortical areas, while not detected in deep structures. Co-localisation of atrophy and lesions was limited compared to areas in which lesions or atrophy occurred independently.

MS subtype	Region	Side	cm³	Peak T-value	MNI coordinates of local maxima		
					x	y	z
PP	Hippocampus	L	0.02	5.82	-13	-34	2
	Lingual	L	0.01	5.77	-13	-33	0
	Postcentral	L	0.01	5.45	-52	-13	31
	Putamen	L	0.05	5.49	-33	-10	-1
	Thalamus	L	0.40	6.37	-15	-29	2
	Thalamus	R	0.28	5.75	15	-27	5
	Temporal superior	L	0.09	5.78	-60	-28	14
RR	Caudate	R	0.15	5.58	13	6	20
	Thalamus	L	0.19	7.37	-10	-26	6
	Thalamus	R	0.15	6.59	10	-22	9
SP	Hippocampus	R	0.03	6.06	29	-9	-10
	Amygdala	R	0.10	6.30	31	-7	-10
	Occipital inferior	R	0.01	5.36	31	-97	-4
	Caudate	R	0.01	5.29	14	8	19
	Putamen	L	4.21	6.55	-26	6	-5
	Putamen	R	3.02	7.04	33	-6	-6
	Pallidum	L	0.47	6.35	-25	2	-3
	Pallidum	R	0.21	6.53	30	-9	-5
	Thalamus	L	1.37	8.99	-14	-25	5
	Thalamus	R	1.62	8.04	14	-25	5

Table 4.3. Clusters of atrophic voxels in different MS subtypes at p<0.05 FWE corrected. All MS subtypes show deep GM volume loss (caudate, pallidum, putamen and thalamus). Particularly patients with relapse onset have consistent deep atrophy.

MS subtype	Region	Side	cm³	Peak T-value	MNI coordinates of local maxima		
					x	y	z
PP	Precentral gyrus	L	0.05	3.13	-32	-9	68
	Frontal superior	R	0.01	2.64	23	63	-5
	Hippocampus	L	0.01	3.98	-35	-19	-16
	Occipital superior	L	0.03	4.24	25	-74	24
	Occipital middle	L	0.01	2.93	-26	-74	24
	Parietal inferior	L	0.07	3.14	-50	-69	30
	Temporal superior	R	0.01	2.84	53	-18	-6
	Temporal middle	L	0.08	3.91	-50	-6	-15
	Cerebellum	R	0.03	5.11	19	-66	-28
RR	Temporal superior	R	0.01	4.16	60	-19	-5
	Cerebellum	R	0.17	3.62	29	-68	-29
SP	Postcentral gyrus	R	0.01	2.51	14	-42	62

Table 4.4. Areas in patients showing a significant association between smaller grey matter volume and increased lesion load at p=0.01 uncorrected. Co-localisation of both forms of pathology was largest in patients with PPMS, throughout virtually the entire brain with the exception of deep grey matter. Particularly the cerebellum in RRMS patients showed a great association between these forms of pathology. Overall, lesion-atrophy clusters were small when compared with the volume of the brain.

4.4 Discussion

The present study assessed the distributions of GM lesions and GM atrophy in patients with different subtypes of MS, aiming to determine if they co-localise and if they both contribute to clinical outcomes. GM lesions were found to regionally correlate with atrophy most in people with PPMS and least in SPMS. However, co-localisation was at best modest, with the majority of regionally consistent atrophy not corresponding to regions most likely to contain GM lesions. Of the GM regions found to be consistently atrophied or to contain lesions, only the cerebellum and postcentral gyrus showed associations between both types of pathology and physical and cognitive function.

In line with previous studies (Audoin et al. 2006; Sepulcre et al. 2006; Ceccarelli et al. 2008; Henry et al. 2008; Mühlau et al. 2013; Deppe et al. 2016), reduced DGM volume was found in the whole MS cohort compared to controls. Regional predilections for cortical atrophy have previously been demonstrated in the right lateral prefrontal cortex (Audoin et al. 2006), in the left temporal and prefrontal cortex (Morgen et al. 2006), and bilaterally in the superior and medial frontal gyrus, frontobasal regions near the frontal poles, as well as thinning of the medial temporal gyrus (Sailer et al. 2003), and my results are broadly in agreement with them. However, in addition consistent atrophy was also found in small regions in the frontal, insular, and temporal lobes, as also reported in other studies that found cortical thinning throughout the entire cortex (Calabrese, Atzori, et al. 2007; Calabrese, Battaglini, et al. 2010). GM lesions were found throughout the cerebral and cerebellar cortex, but rarely in DGM structures. Lesions consistently occurred only in the right cerebellum. Co-localisation between GM atrophy and GM lesions was observed only when lower statistical thresholds were used, and then mainly in regions within the cerebral and cerebellar cortices, and to a lesser extent in deep structures that were particularly affected by atrophy. Previous work (Wegner et al. 2006) has shown

changes in cortical lesions and, to a lesser degree, in non-lesional cortex, but did not find an association between demyelination and cortical thickness, suggesting that demyelination *per se* is not directly responsible for cortical atrophy. The present findings are in agreement with this, and therefore suggest, with caveats (see discussion of limitations below) that GM atrophy and GM lesion formation are often not directly linked. A longitudinal study specifically addressing the relation between cortical lesions and cortical thickness showed that these two forms of pathology share a spatiotemporal distribution pattern in CIS and early RRMS, but that they are distinct pathological processes and particularly later in the MS disease course diffuse pathology and cortical lesions occur separately (Calabrese et al. 2015). This is in line with a VBM study of the distribution of cortical MTR abnormalities and atrophy (Mallik et al. 2015), which uses the assumption that abnormal MTR reflects demyelination. This study showed that MTR abnormalities and atrophy do not co-localise much, particularly in people with SPMS and PPMS.

I found that MS subtypes differed noticeably in patterns of GM atrophy. People with PPMS showed relatively little consistently localised DGM and no consistent cortical atrophy at stricter thresholds. In contrast, those with RRMS had a rather different pattern of GM damage with more substantial and consistent DGM volume loss, and in SPMS this appeared to be regionally similar but larger areas, with additional cortical involvement. While my main observation is consistent DGM atrophy, it has been suggested that progressive MS has a relatively specific CGM neurodegenerative component to its pathology (Stys et al. 2012; Geurts 2008), and the present results suggest that this is more likely to be the case in people with SP compared with PPMS. Previous work has also shown that PPMS patients have relatively little DGM volume loss, at least early in the course of the disease (Sepulcre et al. 2006), particularly when compared to SPMS patients (Ceccarelli et al. 2008). In contrast, RRMS patients have been shown to have increasing

thalamic atrophy over time, which relates to physical and cognitive disability, but have less cortical atrophy than SPMS (Ceccarelli et al. 2008).

GM lesions, on the other hand, were most consistently clustered in PPMS, in both the cerebral and cerebellar cortex, and much less so in RR and SPMS. Previous work has mainly shown similarities between patients with PPMS and RRMS in terms of cortical lesion load (Calabrese, Battaglini, et al. 2010), while other work showed that progressive MS patients have a larger degree of cerebellar cortical demyelination when compared with RRMS and SPMS patients (Kutzelnigg et al. 2007; Calabrese, Mattisi, et al. 2010). My results suggest cerebellar lesion clustering is more the case in PP compared with SPMS. Given this, it is perhaps not surprising that co-localisation of GM lesions and atrophy (examined at lower thresholds) was most pronounced in the PPMS group, although overall to volume of co-localisation was very small (less than $1cm^3$) when compared with total brain GM volumes of $>500\ cm^3$ (Miller et al. 1980).

The ROI analyses and voxel-wise analyses revealed significant associations between both cerebellar lesion load and atrophy, and lower physical and cognitive performance scores (Appendix I, supplemental table 4.1). This fits with the known involvement of the cerebellum in sensorimotor and cognitive function (Stoodley et al. 2012; Koziol et al. 2014), and is in agreement with recent work showing that loss of cerebellar volume in MS patients is associated with a decline in cognitive function (Weier et al. 2014). While consistent atrophy was most pronounced in DGM structures, particularly in RR and SPMS, it did not appear to correlate significantly with functional outcomes. This corresponds with recent studies which indicate that changes in GM microstructure, assessed by diffusion MRI, and metabolic function, assessed by MR spectroscopy, can explain additional variance in cognitive function over GM volumes (Koziol et al. 2014; Weier et al. 2014), but contrasts with a recent study finding a modest correlation between

DGM atrophy and poorer cognitive function in people with RRMS (Debernard et al. 2015), and a study showing that particularly atrophy of the anterior nucleus of the thalamus was related to slower cognitive processing (Bergsland et al. 2015). It is possible that the heterogeneity of the present cohort did not allow the detection of these subtle associations, and that more refined spatial analyses are needed to detect the clinical impact of atrophy and microstructural changes in specific nuclei of the thalamus (as will be discussed in chapter 5). A key finding from the present study is the role of damage to somatosensory networks in clinical dysfunction. Both GM lesion volume and atrophy in the postcentral gyrus (the primary somatosensory cortex) were linked to worse performance in almost all cognitive domains and clinical scores assessing physical disability. In addition, the postcentral gyrus and cerebellum, which is both functionally and structurally connected to the postcentral gyrus (Stoodley et al. 2012; Stoodley & Schmahmann 2009), were the only regions in which lesion burden and volume loss were linked (Stoodley et al. 2012; Koziol et al. 2014), and is in agreement with recent work showing that loss of cerebellar volume in MS patients is associated with a decline in cognitive function (Weier et al. 2014). Further work focussing on the somatosensory network may shed light on the mechanisms underlying the progression of disability in MS.

4.4.1 Study limitations

A priori a number of brain areas were chosen to assess in statistical analyses. Of the DGM structures only the thalamus was included in the analyses presented here. However, the ROI analyses could have benefitted from also including other DGM areas (i.e. the caudate, putamen, and pallidum) in light of the voxel based results presented here, as well as increasing evidence emphasising early injury to and the clinical impact of damage to these DGM structures (Schmalbrock et al. 2016; Debernard et al. 2015; Krämer et al.

2015). When considering the LPM results, it should be recalled that of the four different cortical lesion types that have been described (Bø et al. 2003b), DIR scans only detect approximately 18% of cortical lesions and 7.7% of DGM lesions, and while subpial lesions are the most abundant type seen in *post mortem* studies, these are rarely observed using DIR (Seewann et al. 2012). This insensitivity for DGM lesions may partly explain the limited overlap found between lesions and atrophy in deeper GM structures. Phase sensitive inversion recovery (PSIR) MRI detects two to three times more GM lesions, and so may increase the overall sensitivity of an LPM analysis (once technical issues related to LPM of PSIR scans have been overcome), but this sequence may still be relatively less sensitive to subpial compared with other GM lesion subtypes (Sethi et al. 2013; Sethi et al. 2012). While DIR scans allow detection of only a minority if GM lesions, recent work has similarly shown a dissociation between atrophy and demyelination as measured by MTR (Mallik et al. 2015). As mentioned above, for voxel-wise LPM, an alpha value of 0.001 (uncorrected) was used. This threshold was used as no consistent lesion clustering was found at 0.05 (FWE corrected) due to the wide spread nature of binary lesions (albeit smoothed), rather than having a continuous distribution. While lowering the threshold increases the chance of a type 1 error, only one per 1000 voxels would show a false positive. In addition, the applied cluster threshold reduces the number of false-positive findings further. The clinical scales used to assess motor and cognitive function have a number of limitations that should be kept in mind when interpreting the present findings. Firstly, EDSS in non-linear and irreversible. Secondly, scores between 5.0 to 9.5 are defined by ambulation, while lower scores on the lower end are for people who are fully ambulatory, and is defined by function in other domains, leading to 'clustering' of patients in the lower end of the scale. The combination of the challenge of differentiating people with MS on the lower end of the scale and its non-linearity complicate the use of EDSS in statistical analyses, as the scale may violate parametric tests' assumption of normality

of residuals. The PASAT has been found to be good at differentiating people with MS from controls, but it has been suggested that performance differences may be difficult to detect as the task gets more difficult because of the use of 'chunking strategies', and may therefore not fully reflect processing speed and working memory (Fisk & Archibald 2001). In addition, learning effects on the PASAT as well the 9HPT, affect the ability of these MSFC subtests to assess long term function (Polman & Rudick 2010). Finally, while where possible z scores were calculated on the basis of published scores, not all tests had such published scores available, limiting the generalisability of the present findings.

4.4.2   Conclusion

The present study assessed the distributions of GM lesions and GM atrophy in patients with different subtypes of MS, aiming to determine if co-localisation of these forms of pathology occurs, and if they both contribute to clinical outcomes. I hypothesised that GM lesions and GM atrophy do no co-localise to a large extent, and that disruption of clinically relevant regions by either form of pathology results in clinical dysfunction. GM lesions (as seen using DIR) and GM atrophy were found to not usually co-localise, suggesting that they are not directly spatially linked. In addition, both GM lesions and atrophy contributed to disability, suggesting that the substrates of disability in MS are both pathologically and spatially heterogeneous.

As GM pathology is substantial in the MS disease course, it is important to assess how this develops longitudinally in relation WM pathology to gain insight into the ongoing pathophysiological processes in MS. To this end, the next chapter describes the longitudinal development of microstructural damage in the thalamus, and how this relates to injury to connected WM tracts and cortical projections.

Chapter 5

Magnetisation transfer ratio changes to thalamo-cortical tracts precede thalamic and cortical grey matter abnormalities

5.1 Introduction

As both GM and WM pathology are clinically important in the MS disease process, this chapter assesses the spatio-temporal relationship between these forms of damage. As shown in the previous chapter, GM injury is extensive, and particularly the thalamus is affected in the MS disease process. The present chapter will therefore focus specifically on thalamo-cortical systems and the longitudinal development of non-lesional myelin and neuro-axonal loss (as assessed by MTR) in these areas.

The thalamus is an integrated heterogeneous structure composed of a large number of independent nuclei involved in relaying neuronal information. Increasingly, this subcortical structure is seen as more than a relay hub, and is found to be involved in processing and modifying the input it receives from a large number of structures including the majority of cortical areas, basal ganglia, spinal cord, and sensory organs (Sherman 2007; Kipp et al. 2015). With its large number of connections to key subcortical and cortical areas, the thalamus is part of the thalamo-cortical loop, producing high and low rhythmic activity important in a wide range of functions. including auditory, visual, motor, and cognitive function (Kipp et al. 2015; McCormick 1999), and damage to the thalamus and its networks has been shown to affect clinical function in people with MS (Kern et al. 2015; Bergsland et al. 2015; Schoonheim et al. 2015; Magon et al. 2014).

As the thalamus is a functionally important structure that is affected early and disproportionally in the MS disease process (Henry et al. 2008; van de Pavert et al. 2016;

Audoin et al. 2006; Chard et al. 2002; Ceccarelli et al. 2007), it has been suggested that due to its integrated anatomy both GM pathological processes and WM injury (through Wallerian degeneration) contribute to MRI detected thalamic damage (e.g. neuro-axonal and myelin loss, or atrophy), potentially making MRI assessment of this structure an ideal biomarker for MS neuroprotective clinical trials (Kipp et al. 2015; Zivadinov et al. 2013). To gain a better understanding of thalamo-cortical system damage in MS, it is key to understand how injury to thalamic and cortical GM relates to WM thalamo-cortical tract injury over time. In addition, it is important to understand the clinical consequences of damage to these systems. To this end, I will here give an overview of our current understanding of pathology to thalamo-cortical systems in MS, followed by a longitudinal study in which the spatiotemporal characteristics of MTR in the components of these systems are investigated, and how they relate to clinical function.

5.1.1 Thalamic pathology and its relation to white matter tract injury

Thalamic pathology is extensive in MS, and can already be seen in people with CIS (Henry et al. 2008), as reflected by changes in metrics for diffuse tissue damage, including increased FA (Cappellani et al. 2014), T2 hypo-intensity (Ceccarelli et al. 2010), and an increase in Fe^{2+} concentration (Al-Radaideh et al. 2013). Neuronal loss in non-lesional thalamic GM in people with MS is substantial and is estimated to be around 35% compared to controls (Cifelli et al. 2002), which is similar to a previously reported loss of non-lesional WM axons in the corpus callosum (Evangelou, Konz, et al. 2000). While the thalamus and corpus callosum are not anatomically connected, the comparable estimates of neuronal loss in DGM and WM tracts suggest a possible link between pathology in these tissue types. Diffuse thalamic pathology has been linked to FA reduction of NAWM, but not with T2 lesion load, suggesting that diffuse non-lesional WM damage, but not WM lesions directly, may lead to thalamic pathology (Cappellani

et al. 2014). Other previous work has elegantly shown that atrophy of the lateral geniculate nucleus of the thalamus could be linked to the presence of WM lesions in the connected optic radiation, while occipital lobe atrophy was not associated with this WM pathology, suggesting that retrograde, but not anterograde, degeneration from axonal damage is important to GM atrophy (Sepulcre et al. 2009). While the above studies point to a link between WM lesions and thalamic injury, a recent cross-sectional DTI study specifically assessing early thalamic microstructural pathology showed that thalamic damage in CIS and RRMS patients could not be fully explained by the presence of adjacent WM lesions (Deppe et al. 2016). The differing spatial distribution between voxels associated with thalamic pathology and WM lesions in this study suggests that thalamic microstructural damage has additional contributing pathogenic processes than WM lesions alone. Similarly, another cross-sectional study showed an association between WM tract damage and DGM volume, and to a lesser extent with CGM volume (Steenwijk et al. 2015). Combined, the above studies show that thalamic injury in MS is likely to have a number of contributing processes, including possible neurodegenerative processes inside the thalamus and Wallerian degeneration from WM lesions or diffuse WM tracts injury, but it remains unclear to what extent each of these processes contribute, and how these forms of pathology relate spatiotemporally.

5.1.2 The relationship between cortical and white matter tract injury

As described in more detail in chapter 4, in addition to DGM pathology, CGM pathology is well-recognised in MS (Audoin et al. 2006; Ceccarelli et al. 2007; Chard & Miller 2009a; Chard et al. 2002), occurs early in the disease (Labiano-Fontcuberta et al. 2016; Deppe et al. 2016), is correlated with neurological and cognitive deficits (Amato et al. 2004; Calabrese, Agosta, et al. 2009; Benedict et al. 2006; Chard & Miller 2009a; Rinaldi et al. 2010; Calabrese, De Stefano, et al. 2007; Chard et al. 2002; Fisher et al. 2008;

Fisniku et al. 2008; Roosendaal et al. 2011), and appears to accelerate as people with MS enter a progressive phase (Fisher et al. 2008). Histopathological studies have identified extensive cortical demyelination in people with MS, and in those with progressive disease GM lesion volume may exceed that of WM (Bø et al. 2003b).

Studies addressing how WM tract pathology relates to cortical pathology have provided inconsistent findings. On the one hand, cortical GM and WM pathology have been suggested to be linked and to be dependent on anatomical connectivity (Gorgoraptis et al. 2010; Bodini et al. 2016; Steenwijk et al. 2015; Kolasinski et al. 2012), while on the other hand other work found tract-unspecific associations between WM and regional CGM pathology (Louapre et al. 2016). As pointed out in the latter study, the discrepancy between these findings may be attributed to the fact that these previous studies (except one post mortem study (Kolasinski et al. 2012)) did not assess spatial specificity by also comparing tracts with anatomically non-connected cortical areas. In addition, to the best of my knowledge, all studies except one (Bodini et al. 2016) on WM pathology in relation to GM damage in MS are cross-sectional in nature, making it difficult to draw conclusions regarding chronology of these potentially distinct forms of pathology.

5.1.3   Chronology of pathology in thalamo-cortical systems

The current chapter aims to answer if thalamic and cortical GM pathology, as detected by in vivo MTR MRI, can be explained by prior damage to connecting WM tracts, or vice versa. Together, the above mentioned studies lead to the following hypothesis of a sequence of events leading to damage to thalamo-cortical systems in MS. WM and GM lesions originate (at least partly) independently (Bø 2009). GM lesions may not directly lead to non-lesional GM pathology, as described in chapter 4. WM lesions, on the other hand, may cause degradation to thalamo-cortical tracts, and WM tract degeneration through Wallerian degeneration in turn causes diffuse non-lesional neuro-axonal and/or

myelin loss in the connected thalamus and cortex (Bodini et al. 2016). GM pathology may mainly be associated (either preceding or following) with *proximal* WM tract damage. While it is conceivable that neuronal damage affects tracts more distal from thalamic nuclei, this is expected to be more readily detected closer to the nuclei. Furthermore, while this is not assessed in the current chapter, I hypothesise the associations between WM and GM MTR to differ between MS subtypes, with relapse-onset MS patients having a larger loss of thalamic GM volume than progressive MS patients (Kutzelnigg et al. 2005). As RRMS is more inflammatory than progressive MS I therefore expect more tract-mediated pathology thalamus. Finally, I hypothesise that injury to any part of the thalamo-cortical systems to affect clinical function associated with the respective system.

5.2 Methods

Fifty-seven people with clinically definite MS (Polman et al. 2011), who had not had a relapse or received corticosteroids within the preceding four weeks, were less than 65 years old and had no other neurological conditions, as well as 25 healthy volunteers with no known neurological disease, were included in the present study. All participants gave written informed consent and this study was approved by our local institutional ethics committee.

5.2.1 Data acquisition

Subjects underwent clinical examination to establish EDSS, and performance on 25TWT, PASAT, and 9HPT, as well as brain MRI on a Phillips 3T Achieva TX system (Philips Healthcare, Best, the Netherlands) using a 32-channel receive-only coil at baseline and at 24 month follow up. The following sequences were acquired: 3D sagittal T1-weighted fast field echo (FFE) scan ($1mm^3$, TI=824ms, TR=6.9ms, TE=3.1ms), dual-echo PD/T2-weighted axial-oblique scans aligned with the anterior to posterior commissure line ($1\times1\times3mm$, TR=3500ms, TE=19/85ms); and high resolution MTR using a 3D slab-

selective FFE sequence with two echoes (1mm^3, TR=6.4ms, TE=2.7/4.3ms, alpha=9° with and without sinc Gaussian-shaped magnetisation transfer pulses of nominal alpha=360°, offset frequency 1 kHz, duration 16 ms). A turbo field echo (TFE) readout was used, with an echo train length of four, TFE shot interval 32.5ms, giving a total time between successive magnetisation transfer pulses of 50ms, and scan time of 25min. The two echoes were averaged (thereby increasing the signal-to-noise ratio) for both the magnetisation transfer on and off data. Finally, a whole-brain, cardiac gated, spin-echo diffusion weighted sequence (TR=24,000ms, TE=68ms and 72 axial slices with an isotropic 2mm resolution) with 61 volumes with non-collinear diffusion gradients (b-value of 1200sec/mm^2) and seven volumes without diffusion weighting.

5.2.2   Image data processing

T1-weighted and T2-weighted scans were n4 bias field corrected (Tustison et al. 2010), and on T2-weighted scans hyper-intense WM lesions were delineated by two independent raters using Jim (version 6.0, Xinapse Systems Ltd., Northants, UK, http://www.xinapse.com) and 3DSlicer (version 4.4.0) (Fedorov et al. 2012) software packages, after which all lesions masks were verified by a third rater. T2 lesions were filled on the T1-weighted scans to improve subsequent registration steps (Chard et al. 2010; Prados et al. 2014). Using rigid body transformations, T1-weighted scans were registered to pseudo-T1-weighted images which are in alignment with T2-weighted images (Hickman et al. 2002). Using a second rigid-body alignment, T2-weighted images were subsequently registered to b0 images which were in alignment with DTI data, as described previously (Muhlert et al. 2013). An average b0 volume of six separately acquired b0 images was used and was merged to the DTI data, after which the DTI data were eddy corrected using FSL eddy, and the b vectors and b files updated to reflect the extra volumes. A mean b0 volume was created averaging all eddy corrected b0 volumes.

FA, MD, RD, and axial diffusivity maps were obtained using MRtrix (Tournier et al. 2012).

In 22 controls, whole brain tractography was performed, effectively up sampling the voxel size from 2mm^3 to 1mm^3 (Calamante et al. 2011). Briefly, this was done by creating a high value FA map by applying a threshold of 0.7, which then was used to estimate the fibre response function. Using the Constrain Spherical Deconvolution method, the fibre orientation density function for each voxel was calculated, which was subsequently used by streamtrack to compute the 1mm^3 track-density imaging (TDI) map sampling from any voxel in the mean b0 brain to any other voxel (step size=0.1mm, 2,500,000 iterations). The above transformations were combined with a nonlinear transformation of the MNI brain to individual lesion filled T1-space to reduce the number of interpolations required. The resulting transformation matrix was applied to source, target and exclusion masks for tractography.

5.2.2.1   Generation of ROI masks

Unilateral thalamic masks were created for three groups of thalamic nuclei, based on Morel's histology atlas (Morel et al. 1997) brought to MNI space for MRI use (Krauth et al. 2010; Jakab et al. 2012), as described in table 5.1: lateral group (LG), medial group (MG), and posterior group (PG).

In T1 space, unilateral cortical masks were created using parcellations created from Geodesic Information Flow algorithms (Cardoso et al. 2015), clustered into areas corresponding to the masks used previously (Behrens et al. 2003), of which three were selected based on their connections with thalamic nuclei: Prefrontal cortex (PFC), sensorimotor cortex (SMC), and occipital cortex (OCC). Inclusion masks were generated covering the left and right cerebral hemispheres, and exclusion masks were generated of

the corpus callosum, and to exclude anatomically implausible tracts from the MG a coronal exclusion plane was placed directly posterior to the most posterior voxel of the MG mask.

Thalamic group	Morel MRI atlas masks
Lateral group	Lateral posterior nucleus
	Ventral anterior nucleus, magnocellular division
	Ventral anterior nucleus, parvocellular division
	Ventral lateral anterior nucleus
	Ventral lateral posterior nucleus, dorsal division
	Ventral lateral posterior nucleus, ventral division
	Ventral medial nucleus
	Ventral posterior inferior nucleus
	Ventral posterior lateral nucleus, anterior division
	Ventral posterior lateral nucleus, posterior division
	Ventral posterior medial nucleus
Medial group	Central lateral nucleus
	Central medial nucleus
	Centre median nucleus
	Mediodorsal nucleus, magnocellular division
	Mediodorsal nucleus, parvocellular division
	Medioventral nucleus
	Parafascicular nucleus
	Paraventricular nuclei
Posterior group	Anterior pulvinar
	Inferior pulvinar
	Medial pulvinar
	Lateral geniculate nucleus, magnocellular division
	Lateral geniculate nucleus, parvocellular division
	Lateral pulvinar
	Limitans nucleus
	Medial geniculate nucleus
	Posterior nucleus
	Suprageniculate nucleus

Table 5.1. Thalamic group masks used for tractography by grouping Morel's atlas (Morel et al. 1997) brought to MNI space for MRI use (Krauth et al. 2010; Jakab et al. 2012).

5.2.2.2 Cortico-thalamic and thalamo-cortical tractography

In 22 controls, the thalamic and cortical ROIs were brought to b0 space, where tractography was performed using the TDI images from the MG, LG, and PG, to the PFC, SMC, and OCC, respectively, as well as the reverse, using the cortical regions as seed regions with the thalamic nuclei as target areas. The thalamic and cortical areas were dilated by 2.0mm to reach into the surrounding WM, excluding voxels belonging to more than one mask. To prevent anatomically improbable tracts a hemisphere inclusion mask was used, and for the MG-PFC tract a coronal exclusion plane was placed directly posterior to the MG. The resulting WM probability tracts were then thresholded at 99% to exclude outliers, after which cortico-thalamic and thalamo-cortical tracts were multiplied, leaving only voxels that were part of tracts in both directions. These bidirectional tracts were subsequently brought to MNI space, where the tracts of the 22 controls were combined and thresholded at 50%. As displayed in figure 5.1, the above steps resulted in tract masks composed of voxels present in tracts of eleven or more controls, in both thalamo-cortical and cortico-thalamic directions. Finally, each of the six resulting WM tracts was subdivided into four segments of equal length.
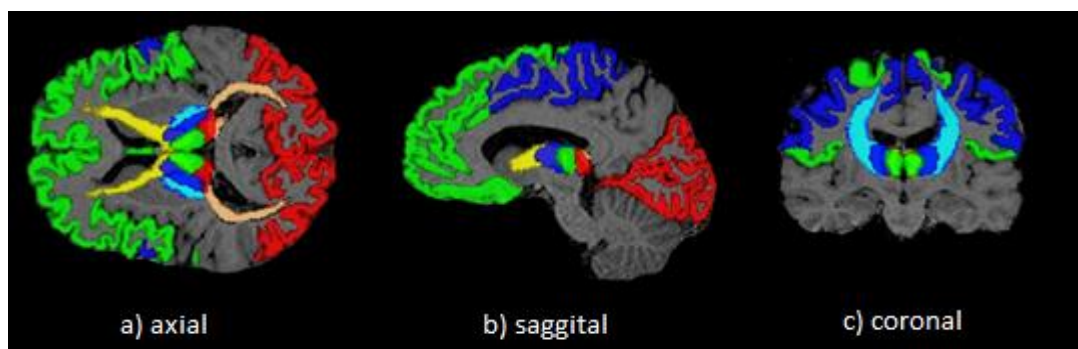
Figure 5.1. An example of an MTR scan overlaid with masks of groups of thalamic nuclei, and their connecting white matter tracts and cortical projections. Medial group - prefrontal cortex (green-yellow-green). Lateral group - sensorimotor cortex (blue-light blue-blue), and the posterior group - occipital cortex (red-orange-red).

5.2.2.3 Extracting MTR and lesional data and statistical analyses

At both time points, the whole tract masks as well as masks for the tract segments and thalamic groups were nonlinearly brought to native T1-space using nearest neighbour interpolations, and along with cortical ROIs and T2 lesion masks for patients (which were already in T1 space) using linear interpolations brought to MTR space. As previously described (Paling et al. 2013), by comparing to the MTR of CSF, partial volume effects were reduced by calculating the proportion of MTR variance in voxels containing several tissue types that could be attributed to each tissue. This segmentation allowed to only include the pure WM part of the tracts and the GM component of the cortical and thalamic ROIs. From the nonzero voxels of the WM tracts, the total WM lesion volume was extracted and from the non-lesional NAWM (created by subtracting voxels dilated by 2.0mm from the WM masks as described previously (Vrenken et al. 2006)) of the tracts and the GM of the thalamic and cortical ROIs, mean MTR was extracted. The masks for the NAWM tracts were created by overlaying the individual's T2 lesions as an exclusion masks (dilated by 2.0mm). To ensure that no 'preactive' lesions were affecting the data extracted from the normal appearing tissue, lesions masks were combined of baseline and follow up, and only tissue that was normal appearing at both time points was included in the subsequent analysis, thereby assuring that new lesion development that occurred between longitudinal MRI scans did not affect the results. MTR was analysed of all components of the thalamo-cortical systems (thalamic groups, WM tracts, and cortical ROIs), while volumes were only analysed of cortical ROIs. This was done because the WM tract and thalamic groups were atlas masks in MNI space brought to common space, while the cortical ROIs were generated in native space and were subject specific.

Age, sex, and EDSS were compared between groups using t-tests and chi-square tests. To cross-sectionally compare global MTR and volumes between subject groups, multiple

regressions of the MTR or volume response variable were performed on group indicators, with age, gender and ICV as covariates for adjustment. To cross-sectionally compare differences in MTR in WM tracts between patients and controls, linear mixed models were used with subject random intercept, group indicator, and side, age, ICV, and gender as covariates for adjustment. The advantage of using the mixed models was that two observations per subject could be analysed, one for each side, and thus adjusting for side rather than averaging sides. To analyse tract data, in addition to analyses using a single mean for each WM tract, separate tract segments were analysed using linear mixed models which could handle the multiple segment values per subject. This enabled examination of the separate WM tract segment means, with an indicator for each segment, and also whether there was a consistent pattern of values across the tract segments. Furthermore, mixed models adjusting for (rather than averaging over) side were used to examine associations between baseline and follow up MTR, both with and without adjustment for side, age, ICV, gender and tract lesion volume. An additional covariate was the baseline value of the response variable, to ensure that any longitudinal association across different regions was independent of, and not induced by, baseline cross-sectional associations.

Comparable to models in previous work (Bodini et al. 2016), the spatiotemporal relationship of non-lesional MTR in thalamo-cortical systems was assessed using two types of statistical models:

1) "Primary WM damage models" for the association between baseline MTR in WM tracts and follow up MTR in cortical and thalamic GM.

2) "Primary GM damage models" for the association between baseline MTR in the thalamic and cortical GM and follow up MTR in WM tracts.

To assess the associations between MTR of different parts of the thalamo-cortical systems and clinical function, the following regression analyses were performed, both at baseline and at follow up.

$$MTR_{ROI} = \text{clinical score} \times B1 + \text{age} \times B2 + \text{sex} \times B3 + \text{side} \times B4 + \text{intercept}$$

The ROIs tested were the cortical ROIs, NAWM of the whole WM tract, and thalamic group from the three thalamo-cortical systems. The clinical scores tested were EDSS, PASAT, 9HPT, and average TWT speed. All statistical analyses were performed in Stata (version 14.1, StataCorp) and R (version 3.2.3, R Core Team).

5.3 Results

Of 57 people with MS who were scanned at baseline, one person with PPMS was not included at follow up because of data analysis issues. Of the 25 controls scanned at baseline, eleven were scanned at 24 month follow up. The reason for not being able to include 14 controls at follow up varied: Three volunteers declined, one control could not leave their partner for whom they cared, one volunteer had a dermal piercing and was unable to remove it, one subject had left the NHS trust, two were unable to come as their health prevented them to come alone and no carer was available, one volunteer lived too far, and no reason was provided for five controls. Demographics are displayed in table 5.2. Age and female-to-male ratios did not differ significantly between the control and MS groups ($p=0.628$ and $p=0.279$, respectively). When assessing the MS group subdivided into MS subtypes, the SPMS group was found to be significantly older than PPMS ($p<0.001$), and the female-to-male ratio was borderline significantly lower different between the groups ($p=0.055$). EDSS was significantly lower in the RRMS group than the PPMS and SPMS group (both $p<0.001$).

	Cohort with baseline and follow up data					Cohort with baseline data only	
	Controls	All patients	PPMS	RRMS	SPMS	controls	PPMS
N Baseline / follow-up	11	56	12	26	18	14	1
Sex (F/M)	7/4	39/17	6/6	20/6	13/5	7/7	0/1
Handedness (R/L)	10/1	50/6	10/2	24/2	16/2	12/2	1/0
Age in years at baseline (SD)	38.42 (12.01)	46.75 (11.14)	48.08 (11.78)	41.54 (10.42)	54.00 (7.34)	36.72 (12.54)	36
Age in years at follow up (SD)	38.00 (12.23)	48.51 (11.16)	49.15 (11.62)	43.31 (10.67)	55.56 (7.29)	N/A	N/A
Median EDSS at baseline (range)	N/A	4.75 (1.0-8.5)	6.0 (1.0-6.5)	2.0 (1.0-6.0)	6.25 (4.0-8.5)	N/A	8.0
Median EDSS at follow up (range)	N/A	5.0 (1.0-8.0)	6.5 (1.0-6.0)	2.0 (1.0-6.0)	6.5 (4.0-8.5)	N/A	N/A

Table 5.2. Baseline and follow up characteristics and demographics of cohort, separated into subjects with baseline data and follow up data and subjects with baseline data only, divided into healthy controls and all patients, and further subdivided per MS subtype.

5.3.1 Cross-sectional group wise comparisons of whole brain metrics

At baseline, people with MS had an average of 11.80ml (SE=1.75ml) T2 lesions, while no controls had lesions. Models correcting for side (i.e. left or right) and excluding a potential interaction for side by subject group (i.e. MS or controls) showed that total thalamic volume was significantly lower in MS (5.29±0.13ml) than in controls

(6.41±0.20ml, p<0.001), and that the left thalamus was significantly larger than the right by 0.15±0.03ml (p<0.001). Total CGM volume, adjusted for age, ICV, and sex, was significantly smaller in controls (465.96±5.04ml) than in the MS group (478.90±3.24ml, p=0.041). MTR was significantly lower in the DGM of people with MS (34.21±0.14) than controls (34.94±0.21, p=0.006), and similarly, whole brain NAWM MTR was lower in people with MS (39.49±0.13) than controls (40.44±0.20, p<0.001). CGM MTR did not significantly differ between MS (32.09±0.11) and controls (32.42±0.17, p=0.113). Cross-sectional analyses at follow up showed a similar pattern and can be found in Appendix II.

5.3.2   Thalamo-cortical systems

Cross-sectional regional baseline differences between the MS group and controls within thalamo-cortical systems are displayed in table 5.3. At baseline, the MS group had significantly smaller volumes of the OCC and SMC than controls. In addition, a highly significant difference between left and right was observed in terms of cortical ROI volume, with the right PFC and OCC being larger than the left, and the inverse for the SMC. Models correcting for age, gender, ICV, side, and excluding potential side by subject group interactions, showed that the MS group had significantly lower MTR than controls in all three thalamic groups and WM tracts, but in none of the cortical ROIs. No significant correlations were found between MTR and volume in any of the cortical ROIs (all p>0.271). Furthermore, in most but not all ROIs a significantly higher MTR was found in the left hemisphere than the right. Follow up comparisons showed similar results and may be found in Appendix II, supplemental table 5.1. Pearson tests did not find any significant correlation between longitudinal change in T2 lesion volume and MTR change in any cortical, thalamic, or WM ROI studied (all -0.21<r<0.22, and p>0.11).

		MS	Controls	p-value	right – left (only presented if significant)	p-value
Thalamic group MTR	MG	35.02±0.19	36.01±0.29	0.005**		
	LG	37.09±0.19	37.90±0.30	0.026*	-0.26±0.09	0.003**
	PG	34.97±0.20	35.90±0.30	0.014*	-0.39±0.08	<0.001***
White matter tract MTR	MG-PFC	39.68±0.15	40.67±0.23	<0.001*	0.36±0.09	<0.001***
	LG-SMC	39.39±0.14	40.37±0.21	<0.001***	-0.35±0.07	<0.001***
	PG-OCC	38.98±0.17	40.51±0.26	<0.001***	-0.89±0.08	<0.001***
Cortical grey matter MTR	PFC	33.28±0.15	33.71±0.22	0.489		
	SMC	34.05±0.14	34.55±0.21	0.214	-0.17±0.06	0.005**
	OCC	32.56±0.17	33.11±0.25	0.181	-0.47±0.06	<0.001***
Cortical grey matter volume (ml)	PFC	64.70±0.40	64.16±0.67	0.513	1.36±0.20	<0.001***
	SMC	31.66±0.21	32.47±0.33	0.043*	-1.92±0.17	<0.001***
	OCC	42.44±0.33	44.06±0.52	0.011*	0.81±0.26	0.002**

Table 5.3. Baseline differences between the MS group and controls in MTR of thalamic nuclei, white matter tracts, and cortical grey matter, as well as cortical grey matter volume. Highly significant left-right differences were observed which did not consistently favour one hemisphere. Except cortical MTR, MTR and volume was larger in controls than patients in almost all parts of the three thalamo-cortical systems.

5.3.3 MTR gradient in tracts

Analyses of WM tracts subdivided into four segments of equal length showed that people with MS had significantly lower baseline MTR in all WM tract segments than controls (all $p<0.05$). Moreover, MTR was heterogeneous within WM tracts. At both baseline and follow up, an MTR gradient was observed along the length of the cortico-thalamic tracts in both patients and controls, as displayed in figure 5.2 and Appendix III, supplemental figure 5.1. The direction of this gradient was different between thalamo-cortical systems: In both patients and controls, in the MG-PFC tract the highest MTR was found proximal to the cortex, whereas in the LG-SMC and PG-OCC tract the segment nearest the

thalamus had the highest MTR. Assuming a linear change between tract segments from the thalamus to the cortex, at baseline a change of 0.54 in MTR was observed with every subsequent segment in controls and 0.38 in MS (both p<0.001) in the MG-PFC tract. This gradient slope differed significantly between groups (p=0.011). In the LG-SMC tract, this gradient was -0.60 for controls, and -0.52 for the MS group (both p<0.001). The difference between gradients in these groups approached significance (p=0.071). In the PG-OCC tract, controls had a gradient of -0.46, differing significantly (p=0.001) from -0.26 in the MS group (both p<0.001).
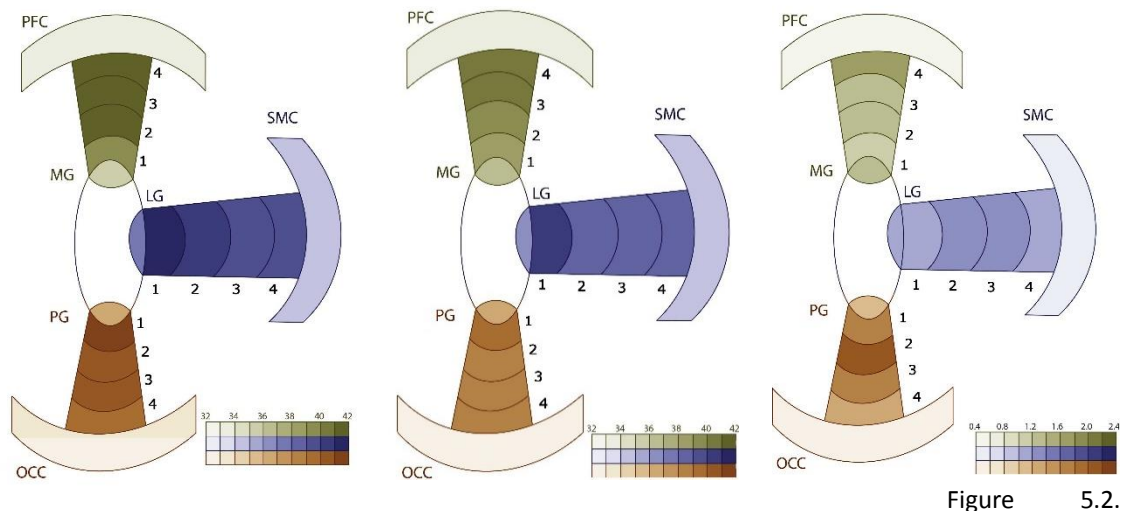
Figure 5.2.

Baseline mean MTR values in controls (left), MS (middle), and difference between MS and controls (right). Within the thalamo-cortical tracts significant MTR gradients could be found with different directions depending on the thalamo-cortical system.

5.3.4 Primary white matter damage

In the MS group, significant associations were found between baseline WM MTR and follow up GM thalamic and cortical MTR. Results are presented in table 5.4 and figures 5.3 and 5.4, which display the (near) significant associations between baseline and follow up MTR in thalamic, cortical, and WM tract ROIs, after correction for covariates and baseline MTR of the respective ROI of which follow up MTR is assessed. Follow up MG

MTR in the thalamic MG was associated with MTR in the connected MG-PFC WM tract, and particularly with tract segment 4 nearest the cortex. In addition, follow up MG MTR was associated with baseline MTR in the non-connected PG-OCC tract ($\beta=0.256\pm0.128$, p=0.045), but this association did not survive correction for baseline PG-OCC MTR (p=0.192). Follow up LG MTR was associated with baseline MTR along the whole non-connected MG-PFC tract, with a stronger association with MTR in the segment nearest the cortex. Furthermore, while correction for baseline MTR removed our ability to detect this link (p=0.585), an additional association was found between follow up MTR in the LG and baseline MTR of segment 1 (nearest the thalamus) of the connected LG-SMC tract ($\beta=0.388\pm0.127$, p=0.002). Finally, follow up PG MTR was associated with baseline MTR in segment 1 of the connected PG-OCC tract, and was additionally associated with baseline MTR of the non-connected MG-PFC tract ($\beta=0.333\pm0.120$, p=0.006), but the latter association disappeared after correcting for baseline PG MTR (p=0.235). Combined these results show an association between baseline MTR in the MG-PFC and follow up MTR in the thalamus, irrespective of anatomical association.

When assessing the relationship between baseline WM tract MTR and follow up cortical GM MTR, follow up MTR in all cortical ROIs was similarly found to be associated with baseline MTR in the PG-OCC tract, which appeared largely irrespective of anatomical connection. Follow up PFC MTR was not associated with MTR in the connected MG-PFC tract, but was associated with baseline MTR in the non-connected PG-OCC MTR, particularly with the tract segment most proximal to the thalamus. Similarly, follow up MTR in the SMC was not associated with baseline MTR in the connected LG-SMC tract, but was significantly associated with MTR in segment 1 of the non-connected PG-OCC tract. Finally, follow up OCC MTR was only associated with baseline MTR of the segment closest to the thalamus of the connecting PG-OCC tract.

5.3.5 Primary grey matter damage

As displayed in table 5.4, when correcting for baseline MTR, no associations were found between follow up MTR of any WM tract and thalamic or cortical GM MTR at baseline. This section will therefore describe the results of models without baseline adjustments. Follow up MTR of the whole MG-PFC tract was associated with baseline MTR of the connected thalamic MG (β=0.282±0.087, p=0.001), while not being associated with baseline MTR of the connected PFC (p=0.152). Baseline MTR in the PG was the only association found with follow up LG-SMC MTR (β=0.241±0.081, p=0.003). Follow up PG-OCC MTR was not associated with baseline MTR in any cortical of thalamic ROI. Together, these results show modest associations between thalamic or cortical MTR and follow up WM tract MTR, which were absent when adjusting for baseline MTR.

Follow up MTR	Baseline MTR associations	β	p
MG	MG - PFC whole tract	0.262±0.110	0.017*
	MG - PFC tract segment 4	0.167±0.062	0.007**
LG	MG - PFC whole tract	0.211±0.115	0.065
	MG - PFC segment 4	0.169±0.065	0.009**
PG	PG - OCC tract segment 1	0.262±0.110	0.017*
PFC	PG - OCC whole tract	0.157±0.082	0.056
	PG - OCC tract segment 1	0.176±0.059	0.003**
SMC	PG - OCC whole tract	0.226±0.096	0.096
	PG - OCC tract segment 1	0.184±0.068	0.007**
OCC	PG - OCC tract segment 1	0.249±0.066	<0.001***
MG - PFC	none		
LG - SMC	none		
PG - OCC	none		

Table 5.4. All associations (significant and those below 0.01) between follow up MTR with baseline MTR in thalamic, cortical, and WM tract ROIs, after correction for side, age, sex, intracranial volume, and baseline MTR of the region of interest of which follow up MTR is assessed. Baseline MTR in the MG-PFC tract was significantly associated with thalamic MTR, while baseline PG-OCC MTR was significantly associated with cortical MTR. Follow up MTR in none of the tracts was significantly associated with baseline MTR in any of the cortical or thalamic GM ROIs. MG: medial group, LG: lateral group, PG: posterior group, PFC: prefrontal cortex, SMC: sensorimotor cortex, OCC: occipital lobe.
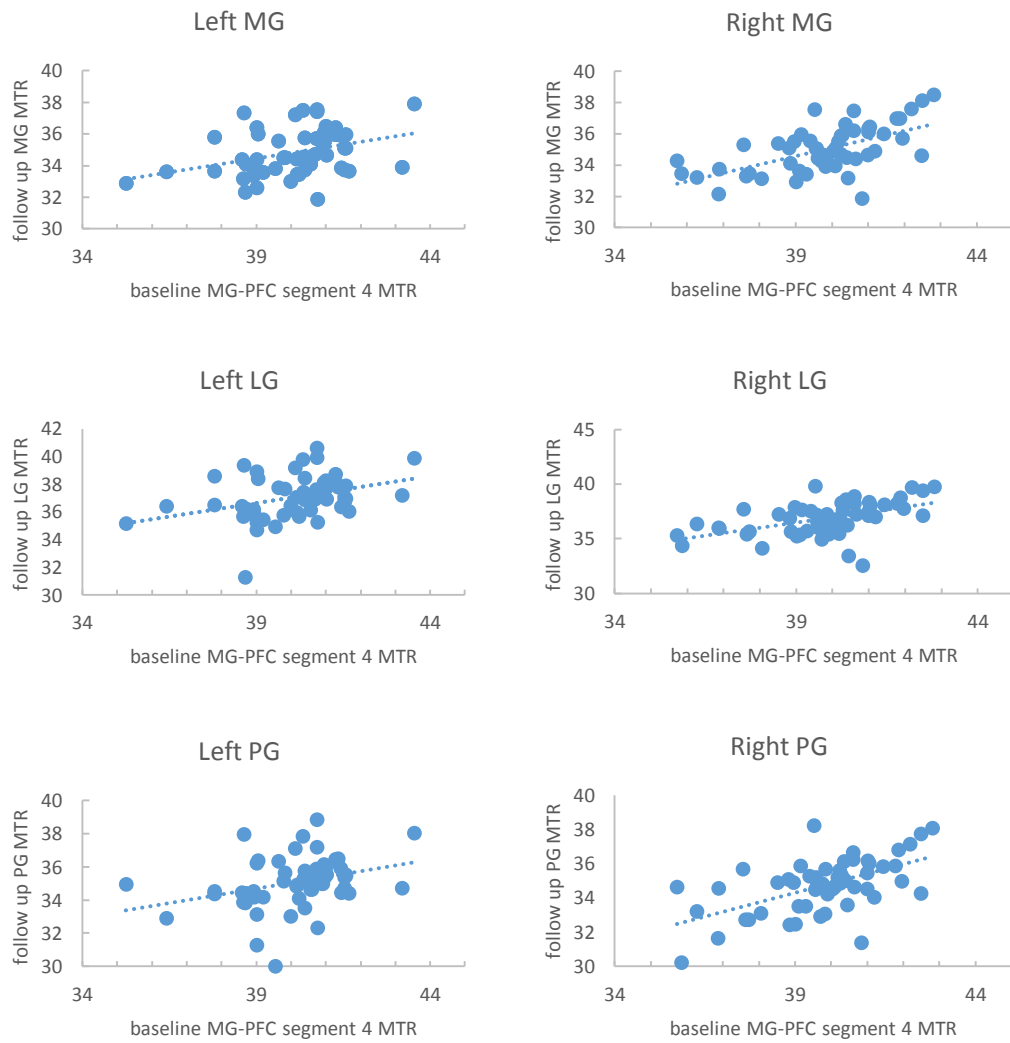
Figure 5.3. Scatterplots of the association between baseline MTR in the MG-PFC tract segment 4 nearest the cortex, and follow up MTR in the different thalamic groups.
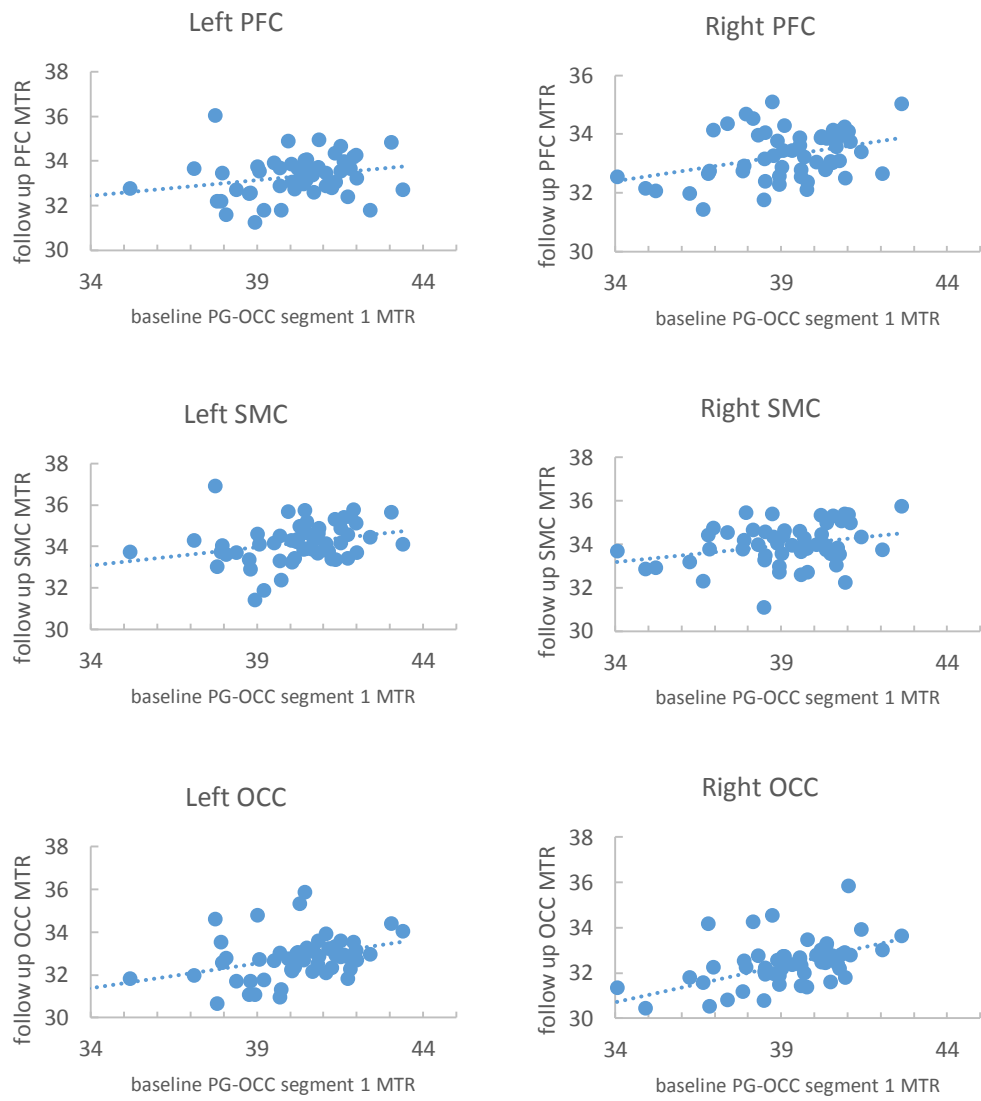
Figure 5.4. Scatterplots of the association between baseline MTR in the PG-OCC tract segment 1 nearest the thalamus, and follow up MTR in the different cortical ROIs.

5.3.6 Associations between MTR and clinical function

Part of thalamo-cortical system		EDSS		PASAT		TWT average speed		9HPT	
		B	p	B	p	B	p	B	p
MG-PFC	tract	-0.19	0.023		n.s.	0.96	0.003	0.41	0.009
LG-SMC	tract		n.s.		n.s.	0.65	0.024		n.s.
PG-OCC	tract	-0.22	0.017		n.s.	1.10	0.003	0.42	0.016
PFC	cortex		n.s.		n.s.		n.s.		n.s.
SMC	cortex		n.s.		n.s.		n.s.		n.s.
OCC	cortex	-0.21	0.003		n.s.	0.88	0.002		n.s.
MG	thalamic group	-0.24	0.020		n.s.	1.25	0.001	0.51	0.005
LG	thalamic group	-0.22	0.036		n.s.	1.18	0.003	0.54	0.006
PG	thalamic group		n.s.		n.s.	1.28	0.002	0.51	0.014

Table 5.5. Baseline associations between MTR in tract, cortex, and thalamic group ROIs of the three thalamo-cortical systems and clinical function assessed by EDSS, PASAT, TWT and 9HPT.

As displayed in table 5.5, except for an association between occipital MTR with EDSS and TWT, MTR of no cortical ROI at baseline had a significant association with any clinical metric. Lower EDSS was associated with higher MTR in multiple ROIs, but did not consistently favour a specific thalamo-cortical system. PASAT performance was not associated with MTR in any ROI. TWT speed was associated with MTR in nearly all ROIs, except two cortical areas, and appeared to have a stronger association with MTR in thalamic ROIs without favouring ROIs from a specific thalamo-cortical system. Similarly, 9HPT performance was most strongly associated with thalamic MTR, and did not favour a specific thalamo-cortical system. As shown in the Appendix II, supplemental table 5.2, associations between MTR and clinical function at follow up showed a similar pattern.

5.4 Discussion

The main findings of the present study are that 1) in both people with MS and healthy controls statistically significant hemispheric differences exist in MTR and regional cortical volume which do no consistently favour one side, emphasising the need to account for this in statistical models to detect disease-specific changes. 2) In both groups NAWM MTR within thalamo-cortical tracts is heterogeneous and shows gradients along the length of the tract. Furthermore, the directions of these gradients differ between thalamo-cortical systems, further emphasising the need to account for these inhomogeneities on a tract by tract basis. 3) Thalamic MTR was lower in the MS group than in controls and was accompanied by lower thalamic volume, whereas lower regional cortical MTR was not consistently associated with lower cortical ROI volume, suggesting that significant cortical microstructural damage can occur in MS in the absence of atrophy. Finally, 4) "Primary WM damage models" are better than "primary GM damage models" at explaining longitudinal MTR changes in thalamo-cortical systems in MS.

5.4.1 Asymmetry and heterogeneity

MTR and volumes were asymmetric and heterogeneous, emphasising the need to adjust for this in more refined statistical approaches to increase our ability to detect disease-specific effects. The present study found highly significant left-right MTR differences in the thalamus, WM tracts, and cortex in both MS and controls. While most left-hemispheric ROIs had significantly higher MTR than their right-hemispheric counterparts, this was not the case for all ROIs. MTR in the left SMC and OCC was higher than in the right, which corresponds to a previously reported higher MTR in these left hemispheric cortical regions (Kang et al. 2011). Furthermore, in WM tracts, a significantly higher MTR was found in the right compared to left MG-PFC tract, and in the left compared to right PG-OCC and the LG-SMC tracts, broadly corresponding to a

previously reported larger MTR in left hemispheric WM (Silver et al. 1997; Armstrong et al. 2004).

Volumes of regional cortical and thalamic ROIs were also asymmetric in both MS and controls, and these left-right differences similarly did not consistently favour one side. Asymmetries in thalamic volume have been reported in lower vertebrate species (Harris et al. 1996), and the current finding of a larger left thalamus complements the finding of a reported lower MD on this side (Fabiano et al. 2005; Fabiano et al. 2003). This left-right difference may be attributed to intrinsic anatomical asymmetries and left-hemispheric dominance in the predominantly right-hand dominant cohort included in this chapter. Volume of the left SMC was significantly larger than the right, whereas the right PFC and OCC were larger than the left, which broadly corresponds to previously reported regional cortical volume asymmetries (Goldberg et al. 2011), and is in line with the previously reported right hemispheric dominance for visual processing (Silva et al. 2014; Hougaard et al. 2015) and left hemispheric dominance for motor processing in right-hand dominant people (Amunts et al. 1996).

Interestingly, in addition to the observed hemispheric asymmetries, NAWM MTR within thalamo-cortical tracts was found to be highly heterogeneous and to follow a gradient along the length of the tract. Furthermore, the directions of these gradients differed between tracts, which highlights the importance to analyse tracts individually, rather than clustering them into single analyses. Combined, these data show that to gain insight into WM pathology, more sophisticated statistical methods may aid to distinguish disease-specific variance from intrinsic tissue heterogeneity. Recent studies addressing GM pathology in MS (Deppe et al. 2016; Schoonheim et al. 2015; Magon et al. 2014; Louapre et al. 2016) have grouped data from the left and right thalamus without adjustments in their statistical models. Considering the present findings, these studies may have

benefitted from accounting for asymmetries in their statistical models. Similarly, correcting for NAWM tract heterogeneities could increase statistical power to detect pathological changes in studies looking at WM tract pathology in MS. This may be done in different ways, including an advanced statistical method that was recently proposed which allows the analysis of individual tract profiles (Dayan et al. 2016), or as done in the present work by subdividing the tract into smaller segments. The present chapter presents the first study to assess thalamic and WM tract pathology in MS taking into consideration the above mentioned asymmetries as well as intrinsic WM tract inhomogeneities.

5.4.2   Cross-sectional comparisons

Baseline MTR was lower in MS than controls in the thalamic groups and in all segments of the WM tracts, but in none of the cortical ROIs. These differences were not all significant at follow up, likely due to the smaller number of controls (11, compared to 25 at baseline). At both baseline and follow up, compared to controls people with MS had significantly lower thalamic, but not cortical, volume. After correction for ICV and age, an unexpected significantly larger overall cortical volume was found in patients than in controls. This was surprising as patients were expected to have smaller baseline CGM volumes. This may be attributed to age and ICV (both of which are nearly significantly different between patients and controls), confounding the unadjusted, non-significant volume difference between the two groups. However, when looking at regional volumes of cortical ROIs, this effect was not reproduced, and volumes were lower in the SMC and OCC in people with MS, as may be expected biologically. The cross-sectional finding of lower regional cortical MTR in MS in the absence of lower regional cortical volume is in line with a voxel based study showing that in MS lower MTR is not consistently co-localised with a lower cortical volume (Mallik et al. 2015), and may be interpreted to be

due to a significant decrease in synaptic density, axonal loss, and reduced neuronal connectivity (Wegner et al. 2006; Jehna et al. 2013; Filippi et al. 2012).

5.4.3 White matter and associated subsequent grey matter injury

As this study is longitudinal in nature, the current findings may allow conclusions regarding chronology of pathology development in MS. As such, the present work provides evidence for the development of pathology from WM tracts to GM, while the inverse hypothesis does not seem to be supported by the data. Primary WM damage models for all three different cortico-thalamic systems yielded significant associations between baseline WM MTR and follow up (cortical and thalamic) GM MTR, while associations detected by primary GM damage models were weaker and were largely insignificant. Importantly, these baseline WM to follow up GM MTR associations remained significant after adjusting for baseline MTR of the respective GM ROI, suggesting that this effect is independent and not induced by two secondary correlations: a significant longitudinal correlation between baseline and follow up MTR in the GM ROI, combined with a baseline association between tract and GM MTR.

Thalamic and cortical pathology were hypothesised to be associated with proximal WM tract damage, and to be tract-specific. While the present findings partly support this hypothesis, significant associations were found between MTR in WM tracts and non-connected GM cortical and thalamic ROIs. On the one hand, the current study provides evidence for tract-specific development of pathology: PG follow up MTR was mainly associated with baseline MTR in the nearest part of the connected PG-OCC tract. This corresponds to previous work that found evidence for retrograde degeneration from WM lesions in the optic radiation, leading to connected thalamic, but not cortical, atrophy (Sepulcre et al. 2009). Further evidence for tract-specific development of MS pathology comes from a post mortem study looking at the correlation between cortical thickness and

histological markers of neurodegeneration and histology in thalamo-cortical systems (Kolasinski et al. 2012). Specifically, this study shows significant correlations between cortical thickness of the prefrontal cortex and primary visual cortex with myelination of their respective WM tract projections to their anatomically associated thalamic nuclei, as well as with cell density in these thalamic nuclei. As significant correlations were confined only to anatomically connected areas and no significant inter-tract correlations were found, this suggests that functional anatomical connectivity is relevant in the spread of multiple sclerosis pathology. Furthermore, a recent longitudinal study in PPMS showed that cortical GM MTR at a 24 month follow up is related to baseline MTR in connected WM tracts, while the hypothesis of pathology evolving from GM to WM was not supported (Bodini et al. 2016). Unfortunately, the latter study did not assess associations between cortical areas and non-connected WM tracts, making it difficult to assess whether the observed WM to GM directionality of pathology development was tract-specific.

On the other hand, the present work provides evidence for a tract-unspecific development of diffuse injury from WM to GM. Follow up thalamic MTR in the MG and LG, and to a lesser extent the PG, was found to be associated with baseline MTR in the MG-PFC tract segment nearest the cortex irrespective of anatomical connectivity. Similarly, follow up MTR in all cortical ROIs was associated with MTR in the PG-OCC tract segment most proximal to the thalamus. Interestingly, these are the segments within their respective tracts with the highest baseline MTR, and may reflect the strength of anatomical connectivity with their cortical and thalamic projections. The findings of a potentially tract-unspecific development of MTR are in line with a recent cross-sectional study that assessed the interdependence of cortical and WM tract pathology using cortical thickness, DTI, and T2* maps (Louapre et al. 2016). This study found that while intracortical and WM tract pathology are concomitant manifestations of MS pathology, they are not

uniquely restricted to their respective thalamo-cortical systems, as significant associations between tract pathology and non-connected cortical areas were also found. The lack of spatial specificity between WM and GM pathology corresponds to the findings found in the present work, and weakens the hypothesis of a mainly tract-driven degenerative process as the main pathogenic mechanism that connects WM and GM injury (Kipp et al. 2015).

5.4.4 Associations between MTR in thalamo-cortical systems and clinical function.

Injury to any part of the thalamo-cortical systems was hypothesised to affect clinical function associated with the respective system. As such, EDSS was thought to be associated mainly with sensorimotor function. However, lower MTR in the cortex, tract, and thalamic groups of all three studied thalamo-cortical systems was associated with higher EDSS, and was not specifically associated with MTR in the LG-SMC thalamo-cortical system. PASAT was expected to be mainly associated performance of the thalamo-cortical system responsible for executive function (i.e. the MG-PFC system), but no associations were found with MTR in any area. TWT function was thought to mainly require sensorimotor function, and to a lesser extent visual function, which was partly reflected in the results. 9HPT requires all three studied thalamo-cortical systems, and function on this test was found to be mainly associated with MTR in the thalamic component of these systems.

Altogether, the present results partially confirm that MTR in thalamo-cortical systems is associated with function of the tasks these systems are involved in, and shows that thalamic has a modestly larger association than cortical and white matter tract MTR. However, the present study also shows associations between MTR in thalamo-cortical and clinical function that was not a priori hypothesised to be linked to the role of these

systems and may partly be explained due to statistical methods applied. In this light it should be noted that the regression analyses performed used the MTR in the respective ROIs as dependent variable, while using clinical function as regressors, which is the reverse of the functional relationship between these variables. The reason this approach was taken is because since the clinical value was the same for both hemispheres no mixed effect models could be fitted and would therefore not have corrected for side, which is important given the previously described hemispheric asymmetries. Future analysis of the present data will apply more refined statistical models that will allow the direct comparison of MTR in different segments and their effect on clinical function, and will furthermore assess longitudinal changes in MTR and how these relate to changes in clinical function.

5.4.5 Methodological considerations

It should be noted that while the present study mainly found tract-unspecific associations between WM and thalamic and cortical GM MTR, these results do not exclude the possibility of a tract-mediated spread of pathology. It is perceivable that different signal-to-noise ratios in ROIs obscured the measurement of MTR due the small size of the masks, and may have led to the inability of the statistical models used to detect possible existing associations. Furthermore, the discrepancy between the present findings of a largely tract-independent WM to GM association of MTR in MS, and the previously suggested tract-specific spread of pathology may be explained by a number of methodological considerations of the present and earlier studies.

With regard to the above mentioned post mortem study which is the only study that indicated a tract-specific association between WM and GM (Kolasinski et al. 2012), it should be noted that this type of study is per definition cross-sectional in nature, and therefore has an intrinsic bias towards including patients with a more advanced or more

active disease state, whereas the current study included people with all MS subtypes. Analysing MS subtypes in the present cohort separately may find differences in pathology development between relapsing and progressive patients (Kutzelnigg et al. 2005). Furthermore, the post mortem MRI study found correlations between cortical thickness and tract and thalamic histology metrics, and as shown in this study and in previous work (Mallik et al. 2015), diffuse pathology as detected by lower MTR does not necessarily co-localise with reduced cortical volume.

The current work has a number of limitations that should be taken into account. Firstly, while at baseline 25 healthy controls were scanned, only 11 were scanned at follow up, which led to lower statistical power to detect group-wise differences at follow up. One male with PPMS was excluded with the relatively high baseline EDSS of 8.0, and the exclusion of this subject at follow up may have skewed the results towards people with milder disease. The controls that had both baseline and follow up data did not differ notably in terms of baseline characteristics. Secondly, in the applied statistical analyses people with all MS subtypes were grouped. As mentioned above, future analyses of the individual MS subtypes may provide insight into differences between progressive and relapsing MS. Thirdly, while sub-thalamic parcellations were applied using a histology based atlas (Morel et al. 1997) brought to MNI space for MRI use (Krauth et al. 2010; Jakab et al. 2012) rather than analysing the whole thalamus, the thalamic group masks consisted of multiple anatomically distinct nuclei with different functions and connections that were grouped into single masks. This was done to have sufficiently large masks to look at MTR changes, but this reduced the specificity of the obtained data. Similarly, while the areas comprising the cortical ROIs were broadly involved in similar cognitive and motor functions (i.e. PFC: executive function, SMC: sensorimotor functions, and OCC: visual processing), the larger cortical ROIs were heterogeneous in anatomical connectivity and function. Further, the WM tracts masks contained a

combination of afferent and efferent fibres (Jones 1985), making it difficult to assess whether the degeneration observed was anterograde or retrograde in nature. These thalamic and WM tract masks were not subject-specific and generated on the basis of an atlas and on tractography in controls. As such, the MTR and lesion volume metrics obtained from these tracts and thalamic group masks were subject to interpolations during registrations, and may not reflect the actual subject-specific anatomical tracts and thalamic nuclei. Furthermore, the WM tract masks did not fully extend to their cortical ROIs, because conservatively only voxels were included that were part of bilateral tracts in more than 50% of controls. As the highest degree of anatomical variation is likely to be in the tract area where the fibres 'fan out' towards the cortex, this makes voxels in those areas less likely to fulfil above criteria, and this resulted in tract masks that appear to terminate in the WM. While using this method increases the likelihood of including only voxels actually belonging to the tract, it reduced the ability to detect whole tract dynamics, and thereby the understanding of the interplay between the cortex and its connected WM. Finally, as scans to detect GM lesions (e.g. DIR) were not available for the current cohort, MTR estimates of cortical and thalamic ROIs may be affected by the presence of unseen GM lesions.

5.5   Conclusions and future directions

The present study is the first to longitudinally analyse MTR changes in WM tracts and their GM connections, while assessing whether potential associations are confined to individual thalamo-cortical systems, by also testing associations between anatomically unconnected regions. The present chapter shows highly significant volumetric and MTR asymmetries as well as heterogeneities within and between thalamo-cortical tracts in healthy controls and MS, emphasising the need to account for this in statistical analyses to detect disease-specific effects. Additionally, this work shows that MTR changes in the

cortex are not consistently associated with lower regional volume, indicating that microstructural damage is not necessarily accompanied by regional volume loss. Finally, the current study provides longitudinal evidence for a WM to GM spread of diffuse myelin and neuro-axonal loss. However, the current data are limited in their ability to conclude on whether this association is tract-specific or not.

The potential tract-unspecific nature of WM to GM development of thalamo-cortical system damage in MS may be interpreted as being part of a wider stage-dependent process leading to both WM and GM tissue damage. Possible pathogenic mechanisms may include wide spread inflammation (Lassmann et al. 2012), and the presence of microglia inducing a more generalised diffuse pathology (Kutzelnigg et al. 2005) (as will be discussed in chapter 6). Alternatively, the perceived association may be due to shared remyelination mechanisms in WM and GM (Franklin & ffrench-Constant 2008). Alternatively, a potential tract-specific spread of pathology may be induced by anterograde trans-neuronal degeneration, retrograde trans-neuronal degeneration, or Wallerian degeneration (Kipp et al. 2015). Results from chapter 4 suggest that GM atrophy is at least partly driven by GM lesion-independent mechanisms, as the spatial overlap between these forms of pathology was at best modest. While the present chapter did not address GM atrophy directly, but assessed diffuse GM pathology using MTR, the results described in this chapter suggest that cortical and subcortical GM injury follow WM tract pathology. Together these two studies demonstrate that GM pathology is highly heterogeneous, and that GM atrophy, GM lesions, and diffuse GM demyelination have limited shared spatio-temporal distribution, and may furthermore only be partly related to injury to connected WM. While there is likely to be a pathogenic link between these forms of injury through mechanisms including Wallerian degeneration, there may be specific pathogenic processes driving these forms of injury. Additional analyses of patient subgroups may provide insight into the ongoing pathogenic events in the different MS

subtypes, as it has been suggested that progressive MS is mainly a GM disease, while WM in these patients is affected to a lesser extent than in relapsing patients (Geurts 2008). To further examine what drives GM and WM injury in MS, the heterogeneity of the MS population may therefore allow a deeper understanding of how these forms of pathology relate to each other.

Further analyses of the data presented in the present chapter will also assess clinical impact of damage to individual cortico-thalamic systems. Previous work has shown that lower MD and thalamic atrophy are associated with poorer cognitive function (Schoonheim et al. 2015; Kern et al. 2015), and has shown that localised atrophy of the anterior nucleus of the thalamus is linked to poorer cognitive function (Bergsland et al. 2015), and atrophy to the ventral thalamic nucleus (included in the LG in the present chapter) is associated with increased EDSS (Magon et al. 2014).

The presented in vivo study provides insight into the spatiotemporal development of MTR abnormalities in MS. As described in chapter 2, MTR is based on magnetic properties of macromolecule-bound hydrogen nuclei, and is therefore indirectly visualising myelin and to a lesser extent neuronal content, with which MTR is correlated (Schmierer et al. 2004; Schmierer, Tozer, et al. 2007a; Schmierer, Parkes, et al. 2010; Tardif et al. 2012). However, it is unclear if this association between histology and MTR is the same in different tissue types. The next chapter will therefore describe the histopathological substrates underlying MRI abnormalities in MS, with a specific focus on MTR.

Chapter 6

Histopathological substrates of magnetisation transfer ratio in lesional and normal-appearing grey and white matter

6.1 Introduction

MRI has proven invaluable in the study of CNS injury *in vivo,* but as described in chapter 2, MRI only indirectly measures pathology by reconstructing images based on MR properties of hydrogen spins. This chapter describes the underlying histopathological substrates of MR detected abnormalities in MS. Out of many correlations between MRI indices and histology, I focussed on the histopathological substrates of MTR, because MTR has been demonstrated to be affected in MS and to be associated with clinical disability (Khaleeli *et al.*, 2007). Combined with chapter 5 in which the spatiotemporal distribution of MTR is outlined, I will in this chapter further refine our understanding of MTR abnormalities in MS by presenting a study performed on 16 post mortem MS cases and four controls, specifically assessing the histopathological correlates of MTR in normal appearing and lesional GM and WM.

To introduce this work, I will present a literature review of all MRI-histology studies on MS brain tissue to date. Fifty studies on MS brain tissue combining MRI and histology have been performed since the first such study (Estes et al. 1990), which include biopsies, post mortem in situ scans, scans of unfixed and fixed tissue, and combinations of in vivo MRI and post mortem histology. I will here outline their main findings, broadly clustered into four categories which will be described in turn: 1) Methodological considerations in post mortem MRI studies, 2) the detection of WM and GM lesions, 3) the visualisation of non-lesional MS pathology, and 4) correlations between quantified histology and MR

indices, with a focus on MTR. This is followed by a post mortem MRI-histology study carried out on the histopathological substrates of MTR in the MS brain.

6.1.1 Methodological considerations

A number of differences between in vivo and post mortem tissue poses challenges to the translation of post mortem MRI findings to in vivo scans (see table 6.1). While the use of MRI improves pathological lesion sampling yield (De Groot et al. 2001), an important methodological consideration in MRI–histology studies is that formalin fixation shrinks brain tissue by 11-25% (Quester & Schröder 1997), which affects co-registration of MR and histology images. To aid MRI-histology registration, tools have been developed including stereotactic navigation (Schmierer et al. 2003) and more recently individualised 3D printed boxes (Absinta et al. 2014). In addition to shrinking tissue, fixation changes hydrogen spin properties as covalent bonds cross-link proteins (Thavarajah et al. 2012). This results in significant changes to MRI metrics compared to in vivo scans, including reduced T1, T2, MD, RD, and MTR, and increased FA and fraction of macromolecular protons (f_b) (Schmierer, Thavarajah, et al. 2010; Schmierer et al. 2008). However, at 1.5T, MR indices in WM and GM are affected similarly (Schmierer, Thavarajah, et al. 2010), allowing easier translation of findings towards in vivo scans, as WM/GM contrasts are preserved. In addition to effects of fixation, the media in which post mortem tissue may be scanned (air, formalin, fomblin, or phosphate buffered saline [PBS]) have different MR properties and affect the tissue differently in terms of histology (Schmierer, Tozer, et al. 2007a; Schmierer et al. 2004; Gilmore, Geurts, et al. 2009b; Geurts, Pouwels, et al. 2005). Finally, tissue temperature affects T1 and T2 signal linearly and below 10° Celsius image contrast is too severely reduced for sufficient signal-to-noise ratio (Tofts et al. 2008; Ruder et al. 2012), but keeping tissue at room temperature affects the integrity of unfixed tissue due to decay. In summary, changes occur to tissue and MR indices

depending on formalin fixation and the medium in which the tissue is scanned. These tissue alterations need to be taken into consideration when comparing histological images to their matching MR images, and when comparing post mortem to in vivo findings.

Factor	Effect on tissue and image quality
Fixation	Tissue shrinkage (Quester & Schröder 1997)
	Histology-MR registration (Schmierer et al. 2003; Absinta et al. 2014),
	Changes in MR metrics (Schmierer, Thavarajah, et al. 2010; Schmierer et al. 2008)
Medium	Susceptibility effects (particularly if tissue is scanned in air)
	Fixation (if placed in formalin)
	Binding affinity antibodies and histological stains (particularly if submerged in fomblin)
Temperature	T1 changes (Tofts et al. 2008; Ruder et al. 2012)
	T2 changes (Tofts et al. 2008; Ruder et al. 2012)
	Decay of unfixed tissue

Table 6.1. The effects of fixation, medium and temperature on image quality, tissue integrity, and histology.

6.1.2 Lesional and non-lesional MS pathology

Studies combining MRI and histology are the only way to evaluate to what extent different MRI sequences are able to visualise (both WM and GM) pathology. Abnormalities on T2-weighted and MTR scans visualise inflammatory WM demyelination (Macchi & Cioffi 1992; Estes et al. 1990; Schmierer, Parkes, et al. 2010; Schmierer et al. 2008; Schmierer et al. 2004; Tardif et al. 2012), whereas changes on T1-weighted scans more closely reflect axonal loss (van Walderveen et al. 1998; van Waesberghe et al. 1999), as can be appreciated in figure 6.1. Post and ante mortem T2-weighted scans have been found to be comparable in their ability to evaluate MS pathology (Barkhof et al. 1993), but the heterogeneity of T2 detected WM pathology highlights the high specificity and low sensitivity of this scan type (van Waesberghe et

al. 1999; Newcombe et al. 1991). Cortical GM lesions are not easily detected on T2-weighted or FLAIR scans, and particularly intracortical lesions are difficult to distinguish (Geurts, Bø, et al. 2005; Geurts et al. 2008). Because on clinical scanners the visibility of cortical lesions is dependent on lesion size and we are merely seeing the "tip of the pathological iceberg" (Seewann et al. 2011), studies have combined T2-weighted and FLAIR with high resolution T1-weighted scans or have used different sequences including DIR (and PSIR) to improve cortical lesion detection rates (Bagnato et al. 2009; Seewann et al. 2012). Even if prospectively many cortical lesions are still missed, their detection rate is significantly higher on 7T scanners than on clinical scanners (Kilsdonk et al. 2016), and the use of R2*, T2*gradient recalled echo (GRE), inversion recovery GRE, and gradient and spin echo sequences allows detection of most cortical lesions (Yao et al. 2014; Pitt et al. 2010; Bagnato et al. 2015). At this field strength, cortical lesion subtypes may even be distinguished; type 3 subpial lesions can be distinguished from NAGM using MTR and FA (Jonkman et al. 2015; Tardif et al. 2012; Kilsdonk et al. 2016). Finally, other tissue characteristics have been studied. Iron may be detected in microglia of active WM lesions and can be visualised using T2 GRE scans, R2* scans, or susceptibility mapping, but the detection of iron may not be selective for pathology (Mehta et al. 2013; Bagnato et al. 2011; Sun et al. 2015; Walsh et al. 2013). Altogether, these studies show that particularly inflammatory demyelinated WM lesions are readily detected on post mortem scans and that the development of novel MR sequences and scanners with higher field strengths allow the detection of iron and cortical lesions.

In addition to WM and GM lesions, several MRI-histology studies identify pathological changes in non-lesional tissue. Non lesional WM with high MR texture heterogeneity is associated with lower axon and myelin content (Zhang et al. 2013), and has post-translational phosphorylation of neurofilaments, affecting T1 and MTR signal (Petzold et al. 2011). NAWM also contains astrocytes and microglia expressing iNOS

immunoreactivity (Broholm et al. 2004; Zeis et al. 2009), suggesting neuronal damage and diffuse inflammation outside lesions. Combinations of MR sequences show that regions normal on T1, T2 and MTR differ from regions abnormal on T2 only by having axonal swelling and axonal loss (Fisher et al. 2007), and that MTR may be combined with DTI, as these sequences reveal different tissue characteristics, which are more abnormal in normal appearing tissue adjacent to lesions (Lindquist et al. 2007; Moll et al. 2011). DAWM, defined as areas with abnormalities on PD and T2-weighted scans between WM lesions and NAWM, is associated with a decrease in axonal content, myelin phospholipids, and increased gliosis compared to NAWM, accompanied by a decreased FA and increased T1, T2, and myelin water fraction (Seewann et al. 2009; Moore et al. 2008; Laule et al. 2011). Studies assessing non-lesional GM pathology show that cortical volume is most strongly associated with neuronal size, neuronal density and axonal density (Popescu et al. 2015), as well as with myelination in the connected tract and connected thalamic nucleus cell density (Kolasinski et al. 2012). Combined, these studies show that subtle diffuse tissue changes occur in non lesional WM, which may be observed using a combination of MRI sequences, and that GM atrophy is driven by neuro-axonal loss and is linked to WM tract pathology.
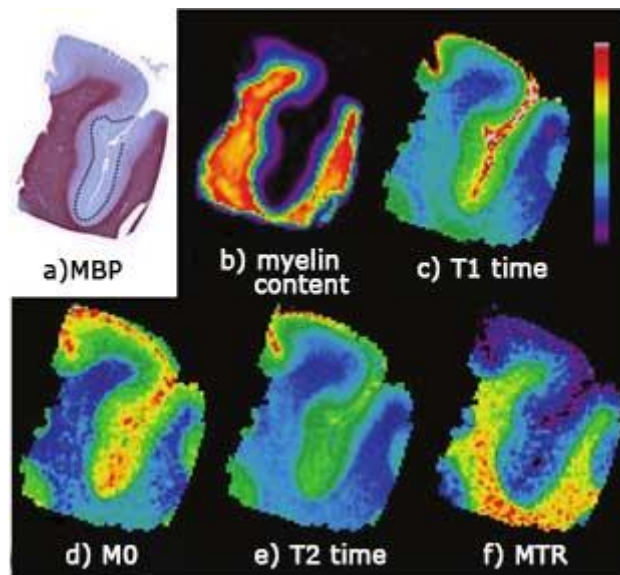
Figure 6.1. Myelin basic protein stain (a), and co-registered myelin content (b; scale: 0-100%) and quantitative MRI maps of post mortem brain tissue of a healthy subject (i.e. T1 time (c; 0.15-0.35s), M0 (d; 3200-4200 a.u.), T2 time (e; 0.03-0.33s), and MTR (f; 5-16%). Myelin content is closely related to MTR. Adapted from Tardif et al 2012.

6.1.3 Correlations between quantified MR and histology

For a more refined understanding of the relationship between MRI scans and the biology they are reflecting, various studies have quantified and correlated MRI and histology metrics. These studies have shown that (short) T2 mainly correlates with myelin content (Moore et al. 2000) and that lower T1 signal is more closely correlated to axonal loss (van Waesberghe et al. 1999), but that the evolution of T1 hypo-intensities corresponds to both myelin and axonal content (Bitsch et al. 2001). FA and MD have been found to be related to myelin concentration, and to a lesser extent with axonal count (Schmierer, Tozer, et al. 2007b).

The present chapter focuses specifically on the association of MTR with myelin, neurons, and astroglia in MS brain tissue, which has been assessed by four MRI-histology studies to date. These four studies show that MTR signal mainly reflects myelin content and to a

lesser extent neuronal content in both GM and WM (Schmierer et al. 2004; Schmierer, Tozer, et al. 2007a; Schmierer, Parkes, et al. 2010; Tardif et al. 2012). The first study at 1.5T showed, in a sample combining NAWM and WM lesions, that MTR correlates most strongly with myelin and to a lesser extent with axon concentration, while not being associated with astrogliosis (Schmierer et al. 2004). A second 1.5T study elaborating on these findings showed that in a comparable sample containing both NAWM tissue and WM lesions f_b as measured by quantitative MTR similarly correlates most strongly with myelin and axonal concentration (Schmierer, Tozer, et al. 2007a). In this study, astrogliosis was also significantly associated with f_b. As f_b was able to distinguish WM lesions from NAWM, and demyelinated and remyelinated lesions, the authors suggested that this metric could be useful in clinical trials for remyelinating agents. A 9.4T study described the difference between NACGM and type 1 and type 3 cortical lesions in different MRI and histological metrics (Schmierer, Parkes, et al. 2010). While this study did not specifically address the underlying histopathological correlates of NAGM and NAWM, it showed that MTR was associated with myelin basic protein concentration. The only study assessing the underlying histopathology of MTR in both GM and WM simultaneously, at a field strength of 3T, was a single brain study which showed that PD, T2, T1 and MTR were all significantly correlated to myelin content (Tardif et al. 2012). Combined, the above studies show that MTR is a valuable tool to detect microstructural pathology in WM and GM, and that MTR is particularly associated with myelin and to a lesser extent with neuronal content.

All four studies on the histopathological substrates of MTR in the MS brain use Pearson correlation analyses combining samples from both lesional and normal appearing tissue in single models, and are based on an implicit assumption that MTR in lesional and normal appearing tissue have the same underlying histopathological substrates. However, at present it is unclear exactly what histopathological substrates contribute to MTR signal

of NAGM, NAWM and lesional GM and lesional WM, and, importantly, whether this is comparable for different tissue types. Furthermore, as these studies use Pearson correlation analyses, it is difficult to draw conclusions regarding the individual contributions of myelin, neurons, and astrocytes to MTR signal, as these metrics may co-vary. To evaluate the individual contribution of these cell types to MTR, the aims of the present study were to (1) compare NAGM, NAWM, and GM and WM lesions in terms of MTR and eleven histological markers, broadly clustering into neuronal integrity, myelin content, inflammation and mitochondrial integrity, and (2) to assess the individual contribution of myelin, axonal, and astrocyte content to MTR signal in these different tissues types. I hypothesise the normal appearing and lesional GM and WM to differ substantially in terms of MTR, and histology. Specifically, MTR is expected to be higher in WM compared to GM and in normal appearing tissue than lesional tissue. Histologically measured myelin content is expected to follow a similar spatial distribution, while neuronal content is expected to be greater in GM than in WM, but also be lower in lesional than normal appearing tissue. Furthermore, markers for inflammation and mitochondria are hypothesised to be higher in lesional tissue than in normal appearing tissue, with a potentially larger presence in WM over GM. Finally, individual contribution of myelin, axonal, and astrocyte content is not expected to be different between tissue types.

6.2 Methods

6.2.1 Tissue handling and MRI image acquisition

Right coronal hemi-slices of sixteen brains of people with MS and four controls with no known neurological condition were collected for the current study. Only limited brain tissue was available as tissue from the brains from which these hemi-slices were taken was also distributed to other research groups. Care was taken that consistently a hemi-

slice from the right hemisphere was taken, in light of brain asymmetries described in chapter 5. For the purpose of this chapter results from five MS cases are presented. Details of the cohort can be found in table 6.2. Of each of these cases a 10-15mm thick slice (P2) was taken of each brain, corresponding to the same anatomical region (i.e. the second slice posterior to the mammillary bodies), as indicated in figure 6.2. This study was approved by our local institutional ethics committee and followed Human Tissue Act guidelines.
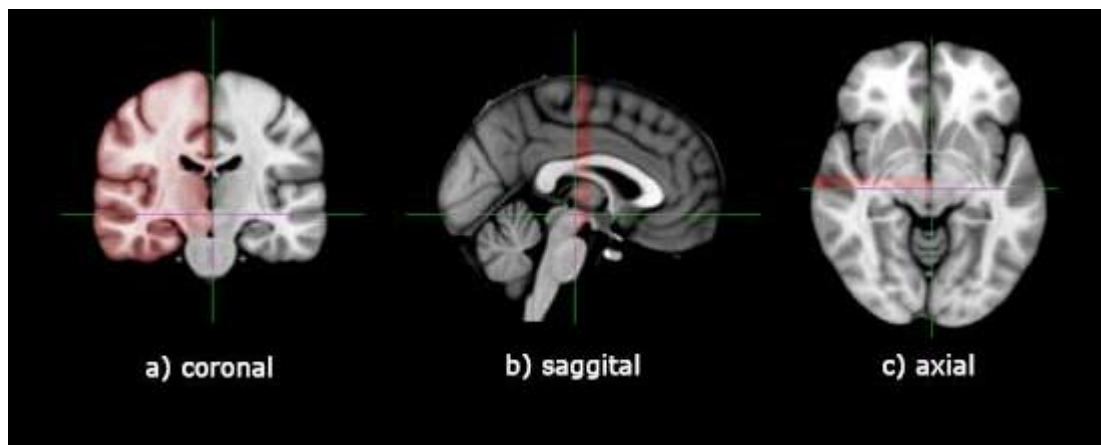
Figure 6.2. MNI brain with a red coloured section indicating the location of the post mortem slice obtained.

Case	Diagnostic classification	Brain weight (g)	Sex	Age (y)	Cause of death	Death-fixation interval (hr)	Histology processing batch
4	PPMS	1413	M	75	MS	25	2
5*	PPMS	1324	F	61	Bronchopneumonia, MS	41	2
9*#	SPMS	1037	F	68	Diabetes type 2, hypertension, MS	47	1
10*#	MS	1225	F	66	Aspiration pneumonia, MS	30	1
11*#	SPMS	1096	F	71	Septicaemia, urinary tract infection, MS	24	1
12*#	SPMS	1126	F	53	Bronchopneumonia, MS	33	1
13	MS		M	50	MS	27	2
14	SPMS	1186	M	64	Bronchopneumonia, MS	33	2
15	SPMS	1184	F	69	Pneumonia	22	2
16	MS	1082	F	75	Food aspiration	48	2
17	SPMS	1021	F	71	Kidney failure, sepsis	12	2
18	SPMS	1471	M	66	Carbon monoxide poisoning	37	2
19#	MS		F	75	Pneumonia	48	2
20#	MS	1561	M	65	Metastatic Colon Cancer, MS	40	3
21	MS		F	63	MS	40	3
22	Control		F	70	Sepsis, stage IV peritoneal cancer, ischemic heart disease		3
23	Control	1315	M	84	Cardiac asthenia amyloid	23	3
24	Control	1324	M	66	Cardiac arrest		3
25	Control	1229	F	70	Metastatic ovarian cancer		3
26#	MS	1221	M	66	Aspiration pneumonia, MS	29	3

Table 6.2. Overview of twenty cases included in the present study. *Fixed tissue MRI and histology data included in present chapter, #tissue scanned both unfixed and fixed.

A detailed tissue handling protocol can be found in Appendix III. In short, out of 20 cases, of which fixed tissue was scanned, tissue of seven cases was scanned both fixed and unfixed. For these cases, unfixed tissue was submerged in PBS and put in an MRI-compatible holder made of Plexiglas and scanned using a 3T Philips Achieva system, with a ~5h protocol at high resolution where possible. MRI sequence parameters can be found in table 6.3. To account for effects of temperature (Tofts et al. 2008; Ruder et al. 2012) tissue was submerged in PBS at room temperature, and temperature measurements were taken before and after scanning. Post MRI, the tissue was submerged fixed through submersion in a 10% buffered formaldehyde solution for a minimum of seven days before the next MRI scan. For the second scan, formalin fixed tissue was washed thoroughly with PBS, submerged in PBS, placed in the MRI compatible holder described above, and scanned using the same protocol as used for unfixed tissue, changing only the PSIR TI to 150ms for improved WM-GM contrast.

	TE (ms)	TR (ms)	Resolution (mm)	Field of view (mm)	
PD/T2	12/80	4000	0.25×0.25×2.00	160×160×16	
3D-T1	6.9	15	0.50×0.50×0.50	160×160×60	
MTR	5.5/12.7	37	0.25×0.25×2.00	160×160×60	
PSIR	13	7000	0.25×0.25×2.00	160×160×16	TI = 400ms (unfixed) and 150ms (fixed)
DTI	69	7000	2.00×2.00×2.00	160×160×16	max B factor = 4000

Table 6.3. Scanning parameters of MRI sequences used.

6.2.2   Histological processing and quantification

For histology, the tissue was subdivided into cassette blocks, ensuring that thalamic grey matter and hippocampal structures were not dissected and would be kept intact. The layout of cassettes was then chosen to include as much tissue as possible for subsequent analyses. The cassette blocks were paraffin-embedded and stained using markers neuronal integrity (NF200), myelin (SMI94), astrocytes (glial fibrillary acidic protein [GFAP]), immune activity (CD20, CD3, CD68, CD8, and IBA1), and mitochondrial function (COX4 and VDAC). To visualise myelin, SMI94 was chosen as this visually gave superior contrast to the commonly used LFB stain. Furthermore, DGM lesions are more difficult to detect on LFB stains compared to stains against myelin specifically (Kipp et al. 2015; Vercellino et al. 2009).

Immunohistochemistry was performed by IQPath (University College London). To minimise within subject variability between cases care was taken to process tissue in three separate batches (as indicated in table 6.2), rather than processing cases individually. The formalin fixed tissues were processed, paraffin-embedded and sectioned at 5μm. Immunohistochemistry staining was performed using the Ventana Discovery XT instrument, and the Ventana DAB Map detection Kit (760-124). See table 6.4 for antibody and epitope damasking detail. When establishing the antibodies initially, the markers are validated with positive and negative controls to ensure the specificity of the epitope. Furthermore, positive controls were used in every run to validate the run if the epitope is not normally or not abundantly present in the brain (i.e. the CD3, CD8, CD68 markers). GFAP, VDAC, COX4, IBA1, SMI94, and NF200 are endogenous to the brain and absence of staining in brain sections would indicate that the run failed. For pre-treatment, either Ventana Protease 1 (760-2018), Ventana CC1 (950-124), equivalent to

EDTA buffer, or Ventana Ribo CC (760-107), equivalent to citrate buffer, was used. Slides were haematoxylin counterstained.

The histology images were subsequently digitised and quantified histology images were generated as follows. Tissue sections were digitised as 8-bit RGB images at ×40 magnification using a Leica SCN400F slide scanner, and digital image analysis was performed using Definiens Developer (version 2.5, Munich) and ×5 resolution for tissue identification and ×10 resolution for stain analysis. A detailed description of the histology quantification can be found in Appendix III. In short, blue and brown staining were separated using different thresholds. The image was segmented into voxels of $250{\times}250\mu m^2$ ($0.0625mm^2$) and the area of tissue, brown stain, dark brown stain, and the number of nucleus objects were exported per pixel with their coordinates within the image for reconstruction purposes. The proportion of surface area covered with dark brown stain was used in the current analyses. From these data, quantified histology images were reconstructed with an in house script in MatLab (version 2012b, The MathWorks Inc., Massachusetts).

Antibody	Clonality	Dilution	Source	Pre-treatment	Primary antibody incubation	Secondary antibody 1:200	
						Swine αrabbit DakoE0353	Rabbit αmouse DakoE0354
SMI94	Monoclonal	1:500	Covance SMI94-R	Extended CC1	32min		32min
NF200	Monoclonal (NE14)	1:200	Sigma N5389	Protease 1 4'	32min		32min
GFAP	Polyclonal	1:1000	DakoZ0334	Protease 1 4'	32min	32min	
CD20	Monoclonal (7D1)	1:200	Dako7D1	Mild Ribo CC	1h		32min
CD3	Monoclonal (LN10)	1:100	Leica PA0122	Standard CC1	1h		32min
CD68	Monoclonal (PG-M1)	1:100	DakoPG-M1	Standard Ribo CC	1h		32min
CD8	Monoclonal (C8/144B)	1:100	DakoM7103	Standard CC1	1h		32min
IBA1	Monoclonal (NCNP24)	1:250	Wako 019-19741	Standard CC1	1h	32min	
COX4	Monoclonal (20E8C12)	1:100	Abcam ab14744	Standard CC1	1h		32min
VDAC	Polyclonal	1:100	Abcam ab15895	Standard CC1	1h	32min	

Table 6.4. Details of stains and antibodies used.

6.2.3 Image processing, histology-MR registration, and generation of ROIs

A histology data set was created grouping eleven digitised stained slides and subsequently down sampled to a resolution of $0.016mm^2$ (from which ten were used for quantification: all except H&E). Most MR volumes (all except T1) consisted of eight planes ($250\times250\mu m^2$) acquired every 2mm; no up sampling was performed. Sub-images, corresponding to the different cassettes within the tissue slice, were obtained by cropping

the original MRI volume to restrict the search space when aligning histology and MRI data (figure 6.3).
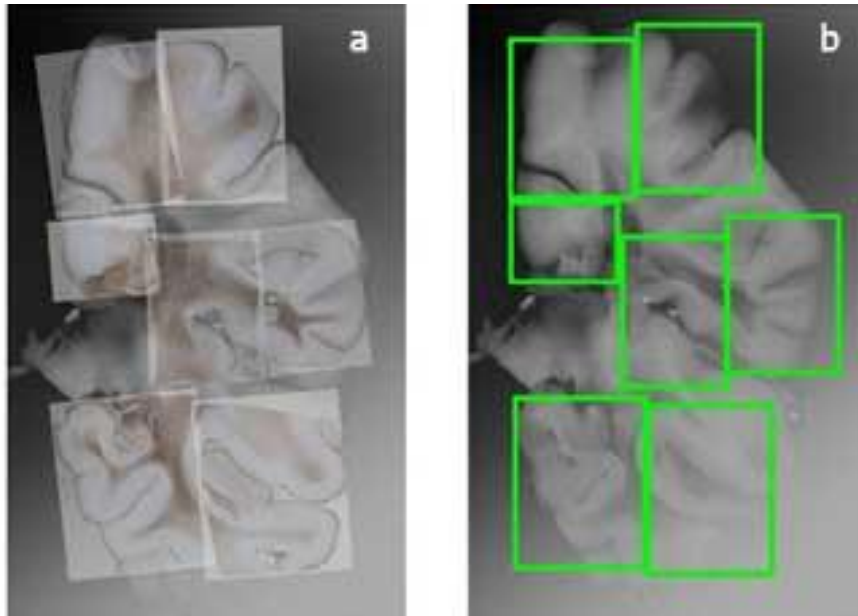
Figure 6.3. Seventh plane from PSIR scan overlaid with GFAP-stained histological slice (a) and corresponding sub regions overlaid on PSIR scan (b).

The process of bringing histology and MR images for each cassette in spatial alignment consisted of the following steps.

1) A group wise space was created by group wise registration of the different stains; which was achieved through consecutive rounds of rigid (1), affine (1) and non-linear (1) registrations (Modat et al. 2010; Modat et al. 2014). The H&E stained images were chosen as a reference.

2) The T2 plane that most resembled the histological slices was chosen and rigid registration was performed between both modalities (Modat et al. 2014). Rigid registration was preferred over non-rigid to preserve the shape of the tissue and to avoid establishing wrong correspondences.

3) The obtained transformations (Modat et al. 2010) were then applied to the selected plane for all the sequences (T2, PD, PSIR, MTR) to bring them into group wise space.

4) Using the transformations obtained during the group wise step, the quantified histology images were resampled into the same space.

After bringing the MR images, histology, and quantified histology images into common space, a single set of ROIs was drawn on the histology and MR images in 3DSlicer (version 4.4.0) (Fedorov et al. 2012). An example can be found in figure 6.4. ROIs for the following thirteen tissue types were drawn: NAWM, NACGM, NADGM, WM lesion (active, chronic active, and chronic inactive), CGM lesion type 1, 2, 3, and 4, DGM lesion, and hippocampal WM and GM. The current chapter includes data from NAWM, NAGM, chronic inactive WM lesions, and GM lesions (grouping GM lesion types 1, 2, 3, and 4). These four tissue types were selected based on the availability of tissue of these tissue classes.
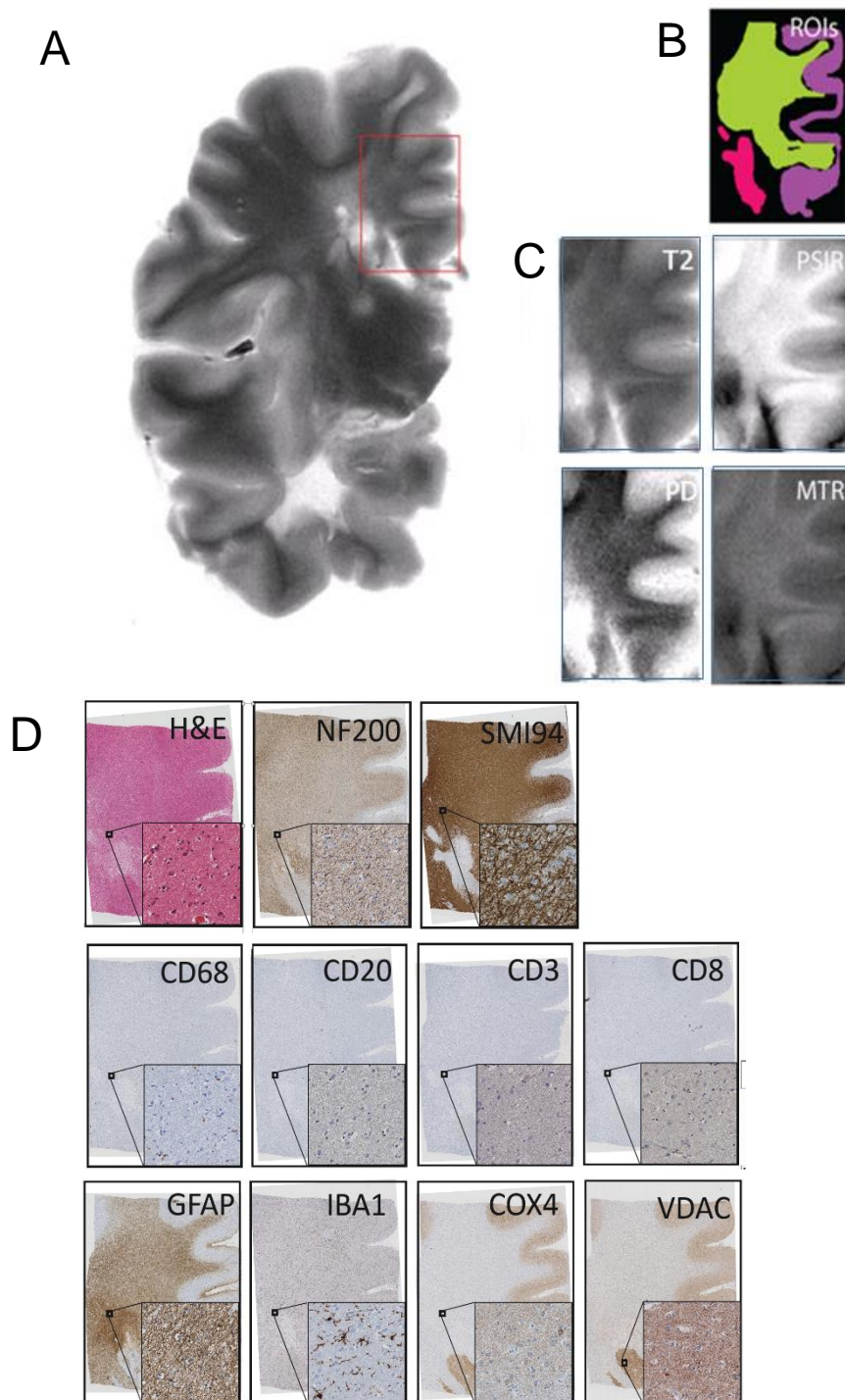
Figure 6.4. Example of a cassette with its corresponding MR images, histology images, and ROIs, from case 12. A) T2-weighted image of whole slice, with a red box indicating the position of a cassette. B) ROIs for normal appearing white matter (green), normal appearing grey matter (purple) and chronic inactive white matter lesions (pink). C) Sections of T2, PSIR, PD, and MTR co-registered to histology images. D) Histology images with high resolution insets at ×40 magnification for cellular presence (H&E), myelin content (SMI94), neuronal content (NF200), lymphocytes positive for CD68, CD20, CD3, and CD8, astrocytic cytoskeleton (GFAP), macrophages (IBA1), and mitochondrial integrity (COX4 and VDAC).

6.2.4 Statistical analyses

From the above mentioned ROIs, using FSLstats, mean MTR and mean histology intensity (from the quantified histology images) was extracted in common space. This was done in two different ways as displayed in figure 6.5: (1) mean signal intensity (for MTR and ten histology images) was extracted from each of the ROIs on each cassette, resulting in eleven values per tissue type per cassette, and (2) to increase power for subsequent statistical analyses, ROIs were subdivided into 'tiles' of 6.4x6.4mm (excluding tiles smaller than 20.48mm^2).

The percentage of dysfunctional mitochondria was calculated as follows.

Percentage damaged mitochondria = (VDAC-COX4)/VDAC
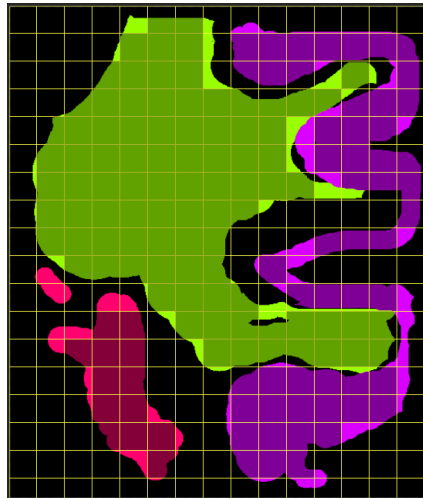
Figure 6.5. Mean MTR and histology intensity was extracted in two different ways. (1) One value is extracted per tissue type i.e. one for normal appearing white matter (green), one for normal appearing cortical grey matter (purple), and one for chronic inactive white matter lesions (pink). (2) The larger ROI is subdivided into smaller 'tiles', of which tiles larger than 20.48mm^2 (dark coloured squares only) are used. From each of these tiles one mean MTR and histology intensity value is taken.

After extracting the MTR and signal intensities, statistical analyses were performed in R (version 3.2.3, R Core Team) on three different data samples: (1) using one mean value per ROI per cassette as described above, (2) using multiple means from the ROI 'tiles' as

described above, and (3) and combining lesional and normal appearing ROIs 'tiles' in a single model at a 1:1 ratio, as previously done in the four only studies to date correlating MTR to histological indices (Tardif et al. 2012; Schmierer, Tozer, et al. 2007b; Schmierer et al. 2004; Schmierer, Parkes, et al. 2010).

To address the first question if tissue types differ in stain intensity and MTR, multilevel mixed models were applied with subject and cassette as nested random effects and the following fixed effects:

$$MTR \text{ or stain intensity} = intercept + ROI$$

For regression analyses to assess the relationship between microglial content and mitochondrial integrity, the following fixed effects were used.

$$Percentage \text{ damaged mitochondria} = intercept + CD68$$

To answer the second question what the individual contributing cellular substrates are to MTR signal intensity within different tissue types, similar mixed effect multiple regression models were performed with the following fixed effects:

$$MTR = intercept + SMI94 \times B1 + NF200 \times B2 + GFAP \times B3$$

Finally, as not all cases had data of all tissue types, in addition to the above analyses on data from all five cases, the above models were performed on data from two cases (case 9 and 12) that had data from tissue types NAWM, NAGM, and chronic inactive WM lesions. This analysis was done to ensure that the inter-subject corrections applied in multilevel mixed effect models did not artificially skew the data due to missing data.

6.3 Results

6.3.1 Different tissue types are associated with specific cellular make up

The 'one mean per ROI per cassette' models and the 'ROI tiles' models gave comparable estimates for mean stain and MTR intensities as displayed in table 6.5 and figure 6.6. The tile models gave highly significant differences in group wise comparisons (all group wise comparisons $p<0.01$, except for CD3 and CD8), but the current section will conservatively focus on results of the 'one mean per ROI per cassette' models in five subjects. Models with data of two and five cases yielded comparable signal intensity estimates, as can be found in Appendix III.

As displayed in table 6.5 and figure 6.6, MTR was significantly higher in NAWM compared to WM lesions ($p<0.05$). SMI94 intensity was significantly higher in NAWM than in NAGM, which in turn had significantly higher SMI94 staining than WM and GM lesions (all $p<0.004$). NF200 staining did not differ significantly between tissue types. Concentration of GFAP was higher in NAWM than in NAGM ($p<0.001$). VDAC was significantly higher in NAGM than in NAWM ($p<0.001$). The proportion of damaged mitochondria was significantly larger in the NAWM than in NAGM ($p<0.001$). CD68 stain intensity was significantly higher in the NAWM than NAGM ($p<0.001$), as was IBA1 stain intensity ($p<0.01$). Further, IBA1 was lower in WM lesions compared to NAWM. CD3 and CD8 staining did not differ between tissue types, and was not significantly different from zero in all tissue types for CD3 and NAGM and GM lesions in CD8. Regression analyses to study the relationship between mitochondrial integrity and CD68 signal showed a significant association in NAWM and WM lesions ($r=0.04$ and 0.135, respectively, and both $p<0.0007$), while in NAGM and GM lesions no such association was found (both $p>0.36$).

		One mean per ROI per cassette				Multiple means from ROI 'tiles'			
		NAGM	**GM lesions**	**NAWM**	**WM lesions**	**NAGM**	**GM lesions**	**NAWM**	**WM lesions**
MTR	mean	30.89	27.00	33.39	26.68	30.58	26.30	34.68	23.20
	SE	3.41	3.84	3.46	3.75	3.55	3.76	3.55	3.64
SMI94	mean	73.31	20.45	93.67	47.5	73.17	7.63	88.28	17.24
	SE	5.56	7.38	5.74	7.24	5.97	6.84	5.96	6.32
NF200	mean	38.27	25.90	48.79	34.81	41.32	21.91	47.09	37.04
	SE	9.80	10.93	9.91	10.72	12.61	12.61	11.92	12.20
GFAP	mean	14.15	18.21	67.31	80.23	2.26	1.01	59.92	46.16
	SE	4.00	5.47	4.14	5.47	12.32	12.91	12.31	12.56
VDAC	mean	71.83	72.10	35.37	36.52	78.43	76.43	39.09	60.16
	SE	6.02	7.69	6.19	7.32	14.57	14.87	14.57	14.69
% mitochondria damaged	mean	0.36	0.27	0.83	0.80	0.42	0.22	0.87	0.60
	SE	0.07	0.09	0.07	0.08	0.10	0.12	0.10	0.10
CD68	mean	0.35	0.26	1.10	0.93	0.49	-0.34	0.98	0.68
	SE	0.19	0.25	0.20	0.24	0.26	0.30	0.98	0.68
IBA1	mean	10.22	10.57	14.87	8.15	13.03	8.1	14.9	9.52
	SE	2.88	3.16	2.91	3.13	4.39	4.50	4.39	4.43
CD8	mean	0.07	0.09	0.09	0.1	0.03	0.01	0.03	0.04
	SE	0.06	0.06	0.06	0.06	0.01	0.03	0.01	0.02
CD3	mean	0.08	0.14	0.09	0.09	0.09	0.16	0.05	0.09
	SE	0.05	0.07	0.05	0.06	0.03	0.05	0.03	0.04

Table 6.5. Mean MTR and histology stain intensity for normal appearing grey matter, grey matter lesions, normal appearing white matter, and chronic inactive white matter lesions, estimated using a single intensity estimate per tissue type and multiple estimates using region of interest 'tiles'. The two statistical approaches yielded comparable estimates.
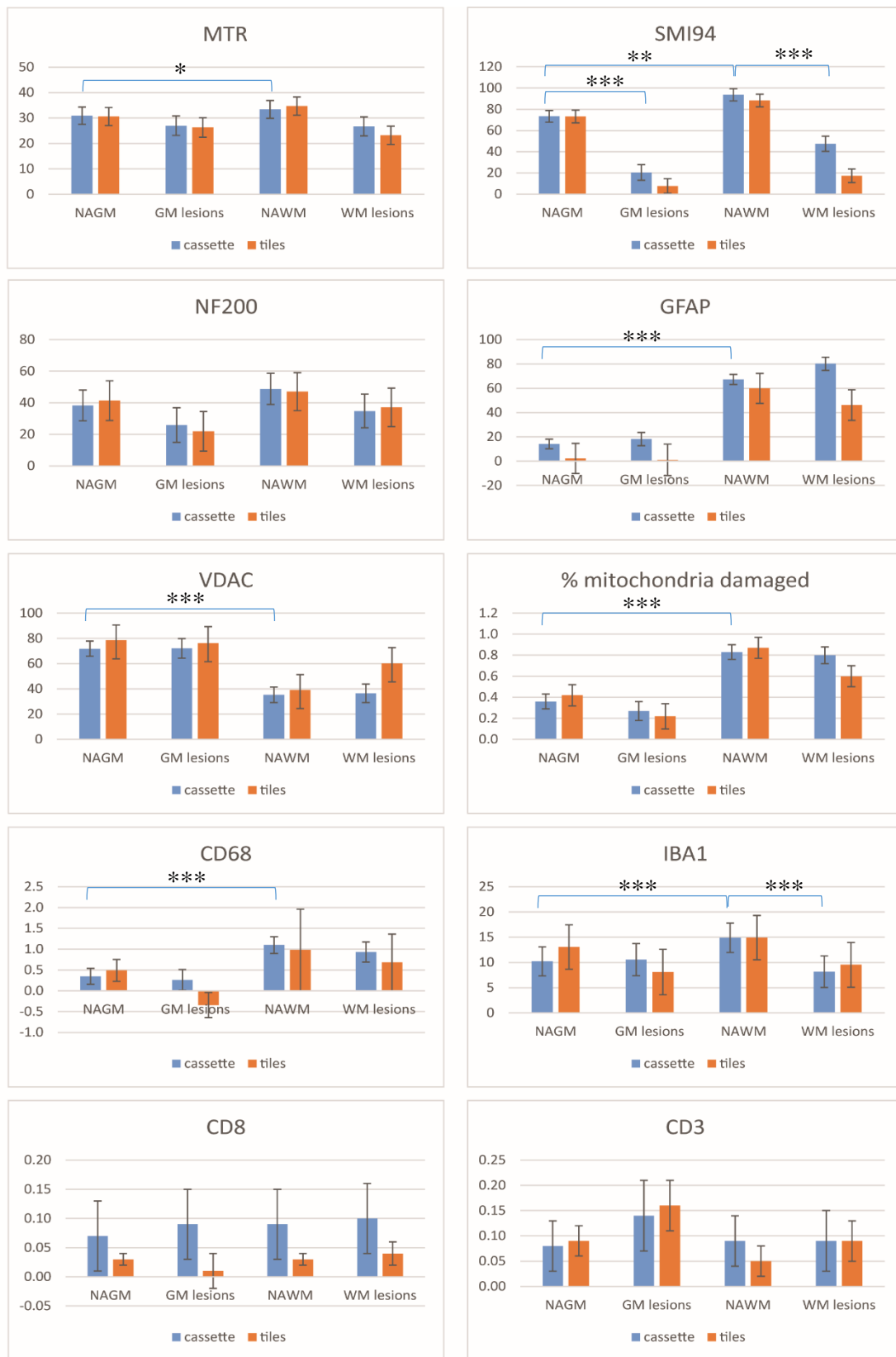
Figure 6.6. Mean MTR and histology stain intensity for normal appearing grey matter, grey matter lesions, normal appearing white matter, and chronic inactive white matter lesions, estimated using a single intensity estimate per tissue type ROI and multiple estimates using ROI 'tiles'. The two statistical approaches yielded comparable estimates. Different tissue types ware associated with specific cellular make up. Statistically significant differences have been indicated. * p<0.05, ** p<0.01, ** p<0.001.

6.3.2 MTR is associated with different cellular substrates depending on tissue type

Results of statistical analyses using samples in which WM lesional and NAWM data were combined in a single model as done previously (Schmierer et al. 2004; Schmierer, Tozer, et al. 2007b; Tardif et al. 2012; Schmierer, Parkes, et al. 2010) showed that SMI94, NF200, and GFAP were all highly significantly associated with MTR (β=0.107, β=0.165, β=-0.125, respectively, all p<0.001), and can be found in Appendix III. The same model for GM lesions and NAGM was not performed, as only a single cassette had both NAGM and GM lesions.

Results from the statistical models on ROI tiles in which data from each tissue type was considered separately showed that the individual contributions of SMI94, NF200, and GFAP to MTR signal intensity differed between tissue types. The results from these analyses are displayed in table 6.6 and figure 6.7. NAWM MTR was predominantly associated with SMI94 (myelin), and had a near significant contribution of NF200 (neurons), but was not associated with GFAP (astrocytes). NAGM MTR was associated positively with SMI94 and negatively with GFAP, but was not associated with NF200. MTR in GM and WM lesions was not associated with any histological marker.

	SMI94			NF200			GFAP		
	β	95% CI	P	β	95% CI	p	β	95% CI	p
NAWM	0.152	0.094 – 0.210	<0.001***	0.028	-0.003 – 0.059	0.072	-0.013	-0.039 – 0.013	0.316
NAGM	0.068	0.020 – 0.116	0.006**	-0.007	-0.049 – 0.034	0.737	-0.057	-0.101 – -0.012	0.013**
WM lesions	0.019	-0.043 – 0.082	0.543	-0.021	-0.014 – 0.102	0.739	-0.048	-0.013 – 0.029	0.229
GM lesions	0.121	-0.179 –– 0.203	0.227	-0.103	-0.288 – 0.081	0.286	-0.199	-0.042 – 0.025	0.097

Table 6.6. Individual associations of SMI94 (myelin), NF200 (neurons), and GFAP (astrocytes) with MTR. MTR was significantly associated with SMI94 in normal appearing white and grey matter, but not in lesional tissue.
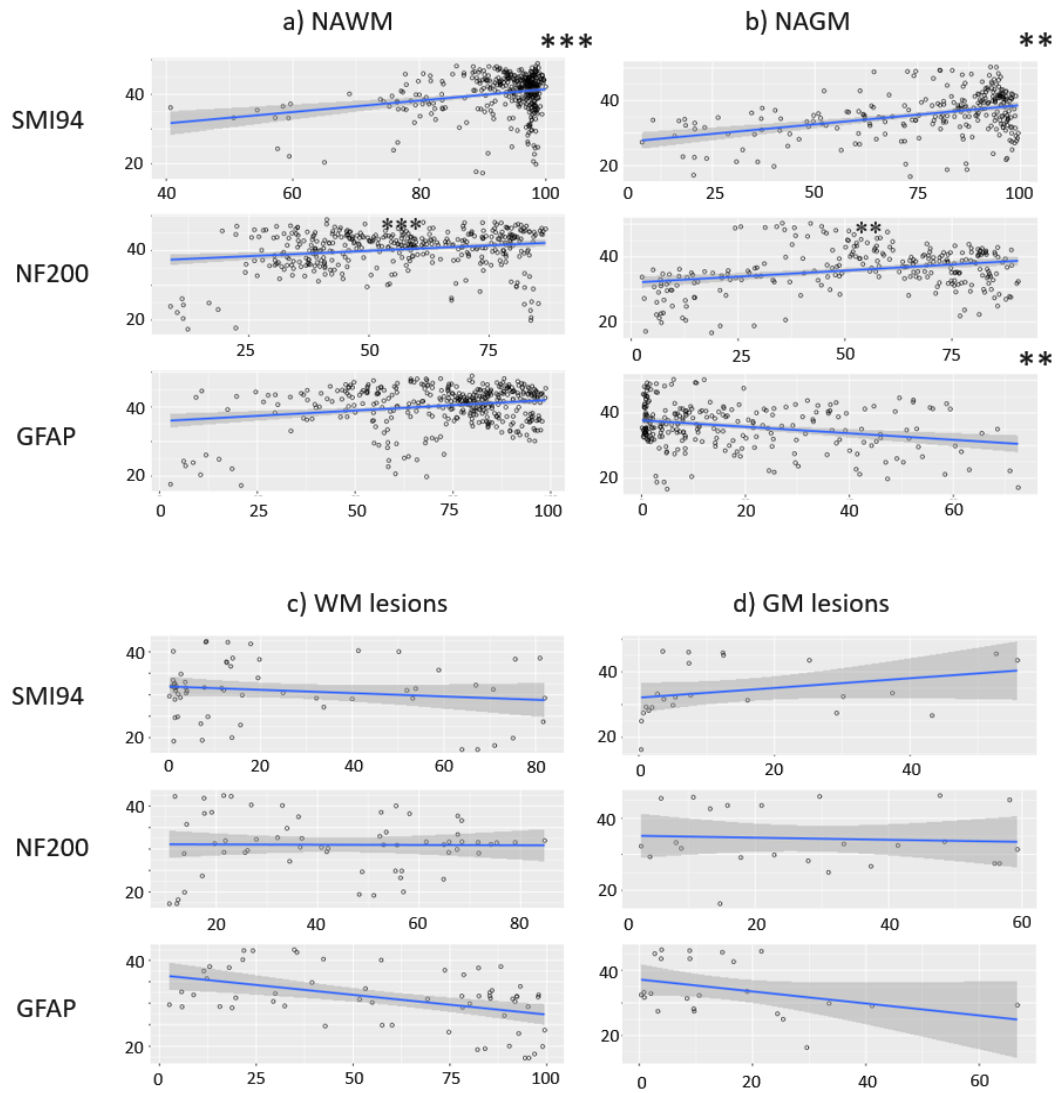
Figure 6.7. Scatter plots of the association of SMI94, NF200, and GFAP with MTR for normal appearing white matter (a), normal appearing grey matter (b), chronic inactive white matter lesions (c), and grey matter lesions (d). Statistically significant association have been indicated ** p<0.01, ** p<0.001

6.4   Discussion

The main findings of the current study are that 1) the cellular make-up of NAWM, NAGM, and WM and GM lesions differs significantly. 2) Diffuse microglial presence may be linked to mitochondrial damage in WM tissue. 3) MTR was underpinned by myelin and to a lesser extent by neuronal content in normal appearing, but not lesional, GM and WM tissue.

6.4.1   Differences in MTR and cellular content between tissue types

NAWM, NAGM, and WM and GM lesions differed significantly in their cellular make up. Methodologically, the 'one mean per ROI per cassette' and 'ROI tiles' models yielded similar estimates of signal intensities, and this section will conservatively discuss the results of the 'one mean per ROI per cassette' models.

As hypothesised, myelin content (as measured by SMI94) was found to be significantly higher in NAWM than in NAGM, and both GM and WM demyelinated lesions showed decreased myelin levels compared to normal appearing tissue. While not significant, levels of phosphorylated neurofilament (as measured by NF200) showed a similar pattern. NF200 is a marker for phosphorylated neurofilament rather than intact neurofilaments and widespread accumulation of hyperphosphorylated neurofilament protein can also be found in MS neuronal somata, particularly in the cortex (Gray et al. 2013). These changes in phosphorylation of neurofilaments have been suggested to play part in the damage to neuro-axonal constructs in MS (Petzold et al. 2011; Petzold et al. 2008), and as such, the observed larger NF200 staining in normal appearing WM and GM compared to lesional WM and GM may reflect two separate pathological processes in the MS disease process, i.e. changes in phosphorylation of neurofilaments, as well as neurodegeneration. In line with previous work (Goursaud et al. 2009), GFAP-expressing astrocytes were more abundant in normal appearing and lesional WM than in GM. As expected, there was an

124

absence of CD8 and CD3-positivity in the different tissue types, as T-cells expressing these markers are mainly found in active lesions and are not abundant in normal appearing tissue or inactive lesions (Tzartos et al. 2008; Haider et al. 2011). In addition, the inherent selection bias in post mortem studies led to the inclusion of tissue of cases with secondary progressive or long standing MS, who therefore show less ongoing inflammatory demyelination.

Overall mitochondrial concentration (as measured by VDAC) was highest in GM (both lesional and normal appearing), compared to WM. However, the proportion of these mitochondria that had COX4 loss, which occurs when the mitochondrial transport chain ceases, was larger in (both lesional and normal appearing) WM than in GM. Previous work observing lesion-independent reduction of mitochondrial function (as measured by N-acetyl aspartate) of 25-33% in CGM and a 36-45% reduction in WM echoes the present findings (Li et al. 2013). The larger proportion of mitochondrial damage in WM compared to GM may be explained by the here observed and previously described (Peterson et al. 2001) higher concentration of microglia/macrophage activity (as measured by CD68 and IBA1), particularly in PPMS and SPMS (Kutzelnigg et al. 2005), and also corresponds to the reported presence of iNOS releasing astrocytes and microglia in the NAWM (Zeis et al. 2009; Broholm et al. 2004). Regression analyses addressing this association show that, while the association is weak, a statistically significant link exist between mitochondrial presence and mitochondrial damage. Independent of myelin loss, these activated microglia may cause diffuse hypoxic mitochondrial damage in the NAWM through mechanisms including the release of reactive oxygen species resulting in oxidative stress (Witte et al. 2010; Witte et al. 2014; van Horssen et al. 2011).

Combined, in line with the hypotheses set out in the beginning of the chapter, the present findings show a difference in cytological make up between NAWM, NACGM and

(chronic inactive) WM and GM lesions, and provide further evidence for diffuse non-lesional pathological mechanisms via microglia-mediated mitochondrial damage.

6.4.2   MTR has different underlying histopathological substrates in normal appearing tissue and lesions

MTR was underpinned by different underlying histopathological correlates in different tissue types, as shown by the models using data from ROI 'tiles'. Methodologically, the 'one value per ROI per cassette' models did not converge as the sample size (20 cassettes of five MS cases) proved insufficient and over parametrised the mixed effect multiple regression models. Therefore, the use of sampling multiple ROIs ('tiles') from the same cassette was evaluated by comparing the means to those from extracting a single value and these approaches gave comparable MTR and stain intensity estimates. In addition to yielding comparable mean estimates, this approach was useful for the purposes of the present study as the main aim of this study was to look for associations between histopathology and MRI and not necessarily comparing findings between cases.

The main finding of the current work is that MTR has different underlying histopathological substrates in normal appearing and lesional tissue. NAWM and NAGM MTR was mainly associated with myelin content, as previously reported (Schmierer et al. 2004; Schmierer, Tozer, et al. 2007b; Schmierer, Parkes, et al. 2010), but no association between MTR and myelin was found in lesional tissue.

NAWM MTR was highly independently associated with myelin content and showed a near significant association with neuronal content. This finding agrees with findings previous work (Schmierer et al. 2004; Schmierer, Tozer, et al. 2007b), which used Pearson correlation analyses in which data from normal appearing tissue and lesions were combined. The current study used more refined statistical mixed effect regression models, in which normal appearing tissue was analysed separately from data from lesional tissue,

126

and these models show that in NAWM MTR was associated with myelin content *independently* of neurons and astrocytes. In addition, these previous studies were done at 1.5T and 9.4T, at different resolutions than described here.

Similarly, NAGM MTR was mainly associated with myelin content, as reported before (Schmierer, Parkes, et al. 2010), and showed a negative association with astrocytes, which contrasts to previous work which reported an absence of a correlation between MTR and gliosis (Schmierer, Parkes, et al. 2010). This discrepancy may partly be explained by the use of multiple regression models in the present study, as opposed to Pearson correlations in the previous work, allowing the study of associations independent of the stronger association between MTR and myelin; the previously described correlation between axonal content and MTR (Schmierer, Parkes, et al. 2010; Schmierer et al. 2004) may be partially explained by the stronger correlation between myelin content and MTR, and between myelin content and axonal content.

Importantly, whereas MTR in NAGM and NAWM was predominantly associated with myelin content, lesional GM and WM MTR did not show any association with histological markers. Both GM and chronically inactive WM lesions have lower MTR and lower SMI94 and NF200 levels, but in these tissue types no link between MTR and myelin (and neurons) was found.

As described above, the discrepancy between the present findings and previous studies may be explained by the statistical methods applied in the present and previous studies. To illustrate the differences between the statistical analyses performed in the current work and in the studies described previously, comparable statistical models that were applied in the previous studies were evaluated on the present data, combining non-lesional and lesional tissue for WM in single models (Schmierer et al. 2004; Schmierer, Tozer, et al.

2007b; Schmierer, Parkes, et al. 2010; Tardif et al. 2012). GM data were not analysed as the sample size was not sufficient. This analysis showed highly significant independent positive associations between WM MTR and myelin and neurons, as reported in these previous studies, (as well as a negative association with gliosis). Grouping lesional and non-lesional data therefore illustrates that independent associations between MTR and myelin, neurons, and gliosis exist, but when refining this model by looking at single tissues only, this association appears absent in lesional tissue, and seems to be mainly driven by their correlation in normal appearing tissue.

6.4.3 Methodological considerations

To interpret the current study, a number of limitation should be taken into consideration. Post mortem studies have an inherent bias towards including tissue of people with late stage or more aggressive MS. Of the sixteen people with MS included in the current study, seven had clinically defined SPMS, confirming this bias.

In previous MRI-histology studies, tissue was scanned submerged in formalin, fomblin, and PBS (Schmierer, Tozer, et al. 2007a; Schmierer et al. 2004; Gilmore, Geurts, et al. 2009b; Geurts, Pouwels, et al. 2005). While not presented in the present work, unfixed tissue was found to be scanned best submerged in PBS compared to formalin, which would fix the tissue, or fomblin, which affects binding affinity of the chosen histological markers. The fixed tissue was scanned in PBS rather than in formalin, which is commonly used in *post mortem* MRI, because free flowing formalin severely reduces T2 relaxation (Bossart 1999). Our average MTR values from fixed tissue were somewhat lower than those reported in vivo: NAGM: 30.7 and 31.9, respectively, and NAWM: 34.0 and 37.9 (Davies et al. 2004).

The current study assesses the relationship between MTR and quantified histological measures. To this end it is important to note that while care was taken to run the histology on tissue in as few processing batches as possible rather than processing the cases individually, the quantification of the histology has a number of limitations reducing the interpretability of the subsequent statistical analyses. Firstly, in addition to average stain intensity, the number (or density) of positive cells could have yielded a more robust metric. Secondly, while to ensure specificity of the makers the histology stains were established using both positive and negative controls and the staining was ran using positive controls, the threshold used for the histology quantification was based on thresholds that were not validated with the use of these controls. The mixed effects models used subsequently reduced within-subject variance, but will not have been able to address this limitation of thresholds. By using additional quantification methods, future analyses of the currently presented data (as well as of the remaining cases) will address this specific limitation. This will include an in-house ImageJ script that in addition to stain intensity also obtains the number and density of positive lymphocytes. Correlation analyses between stain intensity and cell counts will be performed, and both metrics will be used in subsequent statistical analyses.

The MTR scans had a slice thickness of 2mm, whereas the histology image had a slice thickness of 20µm. This means that while in-plane registrations were comparatively accurate, registrations in the third dimension was less precise. Although this is a common limitation in MR-histology studies, this reduces our ability to correlate MR indices to histology, as correlations are evaluated between data from different volumes.

Finally, histology images suffer from deformations/alterations resulting from their preparation, which makes the process of visually matching histology and medical images complicated and biased. The histology-MRI registrations used in the present work were

data-driven, and are likely to introduce less bias than manual registrations using anatomical landmarks as is the most common approach in post mortem MRI studies. The semi-automated histology-MR registration used allows better reproducibility and accuracy through the (automatic) optimisation of a cost function: it takes into account the degree of similarity between two images and other criteria—in the case of deformable registration—that control the transformation by allowing certain behaviours. Aligning histology with an MR plane was performed though a combination of non-linear and linear transformations, which respectively created the histology group wise space and a mapping between both. Non-linear registration was based on free-form deformations and linear registrations were based on a block-matching approach. While the resulting registered images required visual inspection, this method is more robust and reproducible than manual registrations.

6.5   Conclusions and future directions

The current study describes the underlying histopathological substrates of normal appearing and lesional GM and WM, and how these cellular markers relate to MTR to gain better insight in what this scan type represents. The present chapter includes data from five MS cases, and the interpretation of the findings presented here are therefore only applicable to other MS studies. The analysis of data of tissue from healthy controls would add substantial value to this work, as this will allow tissue characteristics that may occur specifically due to the MS disease process. As mentioned below, this is one of the main priorities for the continuation of this project.

A difference in cytological make up was found between NAWM, NAGM and lesional WM and GM, and provide further evidence for diffuse non-lesional pathological mechanisms via microglia-mediated mitochondria damage. Furthermore, MTR was found to have different histopathological substrates depending on whether it is measured

in lesional or normal appearing tissue: MTR is associated with myelin content in normal appearing tissue, but this relationship appears absent in demyelinated cortical lesions or chronic inactive WM lesions, and this finding may have consequences for the interpretability of in vivo MTR scans and the use of this scan type in remyelination trials. Further analyses of the acquired data, comparisons to controls, and other tissue types (active WM lesions, DGM, etc.) will provide further insight into the biological correlates of MTR. Particularly, in light of the finding of substantial damage to DGM structures including the thalamus, as also presented in chapters 4 and 5, one of the main priorities of future work is to analyse data obtained from ROIs with DGM tissue.

The current work may be elaborated upon in five specific ways. Firstly, in this chapter data of twenty cassettes of five cases have been included. Even in this subsample of the twenty cases scanned, important significant differences were detected between tissue types. These findings are expected to be strengthened after analysing the remaining data, which also include control data. Secondly, as mentioned above, only four types of tissue have been analysed (i.e. normal appearing CGM, NAWM, GM lesions, grouping cortical lesion type 1, 2, 3, and 4, and chronic inactive WM lesions), and to aid interpretability of MTR scans in remyelination trials, it is particularly valuable to analyse different (demyelinated and remyelinated) lesion subtypes. Furthermore, as DGM pathology occurs early and disproportionally in the MS disease process, as also described in chapter 4 and 5, it of particular importance to expand the current work to establish the histopathological correlates of DGM abnormalities. Thirdly, while in the current study data was not obtained from tissue from both hemispheres, the brain asymmetries described in chapter 5 may be evaluated with future work by taking samples from both hemispheres for comparative analyses Fourthly, in this chapter MRI data of fixed post mortem tissue is presented which will have been affected by the fixation process. It has been reported that GM and WM T1 and MTR signal is affected similarly (Schmierer,

Thavarajah, et al. 2010). To reproduce these findings and to describe these changes in lesional tissue, future analyses of fixed and unfixed these data will be performed to translate the current findings towards clinical scans. Finally, more refined statistical analyses may be applied, including partial component analyses to assess if the histological markers used cluster into different categories which may have stronger independent associations with MTR (and the yet unanalysed DTI data) than the individual histological markers alone.

Chapter 7

Conclusions and future directions

The current thesis aimed to provide insight into the clinical impact, the spatiotemporal distribution, and histopathological correlates of MRI-detected MS pathology, with a specific focus on GM. As outlined in chapter 3, this work consists of three independent MRI studies which include in vivo, post mortem, and histological investigations, and specifically aimed to answer the following questions.

1) Do GM lesions and GM atrophy co-localise, and what is their independent contribution to clinical disability in vivo?

2) Can thalamic and cortical GM pathology, as detected by in vivo MTR MRI, be explained by prior damage to connecting WM tracts, or vice versa?

3) What are the independent underlying histopathological substrates of MTR abnormalities of CNS pathology in MS? Are they the same in NAGM, NAWM, and lesional GM and WM?

7.1 Key findings

The main findings of the present work are as follows.

1) DIR-detected GM lesions do not consistently co-localise with GM atrophy, as these GM lesions are mainly found throughout the entire cerebellar and cerebral cortex, whereas consistent atrophy was found predominantly in subcortical GM structures. Both GM lesions and atrophy contributed to disability, suggesting that the substrates of disability in MS are both pathologically and spatially heterogeneous.

2) WM injury to thalamo-cortical systems is found to precede (both thalamic and cortical) GM damage. Furthermore, lower regional cortical MTR was not found to be associated with lower volume, suggesting that significant cortical microstructural damage can occur in MS in the absence of atrophy. Finally, in both people with MS and healthy controls highly significant hemispheric differences exist in MTR and regional cortical volume, as well as significant MTR heterogeneities within and between thalamo-cortical tracts, emphasising the need to account for this in statistical models to detect disease-specific changes.

3) MTR is associated with histologically quantified myelin (and to a lesser extent neuronal content) in NAGM and NAWM tissue, whereas this relationship appears absent in demyelinated cortical lesions or chronic inactive WM lesions. This finding may have consequences for the interpretability of in vivo MTR scans and the use of this scan type in remyelination trials. In addition, the cytological make-up has been found to differ between NAWM, NAGM and lesional WM and GM, and provides additional evidence for microglia-mediated mitochondria damage in normal appearing MS tissue.

7.2   Specific conclusions regarding methodology

As described in chapter 2, MRI has proven invaluable in the study of GM injury in MS. The MRI sequences used in the current thesis allow the visualisation and the study of different manifestations of GM pathology.

In chapter 3, 3D T1-weighted volumetric scans allowed an estimate for regional and global atrophy via registrations to a cohort-specific DARTEL template, while DIR scans visualised GM lesions. As mentioned in the discussion of chapter 3, DIR scans are suboptimal in the visualisation of GM lesions, and prospectively only detect an estimated 18% of histopathologically detected cortical lesions (Seewann et al. 2012). Novel MRI

sequences with fewer artefacts, such as the PSIR scan (Sethi et al. 2012), may allow better assessment of GM lesions in vivo.

As significant anatomical asymmetries exist in the brain, as well as MTR heterogeneities within and between cortico-thalamic tracts, as described in chapter 5, studies assessing CNS pathology may benefit from more refined statistical analyses in which left and right ROIs are analysed separately, or where adjustments are made for side. Similarly, subdividing WM into smaller ROIs may aid in distinguishing disease-specific changes in MTR from intrinsic tissue heterogeneities.

Finally, in chapter 4 and 5, MTR was used to study GM abnormalities. MT scans make use of cross-relaxation properties of freely moving protons and protons with restricted motion which are thought to be bound to macromolecules (Enzinger et al. 2015; Henkelman et al. 2001), as described in chapter 2. It has previously been shown that MTR signal correlates predominantly with histologically quantified myelin content in the brain (Schmierer et al. 2004; Schmierer, Tozer, et al. 2007b; Schmierer, Parkes, et al. 2010). However, the associations I these previous studies between myelin and MTR may be partly attributed to the statistical models used, in which data of normal appearing and lesional tissue were combined, whereas the study described in chapter 6 suggests that MTR may have different histopathological substrates in lesional and normal appearing tissue.

7.3   Specific conclusions regarding MS pathology

Chapter 4 describes that DIR-detected GM lesions and atrophy do not consistently co-localise, as DIR-detected lesions were mainly found throughout the entire cerebellar and cerebral cortex, whereas GM atrophy mainly affects DGM structures. This spatial dissociation suggests that different pathogenic processes may underlie these forms of

injury, and is further supported by the observed differences between MS subtypes differed in patterns of GM lesions and atrophy.

Chapter 5 describes longitudinal associations of MTR thalamo-cortical WM tracts with subsequent MTR in thalamic and cortical GM. While the results of this chapter suggest a potential WM to GM evolution independent of anatomical connectivity, this study was not able to exclude tract-mediated pathology as a link between these forms of tissue damage. These findings may be interpreted as being part of a wider stage-dependent process leading to both WM and GM tissue damage. Possible pathogenic mechanisms may include wide spread inflammation (Lassmann et al. 2012), and the presence of microglia inducing a more generalised diffuse pathology (Kutzelnigg et al. 2005). This is in line with the finding of diffuse microglial activation, and corresponding mitochondrial damage in NAWM and NAGM in chapter 7. Alternatively, or additionally, a tract-specific spread of pathology may be induced by anterograde trans-neuronal degeneration, retrograde trans-neuronal degeneration, or Wallerian degeneration (Kipp et al. 2015).

7.4 Future directions

To gain further insight into pathophysiology of clinically relevant GM injury in MS, analyses in chapter 5 may be refined by looking at differences between MS subtypes, as the MS subtypes differ in terms of GM and WM damage. Furthermore, it is important to assess the correlations between damage to individual cortico-thalamic systems and clinical performance.

In addition, chapter 6 presents data of five cases, while data have been obtained of 20 cases including four controls. Analyses of the remaining cases is likely to strengthen the findings by making the statistical models more robust. Additionally, analyses of different tissue types may provide insight into if the histopathological substrates of MTR (and DTI)

136

differ between these other tissue types. Finally, more sophisticated statistical models may be applied, including partial component analyses and machine learning approaches to assess whether the histopathological metrics cluster into different groups.

Appendix I - Supplemental material chapter 4

Domain	Region	Side	cm³	Peak T-value	MNI coordinates of local maxima		
					x	y	z
Executive function	Precentral Gyrus	R	0.08	3.75	48	8	29
	Inferior Frontal Operculum	R	0.24	3.84	49	9	28
	Anterior cingulum	L	0.07	3.48	-2	43	14
	Cerebellum Crus1	R	0.18	3.51	40	-65	-37
	Cerebellum Crus2	R	0.04	3.48	40	-65	-38
	Cerebellum 8	R	0.01	3.32	38	-57	-47
Memory function	Superior frontal lobe	R	0.01	3.29	17	3	72
25TWT	Cerebellum Crus2	L	0.02	3.31	-30	-77	-36
zPASAT	Supramarginal gyrus	R	0.01	3.28	58	-39	33
	Cerebellum Crus1	L	0.01	3.34	-29	-60	-38
	Cerebellum 6	L	0.03	3.59	-27	-58	-35
z9HPT	Precentral gyrus	R	0.04	3.36	11	-24	75

Supplemental table 4.1. Regions with increased lesion probability associated with poorer performance in clinical domains thresholded at p=0.001 uncorrected. Lesion load in the cerebellum in particular is related to poorer executive, TWT speed, and PASAT performance.

Domain	ROI	Total grey matter volume				GM lesion volume			
		B	**SE**	**p**	**Adj R²**	**B**	**SE**	**P**	**Adj R²**
EDSS	Cerebellum	-0.053	0.022	0.018	0.203	*2.562*	*0.960*	*0.009*	*0.216*
	Postcentral gyrus	*-0.294*	*0.093*	*0.002*	*0.242*	5.441	2.326	0.022	0.199
Executive function	Cerebellum	*0.042*	*0.015*	*0.006*	*0.067*	-1.567	0.665	0.021	0.038
Memory function	Cerebellum	0.026	0.011	0.020	0.066	*-1.205*	*0.483*	*0.015*	*0.072*
	Postcentral gyrus					-2.695	1.164	0.023	0.062
25TWT	Cerebellum	*0.014*	*0.006*	*0.020*	*0.156*	-0.543	0.244	0.029	0.148
	Postcentral gyrus	0.062	0.024	0.014	0.164	*-1.574*	*0.574*	*0.008*	*0.176*
zPASAT	Cerebellum	0.047	0.012	<0.001	0.150				
	Insula	0.336	0.099	0.001	0.122				
	Medial temporal lobe	0.286	0.094	0.003	0.098				
	Postcentral gyrus					-2.842	1.399	0.032	0.076
	Prefrontal lobe	0.026	0.011	0.025	0.052				
z9HPT	Cerebellum	0.023	0.009	0.016	0.100				

Supplemental table 4.2. MRI abnormality (volume loss and/or lesions) in ROIs significantly associated with poorer clinical function. If both volume loss and increased lesion burden is associated, the strongest contributor is presented in italics.

Appendix II – Supplemental material chapter 5

Follow up global comparisons

At follow up, average T2 lesion volume in the MS group was 11.51±1.73ml. No controls had lesions. Using the same models as for baseline, thalamic volume was similarly found to be significantly lower in MS (5.27±0.12ml) than controls (6.90±0.28ml, p<0.001), with the left thalamus being significantly larger than the right (0.15±0.03ml, p<0.001). Total CGM volume was not significantly different between the MS group (478.68±3.47ml) and controls (485.92±.0.80ml, p<0.419). Global cortical MTR, NAWM MTR, and DGM MTR were not significantly different between people with MS (CGM: 31.56±0.15, WM: 39.35±0.15, DGM: 33.82±0.14) and controls (CGM: 31.97±0.35, WM: 39.78±0.34, DGM: 34.42±0.32, all p>0.101).

		MS	Controls	p-value	Right – left (only presented if significant)	p-value
Thalamic group MTR	MG	34.69±0.19	35.34±0.34	0.178		
	LG	36.79±0.22	37.30±0.51	0.366	-0.23±0.09	0.015*
	PG	34.68±0.20	35.43±0.46	0.140	-0.42±0.10	<0.001***
White matter tract MTR	MG-PFC	39.34±0.17	39.93±0.38	0.168	0.30±0.11	0.007**
	LG-SMC	39.09±0.17	39.53±0.40	0.333	-0.41±0.09	<0.001***
	PG-OCC	38.58±0.20	40.10±0.46	0.003**	-0.81±0.11	<0.001***
Cortical grey matter MTR	PFC	32.60±0.17	33.08±0.37	0.934		
	SMC	33.60±0.18	33.94±0.39	0.973		
	OCC	32.11±0.20	32.84±0.43	0.318	-0.38±0.08	<0.001***
Cortical grey matter volume (ml)	PFC	64.32±0.45	62.59±1.07	0.143	1.44±0.23	<0.001***
	SMC	31.47±0.21	32.43±0.50	0.081	-2.02±0.19	<0.001***
	OCC	44.27±0.33	44.36±0.80	0.018*		

Supplemental table 5.1. Follow up differences between the MS group and controls in MTR and volume of thalamic nuclei, WM tracts, and cortical grey matter. Highly significant left-right differences were observed. MTR and volume differences between patients and controls were only seen in the posterior-group-occipital cortex system.
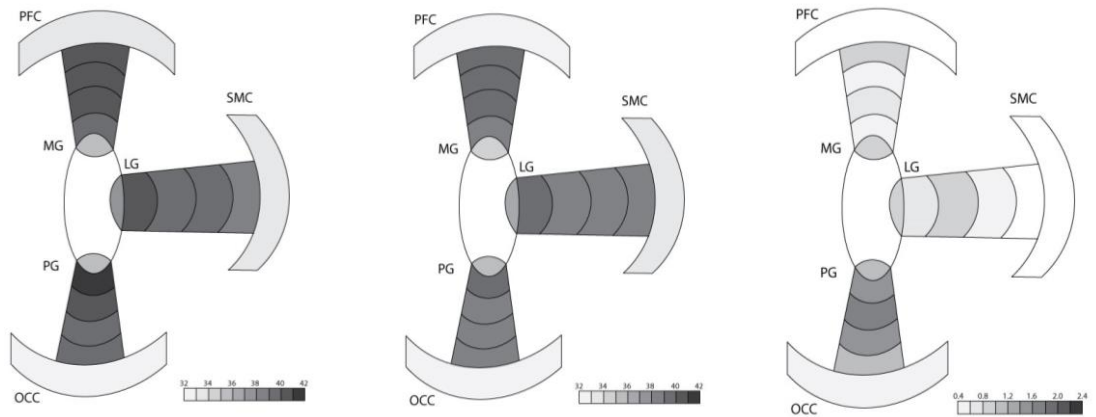
Supplemental figure 5.1. Follow up mean MTR values in controls (left), MS (middle), and difference between MS and control (right).

Part of thalamo-cortical system		EDSS		PASAT		TWT average speed		9HPT	
		B	p	B	p	B	p	B	p
MG-PFC	tract		n.s.		n.s.		n.s.	0.28	0.050
LG-SMC	tract		n.s.		n.s.		n.s.		n.s.
PG-OCC	tract	-0.22	0.024	0.03	0.039	0.94	0.037	0.44	0.010
PFC	cortex		n.s.		n.s.	0.62	0.049	0.26	0.029
SMC	cortex	-0.17	0.046		n.s.	0.75	0.046		n.s.
OCC	cortex	-0.23	0.004		n.s.	1.00	0.005	0.46	0.001
MG	thalamic group	-0.23	0.023	0.03	0.031	1.18	0.009	0.58	<0.001
LG	thalamic group	-0.28	0.028		n.s.	1.28	0.016	0.61	0.002
PG	thalamic group	-0.26	0.012	0.03	0.031	1.28	0.006	0.61	<0.001

Supplemental table 5.2. Follow up associations between MTR in tract, cortex, and thalamic group ROIs of the three thalamo-cortical systems and clinical function assessed by EDSS, PASAT, TWT and 9HPT.

Appendix III - Supplemental material chapter 6

NMR Research Unit
UCL Institute of Neurology

Post mortem tissue handling protocol

Steven van de Pavert
Queen Square MS Centre, Institute of Neurology
University College London

Tissue transport

1) Upon patient death, Djordje Gveric from the Multiple Sclerosis and Parkinson's Tissue Bank, Imperial college, calls Steven van de Pavert
2) Steven books MRI scanner time that evening
3) Steven takes 4% PBS solution out of fridge for it to reach room temperature or creates new PBS solution
4) Steven notifies Marie Braisher that he is collecting fresh tissue
5) Steven travels to Imperial College brain bank with
   - Cool bag
   - Tupperware container with Plexiglas plates
   - Zip lock bags
   - Thermometer
   - Folder with Human Tissue Act form, Site transfer form, and Sample tracker forms
6) Steven attends dissection
7) Photos are taken of tissue on mm grid paper
8) Temperature of tissue is recorded
9) Steven receives tissue and puts it in zip lock bag in Tupperware container without addition of fluids or ice
10) Sample tracker forms are filled out
11) Sample Site Transfer form is filled out
12) Steven travels to Queen Square
13) Steven notifies Marie of arrival at Institute of Neurology, UCL
14) Sample transfer document is filled out and signed

Scanning of fresh tissue

15) In the cut up room of the Division of Neuropathology, Institute of Neurology, UCL, tissue is taken out of zip lock bag
16) Tissue is placed on millimetre grid paper and photographed
17) Tissue is placed between filter paper between Plexiglas plates held in place with nylon bolts
18) Tissue is put in water tight MRI compatible container
19) PBS solution is added, fully submerging tissue, taking care to remove bubbles
20) Temperature of tissue and buffer are recorded
21) Container with tissue is placed in scanner surrounded by tissues/spillage blanket
22) Time of start scan is recorded
23) Scanning proceeds following previously set up sequences for <u>unfixed</u> PM tissue including the following (total time ~4.5 hours)
   - Survey
   - T1
   - PDT2
   - MRS
   - PSIR

- ☒ DTI
- ☒ MTR

24) Record tissue and buffer temperature
25) Remove PBS in cut up room
26) Put tissue in zip lock bag with 10% buffered formaldehyde solution
27) Label bags clearly
28) Put zip lock bag in container for storage on upper shelve in cut up room
29) Sample tracker forms are filled out, one of which will be left with tissue, while the other is kept in study folder for NMR Research Unit administration
30) Container and cut up room are cleaned
31) Steven books scanner time at least 7 days later, allowing full fixation of the tissue.

Scanning of fixed tissue

32) On day of scan new PBS is created and kept at room temperature
33) In the cut up room, formaldehyde is removed from bag
34) Tissue is taken out of zip lock bags
35) Tissue is placed on millimetre grid paper and photographed
36) Tissue is put in MRI compatible container in between Plexiglas plates
37) PBS is added, submerging tissue, taking care to remove bubbles
38) Temperature of tissue and buffer are recorded
39) Container with tissue is placed in scanner surrounded by tissues/spillage blanket
40) Time of scan is recorded
41) Scanning following set up sequences for fixed PM tissue including the following (total time ~4.5 hours)
    - ☒ Survey
    - ☒ T1
    - ☒ PDT2
    - ☒ PSIR
    - ☒ DTI
    - ☒ MTR
42) Measure tissue and buffer temperature
43) Remove PBS or fomblin in cut up room
44) Put tissue in zip lock bag with 10% buffered formaldehyde solution

Processing for histology

45) Steven meets with Angela Richard-Lundt from Division of Neuropathology to process tissue
46) Samples are cut in half using a 5-mm-deep iron angle, resulting in two blocks of equal thickness, with the cut surface corresponding to the centre of the MRI plane
47) Both halves are placed with cut side up on millimetre grid paper
48) On a piece of paper a note is made if tissue is left or right hemisphere, and which half is anterior/posterior

49) Photographs are taken from slice (with piece of paper)
50) Guided by T2w scans, five (~20x30mm) are selected from tissue, including
    - ☒ Thalamus
    - ☒ Normal appearing grey matter

- ☒ Pathological grey matter
- ☒ Normal appearing white matter
- ☒ Pathological white matter

51) Take photo of selected sample location within slice
52) Cassettes are labelled
53) Tissue that is not processed for histology is put in clearly labelled ziplock bags submerged in 10% formaldehyde solution
54) Ziplock bags are placed in dedicated container and kept in store room of Divison of Neuropathology in basement of IoN (access through cut up room)
55) Sample tracker forms are filled out
56) Samples are embedded in paraffin over the weekend
57) Paraffin embedded tissue is kept in dedicated labelled container in storage room in IQPath lab in basement

Histology

58) Sample tracker forms are filled out
59) Angela processes the tissue using the following markers
- ☒ H&E
- ☒ Neurofil2000
- ☒ SMI94
- ☒ CD68
- ☒ CD20
- ☒ CD3
- ☒ CD8
- ☒ GFAP
- ☒ IBA1
- ☒ COXIV
- ☒ VDAC1

60) Data is digitised by Division of Neuropathology
61) Digitised images are quantified by Matthew Ellis from Division of Neuropathology
62) Images are transferred to servers of NMR research group
63) Paraffin embedded blocks and microscope slides will be kept stored in tissue storage room
64) Sample tracker forms are filled out

Project termination

65) Tissue can be disposed of using normal tissue disposal procedure of Division of P Neuropathology. This will be decided upon in discussion with Prof Olga Ciccarelli and prof Sebastien Brandner.

Histology quantification

Tissue areas were separated from background 'glass' using a composite image layer comprised of the lowest pixel value from the 3 colour layers (red, green and blue), and a smoothed version of this composite layer created using a 25×25 pixel filter, assigning the median value to the central pixel. Initial segmentation of the image was performed by applying quadtree method to the filtered image layer; objects were then merged if the difference in mean intensity was below 5. The 10th centile (C10), the threshold that separates the darkest 10% of pixels, was then taken from objects with a mean pixel value below the mean intensity of the whole image in the filtered layer, i.e. background regions. This threshold was then adjusted by -5 (C10-5) to ensure exclusion of lightly stained areas, and all pixels were then classified as ROI<C10-5<Background on the filtered layer, then the background objects were classified as ROI<C10-5<Background on the unfiltered layer. Background objects with area less than 20mm^2 were then merged into the ROI, and ROI objects with area less than 1% of the total area of ROI were removed into the background. Stain analysis was then performed on the tissue region represented by the ROI objects.

Raster images representing the intensity of blue (Bl) and brown (Br) staining were extracted from the RGB image using the hue-saturation-density method (van Der Laak et al. 2000). This gives separate images for each colour (Bl and Br), with values ranging from 0 (colour not present) ~3 (dark stain). A threshold (ThBl) to separate significantly stained blue areas (nuclei) was calculated using a centile based method which compares the threshold given for increasing centiles, searching for significant increases in value. For identification of brown stain an additional image layer was created where each pixel is assigned the value Bl-Br, so that any region with significant brown stain has a negative value. Potential brown areas (Brown) are identified as regions with Bl-Br $\leq$ -0.01.

148

Regions of Brown were split to exclude pixels with optical density (OD=Bl+Br) ≤0.01 (unstained areas). Brown areas with area <5µm were removed, and the 5th centile for Br (C5Br) calculated from Brown pixels; any Brown pixels with Br ≤ C5Br were reclassified as brown background (BrB). The standard deviation of Br within BrB was then calculated to give sBrB. The ROI was then split by classifying all pixels with Br>C5Br+sBrB & Bl-Br ≤ -0.01 as Brown. Two thresholds were then calculated from the ROI not classed as Brown using the mean value of Br ([Equation]) and the standard deviation of Br sBr; ThBr1=[Equation] + 3(sBr) and ThBr2=[Equation] + 6(sBr).

IHC stain identification was performed by classifying all pixels initially identified as ROI as Tissue ≤ ThBr1<Brown Stain ≤ThBr2<Dark Brown Stain based on image layer Br. Nuclear identification was then performed using an image derived from the image layer Bl, using a 3x3 pixel filter and a Gaussian distribution (Bl3). The Tissue region was classified as Tissue ≤ ThBl<Nucleus based on image layer Bl3. The Nucleus regions were subsequently grown into bordering pixels with OD>0.05. Any Tissue object with area <3µm2 enclosed by Nucleus was removed into the surrounding Nucleus, then any Nucleus object with area<20µm2 removed into Tissue. Separation of connected nuclei was performed by applying a rolling ball of 6 pixel diameter to any Nucleus with area >50µm2. This identifies any area of Nucleus into which a 6 pixel ball cannot fit as Blue. Blue objects with area >10µm2 were classified as Nucleus, and then all Nucleus objects were grown into bordering pixels classified as Blue. Any remaining Blue objects were removed into Tissue.

Results of two cases with normal appearing white matter, normal appearing grey matter, and white matter lesion data

Including data of only two patients that had data for NAGM, NAWM and WM lesions, yielded comparable means intensity estimates as including five patients. For two patients, the 'one mean per ROI per cassette' models and the 'ROI tiles' models gave comparable estimates for mean stain and MTR intensities as displayed in supplemental table 6.1 and supplemental figure 6.1. Similar to the analysis for data from five subjects, the tile models gave highly significant differences in group wise comparisons between ROIs (GM-WM, and WM-WM lesions), all group wise comparisons $p < 0.01$, except for CD3 and CD8. The current section will conservatively focus on results of the 'one mean per ROI per cassette' models.

MTR was significantly higher in NAWM compared to WM lesions ($p < 0.05$). SMI94 intensity was nearly significantly higher in NAWM than in NAGM ($p = 0.09$), which in turn had significantly higher SMI94 staining than WM lesions ($p < 0.001$). NF200 staining was lower in WM lesions than in NAWM ($p = 0.03$). Concentration of GFAP was higher in NAWM than in NAGM ($p < 0.001$). VDAC was significantly higher in NAWM than in NAWM ($p < 0.001$). The proportion of damaged mitochondria was significantly larger in the NAWM than in NAGM ($p < 0.001$). CD68 stain intensity was significantly higher in the NAWM than NAGM ($p < 0.001$). IBA1 stain intensity was higher in NAWM than in WM lesions ($p < 0.01$). CD3 and CD8 staining did not differ between tissue types, and was not significantly different from zero in all tissue types for CD3 and NAGM and GM lesions in CD8.

		One mean per ROI per cassette			ROI tiles		
		NAGM	NAWM	WM lesions	NAGM	NAWM	WM lesions
MTR	mean	35.22	38.83	31.40	35.99	41.59	29.61
	SE	1.92	9.84	1.93	1.71	1.70	1.81
SMI94	mean	72.75	92.75	47.10	76.64	93.06	21.68
	SE	13.10	12.87	13.10	3.31	3.23	3.82
NF200	mean	52.13	56.54	45.20	49.38	56.14	45.48
	SE	5.12	4.95	5.12	2.80	2.66	3.68
GFAP	mean	11.95	70.48	80.20	13.79	75.41	60.38
	SE	6.49	6.12	6.49	1.30	1.02	2.49
VDAC	mean	80.56	44.02	44.00	80.88	40.71	62.13
	SE	8.74	8.50	8.71	7.87	7.84	8.05
% mitochondria damaged	mean	0.39	0.83	0.80	0.44	0.92	0.64
	SE	0.08	0.07	0.08	0.02	0.02	0.04
CD68	mean	0.30	0.97	0.86	0.49	1.14	0.78
	SE	0.22	0.22	0.22	0.50	0.50	0.51
IBA1	mean	8.01	10.98	5.14	8.40	10.88	5.30
	SE	6.99	6.98	6.99	8.72	8.72	8.73
CD8	mean	0.02	0.04	0.04	0.03	0.03	0.04
	SE	0.01	0.01	0.01	0.01	0.01	0.02
CD3	mean	0.13	0.11	0.11	0.14	0.08	0.12
	SE	0.09	0.09	0.09	0.07	0.07	0.08

Supplemental table 6.1. Mean intensity estimates for MTR and histological markers in normal appearing grey matter, normal appearing white matter, and chronic inactive white matter lesions, based on two cases only.
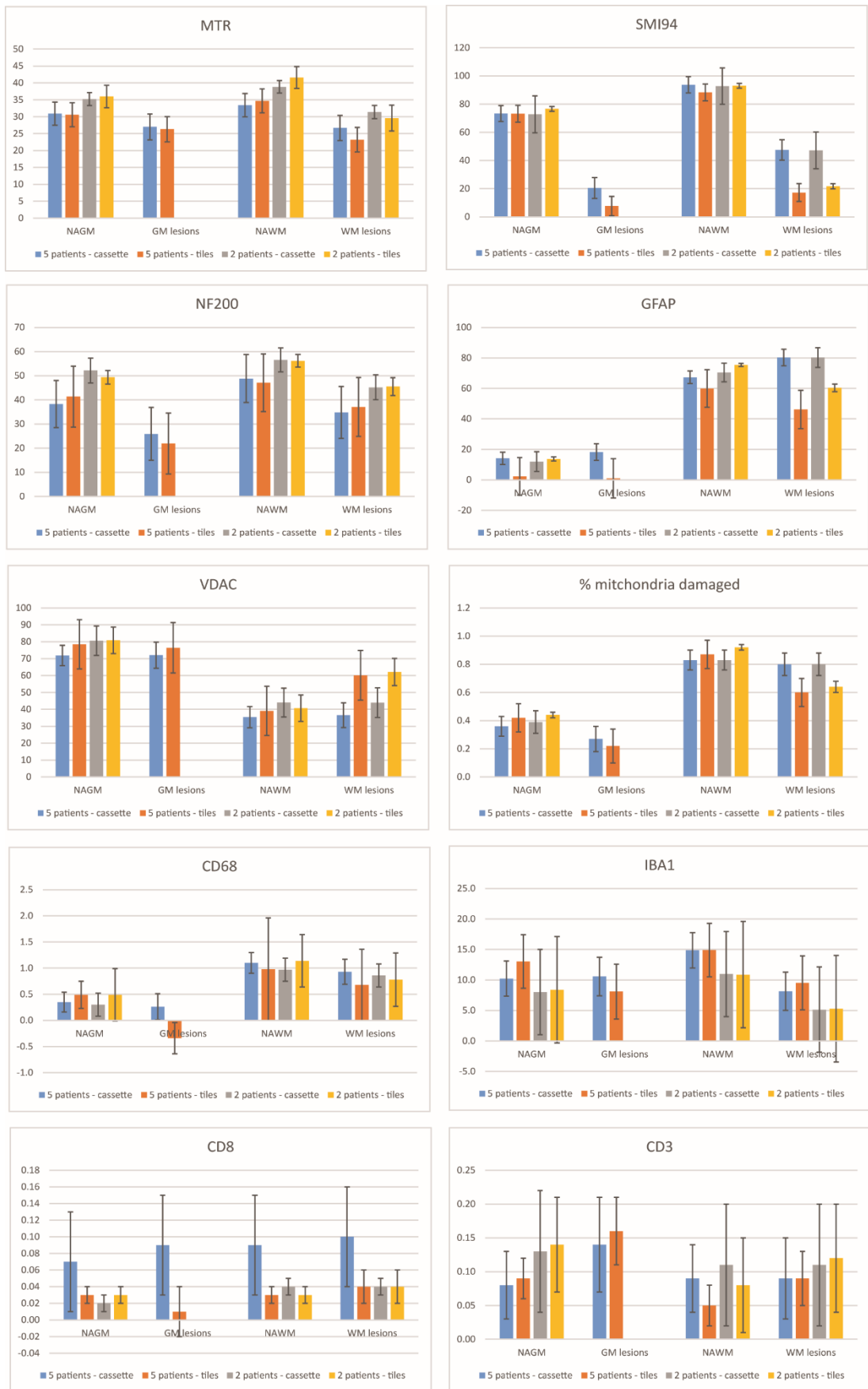
Supplemental figure 6.1. Mean intensity estimates for MTR and histological markers in normal appearing grey matter, normal appearing white matter, and chronic inactive white matter lesions, based on two and five cases.

Bibliography

Absinta, M. et al., 2014. Postmortem magnetic resonance imaging to guide the pathologic cut: individualized, 3-dimensionally printed cutting boxes for fixed brains. *Journal of neuropathology and experimental neurology*, 73(8), pp.780–8.

Al-Radaideh, A.M. et al., 2013. Increased iron accumulation occurs in the earliest stages of demyelinating disease: an ultra-high field susceptibility mapping study in Clinically Isolated Syndrome. *Multiple Sclerosis Journal*, 19(7), pp.896–903.

Allen, I. et al., 2001. Pathological abnormalities in the normal-appearing white matter in multiple sclerosis. *Neurological sciences : official journal of the Italian Neurological Society and of the Italian Society of Clinical Neurophysiology*, 22(2), pp.141–4.

Amato, M.P. et al., 2004. Neocortical volume decrease in relapsing-remitting MS patients with mild cognitive impairment. *Neurology*, 63(1), pp.89–93.

Amunts, K. et al., 1996. Asymmetry in the human motor cortex and handedness. *NeuroImage*, 4(3 Pt 1), pp.216–22.

Armstrong, C.L. et al., 2004. Age-related, regional, hemispheric, and medial-lateral differences in myelin integrity in vivo in the normal adult brain. *American journal of neuroradiology*, 25(6), pp.977–84.

Ashburner, J., 2007. A fast diffeomorphic image registration algorithm. *NeuroImage*, 38(1), pp.95–113.

Ashburner, J. & Friston, K.J., 2009. Computing average shaped tissue probability templates. *NeuroImage*, 45(2), pp.333–41.

Audoin, B., Ibarrola, D., et al., 2005. Functional MRI study of PASAT in normal subjects. *Magma*, 18(2), pp.96–102.

Audoin, B. et al., 2006. Localization of grey matter atrophy in early RRMS : A longitudinal study. *Journal of neurology*, 253(11), pp.1495–501.

Audoin, B., Au Duong, M. Van, et al., 2005. Magnetic resonance study of the influence of tissue damage and cortical reorganization on PASAT performance at the earliest stage of multiple sclerosis. *Human brain mapping*, 24(3), pp.216–28.

Bagnato, F. et al., 2015. 7T MRI-Histologic Correlation Study of Low Specific Absorption Rate T2-Weighted GRASE Sequences in the Detection of White Matter Involvement in Multiple Sclerosis. *Journal of Neuroimaging*, 25(3), pp.370–378.

Bagnato, F. et al., 2009. Multisequence-imaging protocols to detect cortical lesions of patients with multiple sclerosis: observations from a post-mortem 3 Tesla imaging study. *Journal of the neurological sciences*, 282(1–2), pp.80–5.

Bagnato, F. et al., 2011. Tracking iron in multiple sclerosis: a combined imaging and histopathological study at 7 Tesla. *Brain*, 134(12), pp.3602–3615.

Barkhof, F., Scheltens, P. & Kamphorst, W., 1993. Pre-and post-mortem MR imaging of unsuspected multiple sclerosis in a patient with Alzheimer's disease. *Journal of the neurological sciences*, 117(1–2), pp.175–178.

Batista, S. et al., 2012. Basal ganglia, thalamus and neocortical atrophy predicting slowed cognitive processing in multiple sclerosis. *Journal of neurology*, 259(1), pp.139–46.

Behrens, T.E.J. et al., 2003. Non-invasive mapping of connections between human thalamus and cortex using diffusion imaging. *Nature neuroscience*, 6(7), pp.750–7.

Benedict, R.H.B. et al., 2006. Neocortical atrophy, third ventricular width, and cognitive dysfunction in multiple sclerosis. *Archives of neurology*, 63(9), pp.1301–6.

Benedict, R.H.B. et al., 2004. Prediction of neuropsychological impairment in multiple sclerosis: comparison of conventional magnetic resonance imaging measures of atrophy and lesion burden. *Archives of neurology*, 61(2), pp.226–30.

Bergsland, N. et al., 2015. Localized atrophy of the thalamus and slowed cognitive processing speed in MS patients. *Multiple Sclerosis Journal*, 22(10), pp.1327–36.

Bitsch, A. et al., 2001. A longitudinal MRI study of histopathologically defined hypointense multiple sclerosis lesions. *Annals of neurology*, 49(6), pp.793–796.

Bø, L. et al., 2003a. Intracortical multiple sclerosis lesions are not associated with increased lymphocyte infiltration. *Multiple sclerosis (Houndmills, Basingstoke, England)*, 9(4), pp.323–31.

Bø, L. et al., 2003b. Subpial demyelination in the cerebral cortex of multiple sclerosis patients. *Journal of neuropathology and experimental neurology*, 62(7), pp.723–32.

Bø, L., 2009. The histopathology of grey matter demyelination in multiple sclerosis. *Acta neurologica Scandinavica. Supplementum*, (189), pp.51–7.

Bodini, B. et al., 2016. White and grey matter damage in primary-progressive MS: the chicken or the egg? *Neurology*, 86(2), pp.170–6.

Bossart, E.L., 1999. The Effect of Fixative Solutions in Magnetic Resonance Imaging. In *ISMRM*.

Broholm, H. et al., 2004. Nitric oxide synthase expression and enzymatic activity in multiple sclerosis. *Acta Neurol Scand*, 109(4), pp.261–269.

Brownell, B. & Hughes, J.T., 1962. The distribution of plaques in the cerebrum in multiple sclerosis. *Journal of neurology, neurosurgery, and psychiatry*, 25, pp.315–20.

Burgess, P. & Shallice, T., 1997. *The Hayling and Brixton Tests. Test Manual.*, Bury St Edmunds, UK: Thames Valley Test Company.

Calabrese, M., Rocca, M.A., et al., 2010. A 3-year magnetic resonance imaging study of cortical lesions in relapse-onset multiple sclerosis. *Annals of neurology*, 67(3), pp.376–83.

Calabrese, M., Atzori, M., et al., 2007. Cortical atrophy is relevant in multiple sclerosis at clinical onset. *Journal of neurology*, 254(9), pp.1212–20.

Calabrese, M., Agosta, F., et al., 2009. Cortical lesions and atrophy associated with cognitive impairment in relapsing-remitting multiple sclerosis. *Archives of neurology*, 66(9), pp.1144–50.

Calabrese, M., Rocca, M.A., et al., 2009. Cortical lesions in primary progressive multiple sclerosis: a 2-year longitudinal MR study. *Neurology*, 72(15), pp.1330–6.

Calabrese, M., De Stefano, N., et al., 2007. Detection of cortical inflammatory lesions by double inversion recovery magnetic resonance imaging in patients with multiple sclerosis. *Archives of neurology*, 64(10), pp.1416–22.

Calabrese, M., Filippi, M., et al., 2009. Evidence for relative cortical sparing in benign multiple sclerosis: a longitudinal magnetic resonance imaging study. *Multiple Sclerosis Journal*, 15(1), pp.36–41.

Calabrese, M., Battaglini, M., et al., 2010. Imaging distribution and frequency of cortical lesions in patients with multiple sclerosis. *Neurology*, 75(14), pp.1234–40.

Calabrese, M., Mattisi, I., et al., 2010. Magnetic resonance evidence of cerebellar cortical pathology in multiple sclerosis. *Journal of neurology, neurosurgery, and psychiatry*, 81(4), pp.401–4.

Calabrese, M. et al., 2008. Morphology and evolution of cortical lesions in multiple sclerosis. A longitudinal MRI study. *NeuroImage*, 42(4), pp.1324–8.

Calabrese, M. et al., 2015. Regional Distribution and Evolution of Gray Matter Damage in Different Populations of Multiple Sclerosis Patients. *PloS ONE*, 10(8), p.e0135428.

Calamante, F. et al., 2011. Track density imaging (TDI): Validation of super resolution property. *NeuroImage*, 56(3), pp.1259–1266.

Campbell, G.R. et al., 2011. Mitochondrial DNA deletions and neurodegeneration in multiple sclerosis. *Annals of neurology*, 69(3), pp.481–92.

Cappellani, R. et al., 2014. Subcortical deep gray matter pathology in patients with multiple sclerosis is associated with white matter lesion burden and atrophy but not with cortical atrophy: a diffusion tensor MRI study. *AJNR. American journal of neuroradiology*, 35(5), pp.912–9.

Cardinal, K.S. et al., 2008. A longitudinal fMRI study of the paced auditory serial addition task. *Multiple Sclerosis Journal*, 14(4), pp.465–71.

Cardoso, M.J. et al., 2015. Geodesic Information Flows: Spatially-Variant Graphs and Their Application to Segmentation and Fusion. *IEEE Transactions on Medical Imaging*, 34(9), pp.1976–1988.

Ceccarelli, A. et al., 2008. A voxel-based morphometry study of grey matter loss in MS patients with different clinical phenotypes. *NeuroImage*, 42(1), pp.315–22.

Ceccarelli, A. et al., 2010. Deep gray matter T2 hypointensity is present in patients with clinically isolated syndromes suggestive of multiple sclerosis. *Multiple Sclerosis Journal*, 16(1), pp.39–44.

Ceccarelli, A. et al., 2007. Normal-appearing white and grey matter damage in MS. A volumetric and diffusion tensor MRI study at 3.0 Tesla. *J Neurol*, 254(4), pp.513–518.

Charcot, J., 1887. Lectures on the Diseases of the Nervous System. In *Lecture IV. Disseminated Sclerosis. Pathological anatomy*. London: The New Sydenham Society, pp. 157–181.

Chard, D.T. et al., 2002. Brain atrophy in clinically early relapsing-remitting multiple sclerosis. *Brain*, 125(2), pp.327–37.

Chard, D.T. et al., 2010. Reducing the impact of white matter lesions on automated measures of brain gray and white matter volumes. *Journal of magnetic resonance imaging*, 32(1), pp.223–8.

Chard, D.T. & Miller, D.H., 2009a. Grey matter pathology in clinically early multiple sclerosis: evidence from magnetic resonance imaging. *Journal of the neurological sciences*, 282(1–2), pp.5–11.

Chard, D.T. & Miller, D.H., 2009b. Is multiple sclerosis a generalized disease of the central nervous system? An MRI perspective. *Current opinion in neurology*, 22(3), pp.214–218.

Ciccarelli, O. et al., 2003. A study of the mechanisms of normal-appearing white matter damage in multiple sclerosis using diffusion tensor imaging--evidence of Wallerian degeneration. *Journal of neurology*, 250(3), pp.287–92.

Cifelli, A. et al., 2002. Thalamic neurodegeneration in multiple sclerosis. *Annals of neurology*, 52(5), pp.650–3.

Compston, A. et al., 2005. *McAlpine's Multiple sclerosis*, London: Churchill Livingstone.

Coughlan, A. & Hollows, S., 1985. *The adult memory and information processing battery (AMIPB)*, Leeds, UK: St James University Hospital.

Crespy, L. et al., 2011. Prevalence of grey matter pathology in early multiple sclerosis assessed by magnetization transfer ratio imaging. *PloS one*, 6(9), p.e24969.

Dalton, C.M. et al., 2004. Early development of multiple sclerosis is associated with progressive grey matter atrophy in patients presenting with clinically isolated syndromes. *Brain*, 127(5), pp.1101–7.

Davies, G.R. et al., 2004. Evidence for grey matter MTR abnormality in minimally disabled patients with early relapsing-remitting multiple sclerosis. *Journal of neurology, neurosurgery, and psychiatry*, 75(7), pp.998–1002.

Dayan, M. et al., 2016. Profilometry: A new statistical framework for the characterization of white matter pathways, with application to multiple sclerosis. *Human Brain Mapping*, 37(3), pp.989–1004.

Debernard, L. et al., 2015. Deep grey matter MRI abnormalities and cognitive function in relapsing-remitting multiple sclerosis. *Psychiatry research*, 234(3), pp.352–61.

DeLuca, G.C. et al., 2015. Cognitive impairment in multiple sclerosis: clinical, radiologic and pathologic insights. *Brain pathology*, 25(1), pp.79–98.

Deppe, M. et al., 2016. Early silent microstructural degeneration and atrophy of the thalamocortical network in multiple sclerosis. *Human Brain Mapping*, 37(5), pp.1866–1879.

Desikan, R.S. et al., 2006. An automated labeling system for subdividing the human cerebral cortex on MRI scans into gyral based regions of interest. *NeuroImage*, 31(3), pp.968–80.

Duerk, J.L., 1999. Principles of MR image formation and reconstruction. *Magnetic resonance imaging clinics of North America*, 7(4), pp.629–59.

Dutta, R. et al., 2006. Mitochondrial dysfunction as a cause of axonal degeneration in multiple sclerosis patients. *Annals of neurology*, 59(3), pp.478–89.

Enzinger, C. et al., 2015. Nonconventional MRI and microstructural cerebral changes in multiple sclerosis. *Nature Reviews Neurology*, 11(12), pp.676–686.

Esiri, M., Williams, K. & DeLuca, G.C., 2006. Protein co-expression with axonal injury in multiple sclerosis plaques. *CrossRef*, 111(4), pp.289–299.

Estes, M.L. et al., 1990. Stereotactic biopsy of an active multiple sclerosis lesion. Immunocytochemical analysis and neuropathologic correlation with magnetic resonance imaging. *Archives of neurology*, 47(12), pp.1299–1303.

Evangelou, N., Esiri, M.M., et al., 2000. Quantitative pathological evidence for axonal loss in normal appearing white matter in multiple sclerosis. *Annals of neurology*, 47(3), pp.391–5.

Evangelou, N., Konz, D., et al., 2000. Regional axonal loss in the corpus callosum correlates with cerebral white matter lesion volume and distribution in multiple sclerosis. *Brain*, 123(9), pp.1845–9.

Fabiano, A.J. et al., 2003. Thalamic Involvement in Multiple Sclerosis: A Diffusion-Weighted Magnetic Resonance Imaging Study. *Journal of Neuroimaging*, 13(4), pp.307–314.

Fabiano, A.J., Horsfield, M.A. & Bakshi, R., 2005. Interhemispheric asymmetry of brain diffusivity in normal individuals: a diffusion-weighted MR imaging study. *American journal of neuroradiology*, 26(5), pp.1089–94.

Fazekas, F. et al., 1999. The contribution of magnetic resonance imaging to the diagnosis of multiple sclerosis. *Neurology*, 53(3), pp.448–56.

Fedorov, A. et al., 2012. 3D Slicer as an image computing platform for the Quantitative Imaging Network. *Magnetic resonance imaging*, 30(9), pp.1323–41.

Filippi, M. et al., 2012. Association between pathological and MRI findings in multiple sclerosis. *Lancet neurology*, 11(4), pp.349–60.

Filippi, M. & Rocca, M.A., 2012. The neurologist's dilemma: MS is a grey matter disease that standard clinical and MRI measures cannot assess adequately--no. *Multiple Sclerosis Journal*, 18(5), pp.557–8.

Fischl, B. et al., 2002. Whole brain segmentation: automated labeling of neuroanatomical structures in the human brain. *Neuron*, 33(3), pp.341–55.

Fisher, E. et al., 2008. Gray matter atrophy in multiple sclerosis: a longitudinal study. *Annals of neurology*, 64(3), pp.255–65.

Fisher, E. et al., 2007. Imaging correlates of axonal swelling in chronic multiple sclerosis brains. *Annals of neurology*, 62(3), pp.219–228.

Fisher, E. et al., 2000. Relationship between brain atrophy and disability: an 8-year follow-up study of multiple sclerosis patients. *Multiple Sclerosis Journal*, 6(6), pp.373–377.

Fisk, J.D. & Archibald, C.J., 2001. Limitations of the Paced Auditory Serial Addition Test as a measure of working memory in patients with multiple sclerosis. *Journal of the International Neuropsychological Society*, 7(3), pp.363–72.

Fisniku, L.K. et al., 2008. Gray matter atrophy is related to long-term disability in multiple sclerosis. *Annals of neurology*, 64(3), pp.247–54.

Franklin, R.J.M. & ffrench-Constant, C., 2008. Remyelination in the CNS: from biology to therapy. *Nature Reviews Neuroscience*, 9(11), pp.839–855.

Ge, Y., 2006. Multiple sclerosis: the role of MR imaging. *American journal of neuroradiology*, 27(6), pp.1165–76.

Genova, H.M. et al., 2009. Examination of processing speed deficits in multiple sclerosis using functional magnetic resonance imaging. *Journal of the International Neuropsychological Society*, 15(3), pp.383–93.

Geurts, J.J.G. et al., 2011. Consensus recommendations for MS cortical lesion scoring using double inversion recovery MRI. *Neurology*, 76(5), pp.418–24.

Geurts, J.J.G., Bø, L., et al., 2005. Cortical Lesions in Multiple Sclerosis: Combined Postmortem MR Imaging and Histopathology. *American journal of neuroradiology*, 26(3), pp.572–577.

Geurts, J.J.G. et al., 2008. Does high-field MR imaging improve cortical lesion detection in multiple sclerosis? *J Neurol*, 255(2), pp.183–191.

Geurts, J.J.G. et al., 2007. Extensive hippocampal demyelination in multiple sclerosis. *Journal of neuropathology and experimental neurology*, 66(9), pp.819–27.

Geurts, J.J.G., Pouwels, P.J.W., et al., 2005. Intracortical lesions in multiple sclerosis: improved detection with 3D double inversion-recovery MR imaging. *Radiology*, 236(1), pp.254–60.

Geurts, J.J.G., 2008. Is progressive multiple sclerosis a gray matter disease? *Annals of neurology*, 64(3), pp.230–2.

Geurts, J.J.G., 2012. The neurologist's dilemma: MS is a grey matter disease that standard clinical and MRI measures cannot assess adequately--yes. *Multiple Sclerosis Journal*, 18(5), pp.559–60.

Geurts, J.J.G. & Barkhof, F., 2008. Grey matter pathology in multiple sclerosis. *Lancet neurology*, 7(9), pp.841–51.

Gilmore, C.P., Donaldson, I., et al., 2009. Regional variations in the extent and pattern of grey matter demyelination in multiple sclerosis: a comparison between the cerebral cortex, cerebellar cortex, deep grey matter nuclei and the spinal cord. *Journal of Neurology, Neurosurgery & Psychiatry*, 80(2), pp.182–187.

Gilmore, C.P., Geurts, J.J.G., et al., 2009a. Spinal cord grey matter lesions in multiple sclerosis detected by post-mortem high field MR imaging. *Multiple Sclerosis Journal*, 15(2), pp.180–188.

Gilmore, C.P., Geurts, J.J.G., et al., 2009b. Spinal cord grey matter lesions in multiple sclerosis detected by post-mortem high field MR imaging. *Multiple Sclerosis Journal*, 15(2), pp.180–8.

Goldberg, E. et al., 2011. Hemispheric asymmetries of cortical volume in the human brain. *Cortex*, 49, pp.200–210.

Gorgoraptis, N. et al., 2010. Combining tractography and cortical measures to test system-specific hypotheses in multiple sclerosis. *Multiple Sclerosis Journal*, 16(5), pp.555–565.

Goursaud, S. et al., 2009. Cultured astrocytes derived from corpus callosum or cortical grey matter show distinct glutamate handling properties. *Journal of neurochemistry*, 108(6), pp.1442–52.

Gray, E. et al., 2013. Accumulation of cortical hyperphosphorylated neurofilaments as a marker of neurodegeneration in multiple sclerosis. *Multiple Sclerosis Journal*, 19(2), pp.153–161.

De Groot, C.J. et al., 2001. Post-mortem MRI-guided sampling of multiple sclerosis brain lesions: increased yield of active demyelinating and (p)reactive lesions. *Brain*, 124(8), pp.1635–45.

Haider, L. et al., 2014. Multiple sclerosis deep grey matter: the relation between demyelination, neurodegeneration, inflammation and iron. *Journal of neurology, neurosurgery, and psychiatry*.

Haider, L. et al., 2011. Oxidative damage in multiple sclerosis lesions. *Brain*, 134(7), pp.1914–24.

Harris, J.A., Guglielmotti, V. & Bentivoglio, M., 1996. Diencephalic Asymmetries. *Neuroscience & Biobehavioral Reviews*, 20(4), pp.637–643.

Henkelman, R.M., Stanisz, G.J. & Graham, S.J., 2001. Magnetization transfer in MRI: a review. *NMR in Biomedicine*, 14(2), pp.57–64.

Henry, R.G. et al., 2008. Regional grey matter atrophy in clinically isolated syndromes at presentation. *Journal of neurology, neurosurgery, and psychiatry*, 79(11), pp.1236–44.

Hickman, S.I. et al., 2002. Technical note: the comparison of hypointense lesions from "pseudo-T1" and T1-weighted images in secondary progressive multiple sclerosis. *Multiple Sclerosis Journal*, 8(5), pp.433–5.

van Horssen, J. et al., 2011. Radical changes in multiple sclerosis pathogenesis. *Biochimica et Biophysica Acta - Molecular Basis of Disease*, 1812(2), pp.141–150.

Hougaard, A. et al., 2015. Cerebral Asymmetry of fMRI-BOLD Responses to Visual Stimulation. *PloS one*, 10(5), p.e0126477.

Houtchens, M.K. et al., 2007. Thalamic atrophy and cognition in multiple sclerosis. *Neurology*, 69(12), pp.1213–1223.

Huettel, S.A., Song, A.W. & McCarthy, G., 2014. *Functional Magnetic Resonance Imaging,* Third., Sunderland, MA: Sinauer Associates, Inc.

Hulst, H.E. & Geurts, J.J.G., 2011. Gray matter imaging in multiple sclerosis: what have we learned? *BMC neurology*, 11, p.153.

Hutchinson, M., 2012. The neurologist's dilemma: MS is a grey matter disease that standard clinical and MRI measures cannot assess adequately--commentary. *Multiple Sclerosis Journal*, 18(5), pp.561–2.

Jakab, A. et al., 2012. Generation of Individualized Thalamus Target Maps by Using Statistical Shape Models and Thalamocortical Tractography.

Jehna, M. et al., 2013. An exploratory study on the spatial relationship between regional cortical volume changes and white matter integrity in multiple sclerosis. *Brain connectivity*, 3(3), pp.255–64.

Jones, E.G., 1985. *The Thalamus*, Boston, MA: Springer US.

Jonkman, L.E. et al., 2015. Ultra-High-Field MRI Visualization of Cortical Multiple Sclerosis Lesions with T2 and T2*: A Postmortem MRI and Histopathology Study. *American Journal of Neuroradiology*.

Kalkers, N.F. et al., 2001. Optimizing the association between disability and biological markers in MS. *Neurology*, 57(7), pp.1253–8.

Kang, X., Herron, T.J. & Woods, D.L., 2011. Regional variation, hemispheric asymmetries and gender differences in pericortical white matter.

Kern, K.C. et al., 2015. Thalamic–hippocampal–prefrontal disruption in relapsing–remitting multiple sclerosis. *NeuroImage: Clinical*, 8, pp.440–447.

Khaleeli, Z. et al., 2007. Localized grey matter damage in early primary progressive multiple sclerosis contributes to disability. *NeuroImage*, 37(1), pp.253–61.

Kilsdonk, I.D. et al., 2016. Increased cortical grey matter lesion detection in multiple sclerosis with 7 T MRI: a post-mortem verification study. *Brain*, 139(5), pp.1472–81.

Kipp, M. et al., 2015. Thalamus pathology in multiple sclerosis: from biology to clinical application. *Cellular and molecular life sciences*, 72(6), pp.1127–47.

Koenig, K.A. et al., 2014. Hippocampal volume is related to cognitive decline and fornicial diffusion measures in multiple sclerosis. *Magnetic Resonance Imaging*, 32(4), pp.354–358.

Kolasinski, J. et al., 2012. A combined post-mortem magnetic resonance imaging and quantitative histological study of multiple sclerosis pathology. *Brain*, 135(10), pp.2938–51.

Koziol, L.F. et al., 2014. Consensus Paper: The Cerebellum's Role in Movement and Cognition. *Cerebellum*, 13(1), pp.151–77.

Krämer, J. et al., 2015. Early and Degressive Putamen Atrophy in Multiple Sclerosis. *International Journal of Molecular Sciences*, 16(10), pp.23195–23209.

Krauth, A. et al., 2010. A mean three-dimensional atlas of the human thalamus: generation from multiple histological data. *NeuroImage*, 49(3), pp.2053–62.

Kurtzke, J.F., 1983. Rating neurologic impairment in multiple sclerosis: an expanded disability status scale (EDSS). *Neurology*, 33(11), pp.1444–52.

Kutzelnigg, A. et al., 2005. Cortical demyelination and diffuse white matter injury in multiple sclerosis. *Brain*, 128(11), pp.2705–12.

Kutzelnigg, A. et al., 2007. Widespread demyelination in the cerebellar cortex in multiple sclerosis. *Brain pathology*, 17(1), pp.38–44.

Kutzelnigg, A. & Lassmann, H., 2005. Cortical lesions and brain atrophy in MS. *Journal of the neurological sciences*, 233(1–2), pp.55–9.

van Der Laak, J.A. et al., 2000. Hue-saturation-density (HSD) model for stain recognition in digital images from transmitted light microscopy. *Cytometry*, 39(4), pp.275–84.

Labiano-Fontcuberta, A. et al., 2016. Gray Matter Involvement in Radiologically Isolated Syndrome. *Medicine*, 95(13), p.e3208.

Lassmann, H., 2011. Review: the architecture of inflammatory demyelinating lesions: implications for studies on pathogenesis. *Neuropathology and applied neurobiology*, 37(7), pp.698–710.

Lassmann, H., van Horssen, J. & Mahad, D.J., 2012. Progressive multiple sclerosis: pathology and pathogenesis. *Nature reviews. Neurology*, 8(11), pp.647–56.

Laule, C. et al., 2011. Pathological basis of diffusely abnormal white matter: insights from magnetic resonance imaging and histology. *Multiple Sclerosis Journal*, 17(2), pp.144–150.

Li, S. et al., 2013. Decreased NAA in gray matter is correlated with decreased availability of acetate in white matter in postmortem multiple sclerosis cortex. *Neurochemical research*, 38(11), pp.2385–96.

Lin, C. et al., 2001. Measurement of T1 Relaxation times at 3.0T: Implications for clinical MRI. In *ISMRM*.

Lindquist, S. et al., 2007. Histopathology and serial, multimodal magnetic resonance imaging in a multiple sclerosis variant. *Multiple Sclerosis Journal*, 13(4), pp.471–482.

Lockwood, A.H. et al., 2004. Mapping the neural systems that mediate the Paced Auditory Serial Addition Task (PASAT). *Journal of the International Neuropsychological Society*, 10(1), pp.26–34.

Louapre, C. et al., 2016. Is the Relationship between Cortical and White Matter Pathologic Changes in Multiple Sclerosis Spatially Specific? A Multimodal 7-T and 3-T MR Imaging Study with Surface and Tract-based Analysis. *Radiology*, 278(2), pp.524–535.

Lublin, F.D. & Reingold, S.C., 1996. Defining the clinical course of multiple sclerosis: results of an international survey. National Multiple Sclerosis Society (USA) Advisory Committee on Clinical Trials of New Agents in Multiple Sclerosis. *Neurology*, 46(4), pp.907–11.

Lucchinetti, C.F. et al., 2011. Inflammatory cortical demyelination in early multiple sclerosis. *The New England journal of medicine*, 365(23), pp.2188–97.

Macchi, G. & Cioffi, R.P., 1992. An in vivo and post mortem MRI study in multiple sclerosis with pathological correlation. *Italian journal of neurological scence*, 13(9 Suppl 14), pp.97–103.

Magliozzi, R. et al., 2010. A Gradient of neuronal loss and meningeal inflammation in multiple sclerosis. *Annals of Neurology*, 68(4), pp.477–493.

Magon, S. et al., 2014. Label-fusion-segmentation and deformation-based shape analysis of deep gray matter in multiple sclerosis: The impact of thalamic subnuclei on disability. *Human Brain Mapping*, 35(8), pp.4193–4203.

Mallik, S. et al., 2015. Regional patterns of grey matter atrophy and magnetisation transfer ratio abnormalities in multiple sclerosis clinical subgroups: A voxel-based analysis study. *Multiple Sclerosis Journal*, 21(4), pp.423–32.

McCormick, D.A., 1999. Are thalamocortical rhythms the rosetta stone of a subset of neurological disorders? *Nature Medicine*, 5(12), pp.1349–1351.

McDonald, W.I. et al., 2001. Recommended diagnostic criteria for multiple sclerosis: guidelines from the International Panel on the diagnosis of multiple sclerosis. *Annals of neurology*, 50(1), pp.121–7.

McFarland, H.F. & Martin, R., 2007. Multiple sclerosis: a complicated picture of autoimmunity. *Nature immunology*, 8(9), pp.913–9.

Mehta, V. et al., 2013. Iron is a sensitive biomarker for inflammation in multiple sclerosis lesions. *PLoS One*, 8(3), p.e57573.

Miller, A.K., Alston, R.L. & Corsellis, J.A., 1980. Variation with age in the volumes of grey and white matter in the cerebral hemispheres of man: measurements with an image analyser. *Neuropathology and applied neurobiology*, 6(2), pp.119–32.

Modat, M. et al., 2010. Fast free-form deformation using graphics processing units. *Computer methods and programs in biomedicine*, 98(3), pp.278–84.

Modat, M. et al., 2014. Global image registration using a symmetric block-matching approach. *Journal of medical imaging*, 1(2), p.24003.

Moll, N.M. et al., 2011. Multiple sclerosis normal-appearing white matter: pathology-imaging correlations. *Annals of neurology*, 70(5), pp.764–73.

Moore, G.R.W. et al., 2000. A pathology-MRI study of the short-T2 component in formalin-fixed multiple sclerosis brain. *Neurology*, 55(10), pp.1506–1510.

Moore, G.R.W. et al., 2008. Dirty-appearing white matter in multiple sclerosis: preliminary observations of myelin phospholipid and axonal loss. *Journal of neurology*, 255(11), p.1802–11, discussion 1812.

Morel, A., Magnin, M. & Jeanmonod, D., 1997. Multiarchitectonic and stereotactic atlas of the human thalamus. *The Journal of comparative neurology*, 387(4), pp.588–630.

Morgen, K. et al., 2006. Evidence for a direct association between cortical atrophy and cognitive impairment in relapsing-remitting MS. *NeuroImage*, 30(3), pp.891–8.

Mühlau, M. et al., 2013. White-matter lesions drive deep gray-matter atrophy in early multiple sclerosis: support from structural MRI. *Multiple Sclerosis Journal*, 19(11), pp.1485–92.

Muhlert, N. et al., 2013. Diffusion MRI-based cortical complexity alterations associated with executive function in multiple sclerosis. *Journal of magnetic resonance imaging*, 38(1), pp.54–63.

Newcombe, J. et al., 1991. Histopathology of multiple sclerosis lesions detected by magnetic resonance imaging in unfixed postmortem central nervous system tissue. *Brain*, 114(2), pp.1013–23.

Noseworthy, J.H. et al., 2000. Multiple sclerosis. *The New England journal of medicine*, 343(13), pp.938–52.

Paling, D. et al., 2013. Sodium accumulation is associated with disability and a progressive course in multiple sclerosis. *Brain*, 136(7), pp.2305–17.

Papadopoulos, D. et al., 2009. Substantial archaeocortical atrophy and neuronal loss in multiple sclerosis. *Brain pathology*, 19(2), pp.238–53.

van de Pavert, S.H.P. et al., 2016. DIR-visible grey matter lesions and atrophy in multiple sclerosis: partners in crime? *Journal of Neurology, Neurosurgery & Psychiatry*, 87(5), pp.461–467.

Peterson, J.W. et al., 2001. Transected neurites, apoptotic neurons, and reduced inflammation in cortical multiple sclerosis lesions. *Annals of neurology*, 50(3), pp.389–400.

Petzold, A. et al., 2008. Phosphorylation and compactness of neurofilaments in multiple sclerosis: Indicators of axonal pathology. *Experimental Neurology*, 213(2), pp.326–335.

Petzold, A., Tozer, D.J. & Schmierer, K., 2011. Axonal damage in the making: neurofilament phosphorylation, proton mobility and magnetisation transfer in multiple sclerosis normal appearing white matter. *Experimental neurology*, 232(2), pp.234–9.

Pitt, D. et al., 2010. Imaging cortical lesions in multiple sclerosis with ultra-high-field magnetic resonance imaging. *Archives of neurology*, 67(7), pp.812–818.

Polman, C.H. et al., 2005. Diagnostic criteria for multiple sclerosis: 2005 revisions to the "McDonald Criteria". *Annals of neurology*, 58(6), pp.840–6.

Polman, C.H. et al., 2011. Diagnostic criteria for multiple sclerosis: 2010 revisions to the McDonald criteria. *Annals of neurology*, 69(2), pp.292–302.

Polman, C.H. & Rudick, R.A., 2010. The Multiple Sclerosis Functional Composite: A clinically meaningful measure of disability. *Neurology*, 74(Issue 17, Supplement 3), pp.S8–S15.

Popescu, V. et al., 2015. What drives MRI-measured cortical atrophy in multiple sclerosis? *Multiple Sclerosis Journal*, 21(10), pp.1280–90.

Prados, F. et al., 2014. A Modality-Agnostic Patch-Based Technique for Lesion Filling in Multiple Sclerosis. In P. Golland, ed. *MICCAI*. Springer, Heidelberg, pp. 783–790.

Preiningerova, J. et al., 2009. Multiple Sclerosis. *Encyclopedia of life sciences*.

Quester, R. & Schröder, R., 1997. The shrinkage of the human brain stem during formalin fixation and embedding in paraffin. *Journal of neuroscience methods*, 75(1), pp.81–9.

Redpath, T.W. & Smith, F.W., 1994. Technical note: use of a double inversion recovery pulse sequence to image selectively grey or white brain matter. *The British journal of radiology*, 67(804), pp.1258–63.

Rinaldi, F. et al., 2010. Cortical lesions and cognitive impairment in multiple sclerosis. *Neurological sciences : official journal of the Italian Neurological Society and of the Italian Society of Clinical Neurophysiology*, 31(Suppl 2), pp.S235-7.

Roosendaal, S.D. et al., 2011. Grey matter volume in a large cohort of MS patients: relation to MRI parameters and disability. *Multiple Sclerosis Journal*, 17(9), pp.1098–106.

Ruder, T.D. et al., 2012. The influence of body temperature on image contrast in post mortem MRI. *European journal of radiology*, 81(6), pp.1366–70.

Sailer, M. et al., 2003. Focal thinning of the cerebral cortex in multiple sclerosis. *Brain*, 126(8), pp.1734–44.

Sardanelli, F. et al., 2003. Three subsequent single doses of gadolinium chelate for brain MR imaging in multiple sclerosis. *American journal of neuroradiology*, 24(4), pp.658–62.

Sastre-Garriga, J. et al., 2005. Grey and white matter volume changes in early primary progressive multiple sclerosis: a longitudinal study. *Brain : a journal of neurology*, 128(Pt 6), pp.1454–60.

Schmalbrock, P. et al., 2016. Basal Ganglia Iron in Patients with Multiple Sclerosis Measured with 7T Quantitative Susceptibility Mapping Correlates with Inhibitory Control. *American Journal of Neuroradiology*, 37(3), pp.439–446.

Schmierer, K., Wheeler-Kingshott, C.A.M., et al., 2007. Diffusion tensor imaging of post mortem multiple sclerosis brain. *NeuroImage*, 35(2), pp.467–77.

Schmierer, K., Thavarajah, J.R., et al., 2010. Effects of formalin fixation on magnetic resonance indices in multiple sclerosis cortical gray matter. *Journal of magnetic resonance imaging*, 32(5), pp.1054–1060.

Schmierer, K., Parkes, H.G., et al., 2010. High field (9.4 Tesla) magnetic resonance imaging of cortical grey matter lesions in multiple sclerosis. *Brain*, 133(3), pp.858–867.

Schmierer, K. et al., 2004. Magnetization transfer ratio and myelin in postmortem multiple sclerosis brain. *Annals of neurology*, 56(3), pp.407–15.

Schmierer, K. et al., 2008. Quantitative magnetic resonance of postmortem multiple sclerosis brain before and after fixation. *Magnetic Resonance Imaging*, 59(2), pp.268–277.

Schmierer, K., Tozer, D.J., et al., 2007a. Quantitative magnetization transfer imaging in postmortem multiple sclerosis brain. *Journal of magnetic resonance imaging*, 26(1), pp.41–51.

Schmierer, K., Tozer, D.J., et al., 2007b. Quantitative magnetization transfer imaging in postmortem multiple sclerosis brain. *Journal of magnetic resonance imaging*, 26(1), pp.41–51.

Schmierer, K. et al., 2003. Stereotactic co-registration of magnetic resonance imaging and histopathology in post-mortem multiple sclerosis brain. *Neuropathology and applied neurobiology*, 29(6), pp.596–601.

Schoonheim, M.M. et al., 2015. Thalamus structure and function determine severity of cognitive impairment in multiple sclerosis. *Neurology*, 84(8), pp.776–83.

Seewann, A. et al., 2009. Diffusely abnormal white matter in chronic multiple sclerosis: imaging and histopathologic analysis. *Archives of neurology*, 66(5), pp.601–609.

Seewann, A. et al., 2011. Imaging the tip of the iceberg: visualization of cortical lesions in multiple sclerosis. *Multiple Sclerosis Journal*, 17(10), pp.1202–1210.

Seewann, A. et al., 2012. Postmortem verification of MS cortical lesion detection with 3D DIR. *Neurology*, 78(5), pp.302–8.

Sepulcre, J. et al., 2009. Contribution of white matter lesions to gray matter atrophy in multiple sclerosis: evidence from voxel-based analysis of T1 lesions in the visual pathway. *Archives of neurology*, 66(2), pp.173–9.

Sepulcre, J. et al., 2006. Regional gray matter atrophy in early primary progressive multiple sclerosis: a voxel-based morphometry study. *Archives of neurology*, 63(8), pp.1175–80.

Sethi, V. et al., 2016. A longitudinal study of cortical grey matter lesion subtypes in relapse-onset multiple sclerosis. *Journal of neurology, neurosurgery, and psychiatry*, 87(7), pp.750–3.

Sethi, V. et al., 2012. Improved detection of cortical MS lesions with phase-sensitive inversion recovery MRI. *Journal of neurology, neurosurgery, and psychiatry*, 83(9), pp.877–82.

Sethi, V. et al., 2013. MS cortical lesions on DIR: not quite what they seem? *PloS one*, 8(11), p.e78879.

Sherman, S.M., 2007. The thalamus is more than just a relay. *Current opinion in neurobiology*, 17(4), pp.417–22.

Silva, M.F. et al., 2014. Development and aging of visual hemifield asymmetries in contrast sensitivity. *Journal of vision*, 14(12).

Silver, N.C. et al., 1997. Magnetisation transfer ratio of normal brain white matter: a normative database spanning four decades of life. *Journal of Neurology, Neurosurgery & Psychiatry*, 62, pp.223–228.

Sled, J.G. & Pike, G.B., 2001. Quantitative imaging of magnetization transfer exchange and relaxation properties in vivo using MRI. *Magnetic resonance in medicine : official journal of the Society of Magnetic Resonance in Medicine / Society of Magnetic Resonance in Medicine*, 46(5), pp.923–31.

Smith, A., 1982. *Symbol Digit Modalities Test (SDMT): manual (revised)*, Los Angeles: Western Psychological Services.

Sowa, P. et al., 2015. Reduced perfusion in white matter lesions in multiple sclerosis. *European journal of radiology*, 84(12), pp.2605–12.

Steenwijk, M.D. et al., 2015. Unraveling the relationship between regional gray matter atrophy and pathology in connected white matter tracts in long-standing multiple sclerosis. *Human Brain Mapping*, 36(5), pp.1796–1807.

Stoodley, C.J. & Schmahmann, J.D., 2009. Functional topography in the human cerebellum: a meta-analysis of neuroimaging studies. *NeuroImage*, 44(2), pp.489–501.

Stoodley, C.J., Valera, E.M. & Schmahmann, J.D., 2012. Functional topography of the cerebellum for motor and cognitive tasks: an fMRI study. *NeuroImage*, 59(2), pp.1560–70.

Stys, P.K. et al., 2012. Will the real multiple sclerosis please stand up? *Nature reviews. Neuroscience*, 13(7), pp.507–14.

Sun, H. et al., 2015. Validation of quantitative susceptibility mapping with Perls' iron staining for subcortical gray matter. *NeuroImage*, 105, pp.486–92.

Tardif, C.L. et al., 2012. Quantitative Magnetic Resonance Imaging of Cortical Multiple Sclerosis Pathology. *Multiple Sclerosis International*.

Thavarajah, R. et al., 2012. Chemical and physical basics of routine formaldehyde fixation. *Journal of oral and maxillofacial pathology : JOMFP*, 16(3), pp.400–5.

Tofts, P.S. et al., 2008. Imaging cadavers: cold FLAIR and noninvasive brain thermometry using CSF diffusion. *Magnetic resonance in medicine : official journal of the Society of Magnetic Resonance in Medicine / Society of Magnetic Resonance in Medicine*, 59(1), pp.190–5.

Tournier, J.-D., Calamante, F. & Connelly, A., 2012. MRtrix: Diffusion tractography in crossing fiber regions. *International Journal of Imaging Systems and Technology*, 22(1), pp.53–66.

Trapp, B.D. et al., 1998. Axonal transection in the lesions of multiple sclerosis. *The New England journal of medicine*, 338(5), pp.278–85.

Trennery, M.R., 1989. *Stroop Neuropsychological Screening Test manual*, Odessa, Fla: Psychological Assessment Resources.

Tustison, N.J. et al., 2010. N4ITK: improved N3 bias correction. *IEEE transactions on medical imaging*, 29(6), pp.1310–20.

Tzartos, J.S. et al., 2008. Interleukin-17 production in central nervous system-infiltrating T cells and glial cells is associated with active disease in multiple sclerosis. *The American journal of pathology*, 172(1), pp.146–55.

Vercellino, M. et al., 2009. Demyelination, inflammation, and neurodegeneration in multiple sclerosis deep gray matter. *Journal of neuropathology and experimental neurology*, 68(5), pp.489–502.

Vercellino, M. et al., 2005. Grey matter pathology in multiple sclerosis. *Journal of neuropathology and experimental neurology*, 64(12), pp.1101–7.

Vrenken, H. et al., 2006. Normal-appearing white matter changes vary with distance to lesions in multiple sclerosis. *American journal of neuroradiology*, 27(9), pp.2005–11.

van Waesberghe, J.H. et al., 1999. Axonal loss in multiple sclerosis lesions: magnetic resonance imaging insights into substrates of disability. *Annals of neurology*, 46(5), pp.747–754.

van Walderveen, M.A. et al., 1998. Histopathologic correlate of hypointense lesions on T1-weighted spin-echo MRI in multiple sclerosis. *Neurology*, 50(5), pp.1282–1288.

Walsh, A.J. et al., 2013. Multiple sclerosis: validation of MR imaging for quantification and detection of iron. *Radiology*, 267(2), pp.531–542.

Wang, C. et al., 2016. Automated brain volumetrics in multiple sclerosis: a step closer to clinical application. *Journal of neurology, neurosurgery, and psychiatry*, 87(7), pp.754–7.

Warrington, E.K., 1984. *Manual for Recognition Memory Test*, Windsor, UK: NFER-Nelson.

Wegner, C. et al., 2006. Neocortical neuronal, synaptic, and glial loss in multiple sclerosis. *Neurology*, 67(6), pp.960–7.

Weier, K. et al., 2014. Cerebellar abnormalities contribute to disability including cognitive impairment in multiple sclerosis. *PloS one*, 9(1), p.e86916.

Witte, M.E. et al., 2010. Mitochondrial dysfunction: A potential link between neuroinflammation and neurodegeneration? *Mitochondrion*, 10(5), pp.411–418.

Witte, M.E. et al., 2014. Mitochondrial dysfunction contributes to neurodegeneration in multiple sclerosis. *Trends in molecular medicine*, 20(3), pp.179–87.

Yao, B. et al., 2014. 7 Tesla Magnetic Resonance Imaging to Detect Cortical Pathology in Multiple Sclerosis A. Antal, ed. *PLoS ONE*, 9(10), p.e108863.

Zeis, T. et al., 2009. Molecular changes in white matter adjacent to an active demyelinating lesion in early multiple sclerosis. *Brain pathology*, 19(3), pp.459–466.

Zhang, Y. et al., 2013. Pathological correlates of magnetic resonance imaging texture heterogeneity in multiple sclerosis. *Annals of neurology*, 74(1), pp.91–99.

Zivadinov, R. et al., 2013. Thalamic atrophy is associated with development of clinically definite multiple sclerosis. *Radiology*, 268(3), pp.831–41.

Zwanenburg, J.J.M. et al., 2010. Fluid attenuated inversion recovery (FLAIR) MRI at 7.0 Tesla: comparison with 1.5 and 3.0 Tesla. *European Radiology*, 20(4), pp.915–922.